T.R.
GEBZE TECHNICAL UNIVERSITY
GRADUATE SCHOOL OF NATURAL AND APPLIED SCIENCES

MODEL BASED PARTIAL STATE AND OUTPUT FEEDBACK CONTROLLER DESIGNS FOR VARIOUS TYPES OF ELECTROMECHANICAL SYSTEMS

BEYTULLAH OKUR
A THESIS SUBMITTED FOR THE DEGREE OF
DOCTOR OF PHILOSOPHY
DEPARTMENT OF ELECTRONIC ENGINEERING

GEBZE
2016

T.R.

GEBZE TECHNICAL UNIVERSITY

GRADUATE SCHOOL OF NATURAL AND APPLIED SCIENCES

MODEL BASED PARTIAL STATE AND OUTPUT FEEDBACK CONTROLLER DESIGNS FOR VARIOUS TYPES OF ELECTROMECHANICAL SYSTEMS

BEYTULLAH OKUR

A THESIS SUBMITTED FOR THE DEGREE OF DOCTOR OF PHILOSOPHY

DEPARTMENT OF ELECTRONIC ENGINEERING

THESIS SUPERVISOR

PROF. DR. ERKAN ZERGEROĞLU

GEBZE

2016

T.C.
GEBZE TEKNİK ÜNİVERSİTESİ
FEN BİLİMLERİ ENSTİTÜSÜ

FARKLI ÖZELLİKLERE SAHİP ELEKTROMEKANİK SİSTEMLER İÇİN MODEL TABANLI KISMİ DURUM VE ÇIKIŞ GERİ BESLEMELİ DENETLEYİCİ FORMULASYONLARI

BEYTULLAH OKUR
DOKTORA TEZİ
ELEKTRONİK MÜHENDİSLİĞİ ANABİLİM DALI

DANIŞMANI
PROF. DR. ERKAN ZERGEROĞLU

GEBZE
2016

GEBZE TEKNİK ÜNİVERSİTESİ	**DOKTORA JÜRİ ONAY FORMU**

GTÜ Fen Bilimleri Enstitüsü Yönetim Kurulu'nun 27/06/2016 tarih ve 43 sayılı kararıyla oluşturulan jüri tarafından 26/07/2016 tarihinde tez savunma sınavı yapılan Beytullah OKUR'un tez çalışması Elektronik Mühendisliği Anabilim Dalında DOKTORA tezi olarak kabul edilmiştir.

JÜRİ

ÜYE
(TEZ DANIŞMANI) : Prof. Dr. Erkan Zergeroğlu

ÜYE : Doç. Dr. Abdulkadir Balıkçı

ÜYE : Yrd. Doç. Dr. Kadir Erkan

ÜYE : Yrd. Doç. Dr. Janset Daşdemir

ÜYE : Yrd. Doç. Dr. Uğur Hasırcı

ONAY

Gebze Teknik Üniversitesi Fen Bilimleri Enstitüsü Yönetim Kurulu'nun

...../...../..... tarih ve ...../..... sayılı kararı.

İMZA/MÜHÜR

SUMMARY

Model based control algorithms for electromechanical systems provide such advantages like precise and smooth control as well as enlarged stability region. However, comprehensive system models with nonlinear dynamics require complicated controller formulations and more system states to be measured. Increase in the number of system states to be measured brings on some disadvantages like additional sensor costs, noisy feedback signals and implementation difficulty due to non-measurable states. In the literature, there can be seen a variety of examples of observer designs instead of system states to be measured and filter designs to eliminate the need of state measurements.

In this study, the nonlinear model based partial state feedback controller formulations have been investigated for electromechanical systems with parametric uncertainties in the system dynamics. After a robust full–state–feedback solution for the trajectory tracking problem of elastic tendon driven robotic systems, a state–of–the–art adaptive partial–state–feedback formulation have been presented. An extension on a levitation system, composed of both electrical and mechanical dynamical terms, is also presented in order to illustrate the modularity of the design procedure. Backstepping technique have been successfully implemented to both of the system dynamics and stabilities of overall closed loop system dynamics have been proven via Lyapunov based arguments. The performances of the proposed controllers have been verified via numerical simulations. More over some experimental results have been presented for Tendon Driven Robotic system.

Key Words: Partial state feedback control, tendon driven robots, levitation systems.

ÖZET

Model tabanlı denetleyici yöntemleri sistem kararlılığını artırmak ve hassas denetim sağlamak gibi bir çok avantaj sunmaktadırlar. Fakat sistemler karmaşıklaştıkça hem dinamik model denklemleri karmaşıklaşmakta hem de ölçülmesi gereken sistem durumlarının sayısı artmaktadır. Ölçülmesi gereken durumların sayısının artması ilave sensör maliyetleri, gürültülü geri besleme sinyalleri ve ölçülemeyen durumlardan kaynaklı uygulama zorluğu gibi dezavantajlar getirmektedir. Literatürde bu gibi durumlarla başa çıkabilmek adına ölçülmek istenmeyen sistem durumları için tasarlanmış gözlemleyiciler ve ölçüm ihtiyacını ortadan kaldırmaya yönelik tasarlanmış filtreler bulunmaktadır.

Bu çalışmada, parametrik belirsizlikler içeren elektromekanik sistemler için doğrusal olmayan model tabalı kısmi durum geri beslemeli denetleyici formulasyonları üzerine çalışılmıştır. Elastik tendonlarla sürülen robotik sistemlerin yörünge takibi problemi için gürbüz bir tam durum geri beslemeli denetleyici çözümünden sonra uyarlamalı bir kısmi durum geri beslemeli denetleyici formulasyonu sunulmuştur. Bu denetleyici bu tip sistemler için halihazırda literatürdeki en kapsamlı çözümdür. Denetleyici tasarım prosedürünün farklı tipteki elektromekanik sistemler üzerinde de kolaylıkla uygulanabildiğini gösterebilmek adına tek serbeslik dereceli bir levitasyon sistemi için geliştirilmiş bir denetleyici formulasyonu da sunulmuştur. Levitasyon sistemi için sistemin mekanik modeli ve elektriksel modeli kullanılmış ve denetleyici çıkışı olarak bobinlere uygulanacak gerilim değeri hesaplanmıştır. Tasarlanan tüm denetleyicilerin kararlılık analizleri Lyapunov analiz tekniği ile gösterilmiş ve performansları benzetim çalışmaları ile incelenmiştir. Ayrıca tendon robot sistemi ile deneysel çalışmalar da gerçekleştirilmiştir.

Anahtar Kelimeler: Kısmi geri beslemeli denetim, tendon robotlar, levitasyon sistemleri.

ACKNOWLEDGEMENTS

During my graduate studies in the Gebze Technical University several persons collaborated directly and indirectly with my research. Without their support it would be impossible for me to finish my work. That is why I wish to dedicate this section to recognize their support.

I want to start expressing a sincere acknowledgement to my advisor, Dr. Erkan Zergeroğlu for giving me the opportunity to research under his guidance and supervision. I received motivation; encouragement and support from him during my studies and for the completion of my work. I also want to express my gratitude to Dr. Abdulkadir Balıkçı, Dr. Kadir Erkan, Dr. Janset Daşdemir and Dr. Uğur Hasırcı for serving as member of my graduate committee, for reviewing of the thesis and for their valuable advices during my research studies.

At last, but the most important I would like to thank my family, for their unconditional support, inspiration and love.

TABLE of CONTENTS

LIST of ABBREVIATIONS and ACRONYMS

Abbreviations and Acronyms	**Explanations**
$q(t)$	: Robot link position vector
$\dot{q}(t)$	: Robot link velocity vector
$\ddot{q}(t)$	: Robot link acceleration vector
$\theta(t)$	: Actuator position vector
$\dot{\theta}(t)$	: Actuator velocity vector
$\ddot{\theta}(t)$	: Actuator acceleration vector
$l(t)$	: Tendon expansion vector
$M(q)$	: Robot link inertial effects matrix
$V_m(q,\dot{q})$	: Robot link centripetal Coriolis effects matrix
$G(q)$	: Gravitational terms related to the robot
$F_d(\cdot)$	: Robot link viscous friction matrix
d_1, d_2	: Disturbance vectors
J	: Actuator inertia matrix
B	: Actuator viscous friction matrix
R_a	: Radius of pulleys mounted on each actuator
$J_j(q)$	: Jacobian matrix
$f_t(l)$	: Tendon tensile force vector
$f_{t,i}(l_i)$	: Tendon tensile force related to i^{th} tendon
$\tau_a(t)$	: Control input vector applied the actuators
I_n	: $n \times n$ identity matrix
$Y(q,\dot{q},\ddot{q})$	: Robot Model Regression matrix
ϕ_r	: Robot model parameter vector
$\lambda_{\max}\{\cdot\}$	: The maximum eigenvalue of a matrix
f_b	: Bias force vector
$e(t)$	: Output error vector
$q_d(t)$	: Desired link position trajectory vector
$q_{d1}(t)$	: First link desired position trajectory
$q_{d2}(t)$	: Second link desired position trajectory

$r(t)$: Filtered tracking error vector

$\widehat{\phi}_r$: Estimation value of ϕ_r

$\widetilde{\phi}_r(t)$: Parameter estimation error vector

$f_d(t)$: Desired tendon tension force trajectory

$\bar{\theta}_d(t)$: Desired actuator velocity trajectory

$\eta_f(t)$: Auxiliary error vector for tendon tension force

$\eta_\theta(t)$: Auxiliary error vector for actuator velocity

$\rho_i(\cdot)$: Positive bounding functions

$\eta(t)$: A filtered tracking error like term

$e_f(t)$: Error system filter variable

$\eta_L(t)$: Auxiliary error vector for actuator velocity filter

k_{ni} : Constant scalar nonlinear damping gains

t : Time

A_i : i^{th} actuator

L_i : i^{th} link

m : Mass of the levitated body

g : Gravity constant

z : Total air gap of magnetic circuit

i : Total equivalent current

$F_e(\cdot)$: Total electromagnetic attraction force

F_d : Bounded disturbance term

i_c : Current passing through coils

I_{pm} : Equivalent current of PMs

l_{pm} : Thickness of the PMs

φ : Airgap between poles and fixed side

$\lambda(z,i)$: Flux linkage

N : Number of coil turns

S : Cross sectional area of electromagnet poles

μ_0 : Constant permeability of the air

$L(z)$: Inductance of the coils

$B(z,i)$: Back EMF Factor

R : Electrical resistance of the coils

v	: Input voltage of the coils
u	: Auxiliary control input term
u_d	: Desired of the auxiliary control input trajectory
η_u	: Auxiliary error term related to auxiliary control input term
z_d	: Desired trajectory of the airgap
DC	: Direct Current
DOF	: Degree of Freedom
EMF	: Electro-Motive Force
FSFB	: Full State Feedback
PID	: Proportional - Integral - Derivative
PM	: Permanent Magnet
PSFB	: Partial State Feedback
TDRM	: Tendon Driven Robotic Manipulator

LIST of FIGURES

LIST of TABLES

1. INTRODUCTION

For electro–mechanical systems having nonlinearities in their dynamical equations, model based controllers have proven to be more effective compared to their linear counterparts. The main advantages include precise and smoother controller output, enlarged stability region and better performance when dealing with parametric uncertainties and/or unmeasurable system states[1]. However, the main drawback of model based controllers is the complexity of the control algorithms especially when the internal dynamics are also included as the controller implementation requires the measurements of the internal system states. Passivity based approaches [2], back-stepping techniques [3], adaptive [4] and robust [5] controller design procedures are common nonlinear controller design tools applied to cope for the complicated model equations. On the other hand, increase in the number of states used in the controller formulation also increases the total system costs due to the extra sensors required. Therefore researchers are motivated to reduce system cost and complexity by reducing the number of required sensors. In the literature, there can be seen a variety of examples of observer designs [6] instead of system states to be measured and filter designs [7] to eliminate the need of the internal state measurements.

1.1. Motivation and Scope

In order to emphasize the main motivation of this work, consider the following robotic manipulator model

$$M(q)\ddot{q}+V_m(q,\dot{q})\dot{q}+F_d\dot{q}+G(q)=\tau \tag{1.1}$$

where $q(t)$, $\dot{q}(t)$, $\ddot{q}(t) \in \mathbb{R}^n$ represent the link position, velocity and acceleration vectors, respectively, $M(q) \in \mathbb{R}^{n\times n}$ denotes the link inertia effects, $V_m(q,\dot{q}) \in \mathbb{R}^{n\times n}$ represents the centripetal Coriolis effects, $G(q) \in \mathbb{R}^n$ denotes the gravitational terms related to the robot, $F_d \in \mathbb{R}^{n\times n}$ is the constant diagonal link viscous friction matrix and finally $\tau(t) \in \mathbb{R}^n$ is the control input vector applied the actuators. The output of the robotic manipulator system is the link positions and input of the system is link actuation torque

as the actuation system dynamics are not considered in the whole system dynamics. Since the differential equation given in (1.1) is a second order differential equation, it has two system states which are $q(t)$ (link position) and $\dot{q}(t)$ (link velocity). If the whole system states (in this case two states for each link) are measurable, a Full State Feedback (FSFB) controller can be designed easily with the help of the feedback signals. When the system states are not available but the output of the system (in this case position of the links) an Output Feedback (OFB) controller need to be designed to deal with the lack of the state measurements which usually requires some massive mathematical manipulations. For the systems which consider the internal system dynamics like actuator dynamics and/or link elasticity, designing a FSFB controller would be an expensive solution due to the additional sensor costs (some times impossible because of unmeasurable physical variables) while designing an OFB controller becomes a tough problem to solve due to additional complexity in the system dynamics. In such cases, Partial State Feedback (PSFB) controllers could be acceptable solutions with some state measurements including the output of the system and with some mathematical work for unmeasurable system states.

The main motivation of this dissertation is to investigate novel PSFB and/or OFB controller formulations for various kinds of electromechanical systems with complicated system dynamics including parametric uncertainties. Two different kinds of electromechanical systems (i.e. robotic and mechatronic) have been chosen as a scope of this study. As a robotic system, an elastic tendon driven system has been studied in detail and FSFB and PSFB model based controller formulations have been proposed with simulation studies and experimental validations. A one DOF levitation system have been investigated as a mechatronic system a PSFB solution have been also proposed as a last chapter as an extension of the proposed controller algorithm.

1.2. Tendon Driven Robots and System Dynamics

Actuators that mounted on robot links have always been limited the performance of the robotic systems since they add additional bulk, mass and inertia to the mechanical systems. Nevertheless separating actuators from links and actuating links via remote power transmitting methods (i.e. cables, belts, tapes, chains, ropes) brings a re-

spectable complexity and uncertainty to the system dynamics. Besides, actuating links remotely becomes a key design challenge for some applications due to mechanical limitations (i.e. dexterous robotic hands) and/or safety requirements(light-weight robotic manipulators). Among remote power transmitting methods, tendon-driven transmission systems (i.e. steel cable with pulleys) have been widely used to design remotely actuated robotic systems since they provide a good power-to-weight ratio, low backlash, low friction and shock absorbent characteristics.To name some; [9], [10], [11] can be given as examples to small size applications such as robotic hands, and [12], [13], [14] are some examples for large size manipulators. For some background on tendon driven robot manipulators and classical linear control approaches on tendon driven systems, the reader is referred to [15], [16], [17] and the references therein.

The dynamics of an n degree–of–freedom robot manipulator driven by an $m-$tendon mechanism have the following form [13]

$$M(q)\ddot{q}+V_m(q,\dot{q})\dot{q}+F_d\dot{q}+G(q)+d_1=-J_j^T(q)f_t(l) \tag{1.2}$$

$$J\ddot{\theta}+B\dot{\theta}+R_a f_t(l)+d_2=\tau_a \tag{1.3}$$

$$\frac{d}{dt}l=J_j(q)\dot{q}+R_a\dot{\theta} \tag{1.4}$$

where $q(t)$, $\dot{q}(t)$, $\ddot{q}(t)\in\mathbb{R}^n$ represent the link position, velocity and acceleration vectors, respectively, $\theta(t)$, $\dot{\theta}(t)$, $\ddot{\theta}(t)\in\mathbb{R}^m$ represent the actuator position, velocity and acceleration vectors, respectively, $l(t)\in\mathbb{R}^m$ is the $m-$ dimensional tendon expansion vector, $M(q)\in\mathbb{R}^{n\times n}$ denotes the link inertia effects, $V_m(q,\dot{q})\in\mathbb{R}^{n\times n}$ represents the centripetal Coriolis effects, $G(q)\in\mathbb{R}^n$ denotes the gravitational terms related to the robot, $F_d\in\mathbb{R}^{n\times n}$ is the constant diagonal link viscous friction matrix, $d_1\in\mathbb{R}^n$ and $d_2\in\mathbb{R}^m$ are used to represent the bounded (with known upper bounds) disturbance vectors, $J,B\in\mathbb{R}^{m\times m}$ are the diagonal actuator inertia and actuator viscous friction matrices, respectively, $R_a\in\mathbb{R}^{m\times m}$ is the diagonal matrix containing the known radius of pulleys mounted on each actuator, $J_j(q)\in\mathbb{R}^{m\times n}$ is the known Jacobian matrix that maps the joint space to the tendon expansion space, $f_t(l)\in\mathbb{R}^m$ is the known vector

of tendon tensile forces generated by the tendon expansions, and finally $\tau_a(t) \in \mathbb{R}^m$ is the control input vector applied the actuators. A schematic representation of the system dynamics is presented in Figure 1.1. In a model based controller, it is nec-

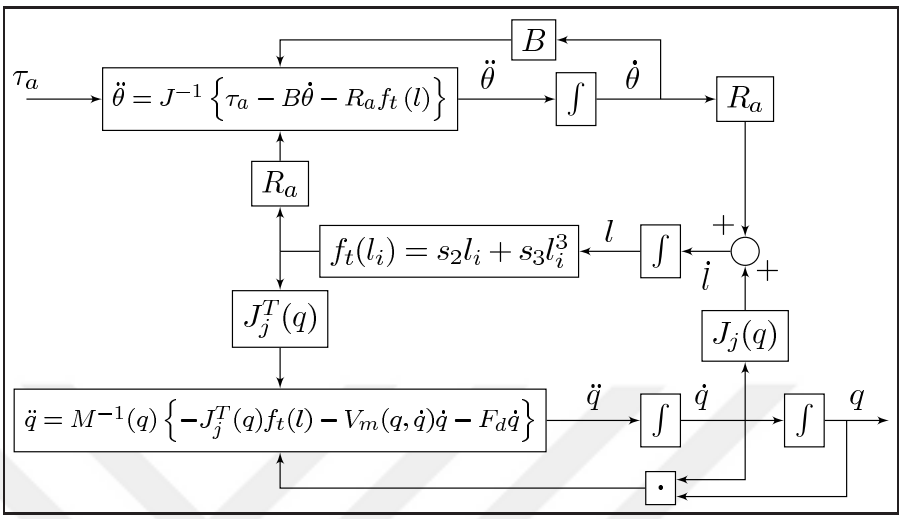

Figure 1.1: Tendon driven System Dynamics: a general view.

essary to include the elastic tendon dynamics to the system model, however, with this inclusion, the control problem becomes more complicated due to the extra dynamics and hence possible extra uncertainties. Agrawal *et al.*[18] and Wang *et al.*[19] investigated the flexibility of the tendons in a tendon-sheath mechanism and revealed that friction has an important effect in the transmission characteristics of a tendon-sheath mechanism. Lee *et al.*[20] suggested a model for robotic mechanisms driven by elastic tendons routed via fixed pulleys and Chang *et al.*[14] investigated the kinematics of similar systems where the friction effects between tendons and pulleys have been neglected. In [9], a detailed investigation of a tendon driven robotic hand system have been presented with tendon elasticity and tendon friction nevertheless the proposed controller in this study requires almost perfect knowledge of the system parameters. A detailed kinematic analysis have been given in [21] with the detailed explanation on calculating the Jacobian matrix between actuator space and link space of tendon driven mechanisms driven via passive and active tendons. The use of tendon driven actuation is more popular in dexterous hands as the resultant task space motion in robotic hand design usually does not need to be accurate[22]. For applications where the main performance criteria is to accurately track a desired task space trajectory, the use of tendon

driven mechanisms are limited which is mostly due to the elastic nature of the tendons where accurate position control and trajectory tracking becomes difficult. A detailed dynamic model of a tendon driven robotic manipulator has been investigated in [23] with the tendon elasticity.

A basic control approach, antagonistic control algorithms for tendon driven robotic manipulators have been studied since the early of nineties [24], [25]. In recent years; some more talented model free controllers have been proposed in the literature [26], [27], [28]. Controller formulations including system dynamics are limited in the literature. In [13], Kobayashi and Ozawa presented an adaptive neural network based controller for tendon driven robotic mechanisms with elastic tendons. In [29], Nakayama and Fujimoto tackled the tracking control of tendon driven robots by applying the delayed reflexive force feedback. In [30] and [31], Haiya *et al.* proposed controllers for multiple degree–of–freedom (dof) tendon mechanisms using nonlinear springs with hysteresis characteristics like stiffness adjustable tendons. For the proposed controllers, error of the equation of spring was estimated by a disturbance observer and compensated by utilizing the estimated disturbance. In [32], Wimbock *et al.* proposed an application of the Immersion and Invariance type framework to tendon driven systems with variable stiffness. The back-stepping approach have been successfully applied in [33]. Among the above cited works, the only work that considered the uncertainties in the system dynamics was given in [13], however the proposed adaptive controller requires the measurement of the second and third time derivatives of link position measurements (see assumption (2) of [13]). Review of the past research on control of tendon–driven robot manipulators has revealed that almost all of the control designs required accurate knowledge of the system model along with exact knowledge of model parameters. The only work considered parametric uncertainties was [13] which utilized link acceleration and jerk measurements.

The dynamic equations of (1.2) exhibit the following useful properties, which will be utilized in the controller development and the subsequent stability analysis.

Property 1.1: The inertia matrix can be bounded from above and below by the following inequalities [34]

$$m_1 I_n \leq M(q) \leq m_2 I_n \tag{1.5}$$

where m_1 and m_2 are positive constants, and I_n is the $n \times n$ identity matrix. Likewise the inverse of the inertia matrix can be bounded as follows

$$\frac{1}{m_2} I_n \leq M^{-1}(q) \leq \frac{1}{m_1} I_n. \tag{1.6}$$

Property 1.2: The inertia and the centripetal Coriolis matrices satisfy the following relationship [35]

$$\xi^T \left(\frac{1}{2} \dot{M}(q) - V_m(q, \dot{q}) \right) \xi = 0 \quad \forall \xi \in \mathbb{R}^n \tag{1.7}$$

where $\dot{M}(q)$ represents the time derivative of the inertia matrix.

Property 1.3: The centripetal Coriolis matrix satisfies the following relationship [36]

$$V_m(q, \nu)\xi = V_m(q, \xi)\nu \quad \forall \xi, \nu \in \mathbb{R}^n. \tag{1.8}$$

Property 1.4: The norm of the centripetal Coriolis matrix, and the gravitational effects with the friction vector can be upper bounded as follows [34]

$$\|V_m(q, \xi)\|_{i\infty} \leq \zeta_{c1} \|\xi\|, \quad \|F_d\| \leq \zeta_f, \quad \|G(q)\| \leq \zeta_g \quad \forall \xi \in \mathbb{R}^n \tag{1.9}$$

where ζ_{c1}, ζ_f, $\zeta_g \in \mathbb{R}$ are known positive bounding constants and $\|\cdot\|_{i\infty}$ denotes the induced infinity norm of a matrix.

Property 1.5: The robot dynamics given in (1.2) *can be linearly parameterized as follows [34]*

$$Y(q, \dot{q}, \ddot{q})\phi_r = M(q)\ddot{q} + V_m(q, \dot{q})\dot{q} + G(q) + F_d\dot{q} \tag{1.10}$$

where $\phi_r \in \mathbb{R}^p$ contains the constant system parameters, and $Y(q, \dot{q}, \ddot{q}) \in \mathbb{R}^{n \times p}$ denotes the regression matrix that is a function of $q(t)$, $\dot{q}(t)$ and $\ddot{q}(t)$. The formulation of (1.10) *can be rewritten in terms of the desired trajectory and its time derivatives in the following manner*

$$Y_d(q_d, \dot{q}_d, \ddot{q}_d)\phi_r = M(q_d)\ddot{q}_d + V_m(q_d, \dot{q}_d)\dot{q}_d + G(q_d) + F_d\dot{q}_d \tag{1.11}$$

where the desired regression matrix $Y_d(q_d, \dot{q}_d, \ddot{q}_d) \in \mathbb{R}^{n \times p}$ is a function of the desired link position, velocity, and acceleration vectors denoted by $q_d(t)$, $\dot{q}_d(t)$, $\ddot{q}_d(t) \in \mathbb{R}^n$, respectively.

Property 1.6: The unknown actuator parameter matrices J and B are bounded by known upper bounds which are determined as follows

$$\lambda_{\max}\{J\} < \bar{J}, \quad \lambda_{\max}\{B\} < \bar{B} \tag{1.12}$$

where $\bar{J}$, $\bar{B} \in \mathbb{R}$ are positive constants, and $\lambda_{\max}\{\cdot\}$ denotes the maximum eigenvalue of a matrix.

Aside from the assumption that the force/elongation characteristics of the tendons being perfectly known, our controller development and stability analysis also utilizes the following assumptions, similar to that of [13]:

Assumption 1.1: $rank(J_j(q)) = n$ for any $q \in \mathbb{R}^n$.

Assumption 1.2: There exists a positive valued vector of bias forces, f_b, such that $J_j(q)^T f_b = 0$ where this bias vector is used to keep the joint tendon tension vector $f_t(l)$ positive without changing the joint forces generated by the tendons.

Assumption 1.3: Each entry of the vector $f_t(l)$ satisfies $f_{ti}(l_i) = 0$ for $l_i < 0$ and $f_{ti}(l_i) \geq 0$, $\frac{\partial f_{ti}(l_i)}{\partial l_i} > 0$ for $l_i \geq 0$ where $i = 1, 2, ..., m$.

Assumption 1.4: The matrix $\frac{\partial f_t(l)}{\partial l} \in \mathbb{R}^{m \times m}$ is non–singular.

1.3. Outline of the Thesis

The outline of this dissertation have been organised to present the detailed studies on tendon driven robots. A FSFB nonlinear robust solution for the link position tracking problem of the tendon-driven robot manipulators with uncertain dynamical system parameters is presented in Chapter 2. A robust backstepping approach has

been utilized to achieve uniformly ultimately bounded tracking performance despite the lack of exact knowledge of the dynamical parameters and presence of additive bounded disturbances. The model based PSFB control of tendon driven robotic manipulators including uncertainty in the system dynamics have been focused on Chapter 3. A backstepping type adaptive controller have been proposed while only link positions, actuator positions and tendon tension measurements are available. An extension for eliminating the actuator side position measurements have been also presented in case of having exact knowledge of the actuator side model parameters. Lyapunov based arguments have been applied to prove the stability of the closed–loop systems at the end of the related chapters. To prove the effectiveness of the proposed controllers some simulation studies have been performed on a two link planar robot manipulator driven by a six tendon mechanism and simulation results are presented in Chapter 4. Besides, experimental results of a standard PID controller, Feed-forward controller and PSFB controller on one link and two links robotic manipulators are presented in Chapter 5. An extension on a one degree-of-freedom magnetic levitation system with hybrid electromagnets have been presentedIn Chapter 6. Nonlinear equations of the magnetic force model have been used to develop the model based controller. The proposed controller can handle parametric uncertainties and only requires air gap and coil current measurements. The output of the controller is the voltage input of the coils and back-stepping procedure have been applied to reach the voltage dynamics over current dynamics. The stability and convergence of the closed loop system have been proved via Lyapunov-type arguments. Simulation results are presented to illustrate the performance of the proposed robust controller. Finally, some conclusions about the overall work are reported in Chapter 7.

2. FSFB ROBUST CONTROLLER

The aim of this chapter is to illustrate the design and the corresponding stability analysis for a full state feedback (*i.e.*, position and velocity information of both the actuators and robot links and tension measurements of each tendon) robust controller. The proposed controller ensures practical joint space trajectory tracking despite the uncertainties associated with the robot and transmission system parameters. Adding the dynamics of the power transmission system and considering tendon elasticity yield a complicated dynamic model, and the resulting system dynamics mandates the use the backstepping technique twice. The stability analysis ensures the boundedness of all the signals under the closed–loop operation and uniform ultimate boundedness of the link position tracking errors.

The rest of the chapter is organized in the following manner. Error system development and controller formulation are given in Sections 2.1. The Lyapunov type stability analysis is presented in 2.2. Finally some concluding remarks are given in Section 2.3.

2.1. Controller Formulation

The control objective is to design a link position tracking controller for the tendon–driven robot manipulator model given by (1.2), (1.3) and (1.4) under the restrictive constraint that the dynamical system parameters of (1.2), (1.3) are uncertain. In the subsequent control design, the full state feedback (*i.e.*, position and velocity information) have been utilized. Specifically, the controller should ensure the robot links follow a desired trajectory as closely as possible, despite the uncertain robot/actuator system parameters. In order to quantify the control objective, the link position tracking error $e(t) \in \mathbb{R}^n$ have been defined as follows

$$e \triangleq q_d - q \tag{2.1}$$

where it is assumed that the desired link position, $q_d(t)$ and its time derivatives are sufficiently smooth and bounded functions of time. To facilitate the subsequent control

development, the filtered tracking error $r(t) \in \mathbb{R}^n$ can be defined as

$$r \triangleq \dot{e} + \alpha e \tag{2.2}$$

where $\alpha \in \mathbb{R}^{n \times n}$ is a positive definite, diagonal control gain matrix. In addition, to provide a method of quantifying robustness, the difference between the actual and estimated parameters can be written as follows

$$\widetilde{\phi}_r \triangleq \phi_r - \widehat{\phi}_r \tag{2.3}$$

where $\widetilde{\phi}_r(t) \in \mathbb{R}^p$ represents the parameter estimation error vector and $\widehat{\phi}_r \in \mathbb{R}^p$ represents the constant best guess estimates of ϕ_r defined in (1.10). The backstepping based controller design procedure requires defining two additional auxiliary error terms $\eta_f(t)$, $\eta_\theta(t) \in \mathbb{R}^m$ as

$$\eta_f \triangleq f_t - f_d \tag{2.4}$$

$$\eta_\theta \triangleq \dot{\theta} - \bar{\theta}_d \tag{2.5}$$

where $f_t(t)$, $\dot{\theta}(t)$ were defined in (1.2) and (1.3), respectively, and $f_d(t)$, $\bar{\theta}_d(t)$ are yet to be designed auxiliary control inputs. Taking the time derivative of (2.2), pre–multiplying the resultant equation by $M(q)$, adding/ subtracting $Y_d\phi_r$, $J_j^T(q)f_d$ and $V_m(q,\dot{q})r$ to the right hand side of the resulting equation, it can be obtained

$$M(q)\dot{r} = -V_m(q,\dot{q})r + \chi + d_1 + J_j^T(q)\eta_f + J_j^T(q)f_d + Y_d\phi_r \tag{2.6}$$

where $\chi(q,\dot{q},t) \in \mathbb{R}^n$ is an auxiliary term defined as

$$\begin{aligned} \chi \;=\; & M(q)\left(\ddot{q}_d + \alpha\dot{e}\right) - M(q_d)\ddot{q}_d \\ & + V_m(q,\dot{q})\left(\dot{q}_d + \alpha e\right) - V_m(q_d,\dot{q}_d)\dot{q}_d \\ & + G(q) - G(q_d) + F_d\dot{q} - F_d\dot{q}_d. \end{aligned} \tag{2.7}$$

Based on Properties *1.1:* and *1.4:*, and using (2.1) and (2.2), it can be proven that (see [34], Chapter 6 Eq: 6.2-9)

$$\|\chi\| \leq \rho_1(\|z\|)\|z\| \tag{2.8}$$

where $z(t) \in \mathbb{R}^{2n}$ is defined as

$$z(t) \triangleq \begin{bmatrix} e^T(t) & r^T(t) \end{bmatrix}^T \tag{2.9}$$

and $\rho_1(\cdot) \in \mathbb{R}$ is a known positive bounding function. From the structure of (2.6) and the subsequent stability analysis, $f_d(t)$ can be designed in the following form

$$f_d = \left(J_j^T(q)\right)^+ \left(-K_r r - k_n\left(\rho_1^2(r,e) + \rho_2^2\right) r - e - Y_d\hat{\phi}_r\right) \tag{2.10}$$

where $(\cdot)^+$ is used to represent the pseudo inverse of a matrix [38], $K_r \in \mathbb{R}^{n\times n}$ is a constant, positive definite, diagonal gain matrix, $k_n \in \mathbb{R}$ is a constant positive damping gain, $\hat{\phi}_r$ was defined in (2.3), and $\rho_2 \in \mathbb{R}$ is a positive bounding constant designed to satisfy

$$\rho_2 \geq \left\|\widetilde{F}\right\| \tag{2.11}$$

where $\widetilde{F}(t) \triangleq Y_d\phi_r - Y_d\hat{\phi}_r + d_1 \in \mathbb{R}^n$. Inserting (2.10) into (2.6), the closed–loop dynamics for the filtered tracking error term $r(t)$ is obtained to have the following form

$$M(q)\dot{r} = -V_m(q,\dot{q})r + \chi + \widetilde{F} + J_j^T(q)\eta_f - K_r r - k_n\left(\rho_1^2(r,e) + \rho_2^2\right) r - e. \tag{2.12}$$

From (2.12), it can be seen that to ensure the stability and convergence of the tracking error signal, the dynamics of the auxiliary signal $\eta_f(t)$ is also required. To this end, one can take the time derivative of (2.4) and make use of (1.2), (1.4), (2.2) and (2.10), to produce

$$\dot{\eta}_f = \Omega_1 + \Omega_2 + \frac{\partial f_t(l)}{\partial l} R_a\dot{\theta} \tag{2.13}$$

where the right hand side is segregated into the auxiliary variables $\Omega_1(q,\dot{q},l,t) \in \mathbb{R}^m$ containing known and measurable parameters, and $\Omega_2(q,\dot{q},l,\phi_r,t) \in \mathbb{R}^m$ containing uncertain system parameters, and are explicitly defined as

$$\begin{aligned}\Omega_1 \triangleq\ & \frac{\partial f_t(l)}{\partial l} J_j(q)\dot{q} + \frac{d}{dt}\left\{\left(J_j^T(q)\right)^+ Y_d \hat{\phi}_r\right\} \\ & -\frac{d}{dt}\left\{\left(J_j^T(q)\right)^+\right\}\left(-K_r r - k_n\left(\rho_1^2+\rho_2^2\right) r - e\right) \\ & +\left(J_j^T(q)\right)^+\left\{\dot{e} + 2k_n\rho_1 r\frac{\partial \rho_1}{\partial e}\dot{e}\right. \\ & \left.+\left[K_r + k_n\left(\rho_1^2+\rho_2^2\right) I_n + 2k_n r\left(\rho_1\frac{\partial \rho_1}{\partial r}\right)\right](\ddot{q}_d + \alpha\dot{e})\right\}\end{aligned} \tag{2.14}$$

and

$$\begin{aligned}\Omega_2 \triangleq\ & \left(J_j^T(q)\right)^+\left\{\left[K_r + k_n\left(\rho_1^2+\rho_2^2\right) I_n + 2k_n r\left(\rho_1\frac{\partial \rho_1}{\partial r}\right)\right]\right. \\ & \left.\times\left[M^{-1}(q)\left(J_j^T(q) f_t(l) + V_m(q,\dot{q})\dot{q} + F_d\dot{q} + G(q) + d_1\right)\right]\right\}.\end{aligned} \tag{2.15}$$

Notice that all the entries of (2.14) are known and/or measurable signals while (2.15) contains uncertain system parameters, therefore cannot be directly used in the controller design. At this stage, motivated to ensure the convergence of $\eta_f(t)$, one should add/ subtract $\frac{\partial f_t(l)}{\partial l} R_a \bar{\theta}_d$ term to the right hand side of (2.13) to obtain

$$\dot{\eta}_f = \Omega_1 + \Omega_2 + \frac{\partial f_t(l)}{\partial l} R_a \eta_\theta + \frac{\partial f_t(l)}{\partial l} R_a \bar{\theta}_d \tag{2.16}$$

where (2.5) was utilized. From the structure of (2.16) and the subsequent stability analysis, the auxiliary signal $\bar{\theta}_d(t)$ can be designed in the following form

$$\bar{\theta}_d = \Lambda\left(-K_f\ \eta_f - J_j(q)\, r - \Omega_1 - \widehat{\Omega}_2 - v_{R1}\right) \tag{2.17}$$

where the auxiliary variable $\Lambda(l) \in \mathbb{R}^{m\times m}$ is defined as

$$\Lambda \triangleq \left(\frac{\partial f_t(l)}{\partial l} R_a\right)^{-1}, \tag{2.18}$$

K_f is a positive definite, constant, diagonal gain matrix, $\Omega_1(\cdot)$ was defined in (2.14), $\widehat{\Omega}_2\left(\hat{\phi}_r, t\right)$ is the estimate of $\Omega_2(\phi_r, t)$ with $\hat{\phi}_r$ being the constant best guess estimates of ϕ_r, and $v_{R1}(t)$ is a differentiable robust term defined in the following form [39]

$$v_{R1} = \frac{\rho_3^2}{\varepsilon_1}\eta_f \tag{2.19}$$

where $\varepsilon_1 \in \mathbb{R}$ is a positive constant, and $\rho_3(e, r, l, t) \in \mathbb{R}$ is a positive bounding function designed to satisfy

$$\rho_3(e, r, l, t) \geq \left\|\widetilde{\Omega}_2\right\| \tag{2.20}$$

with $\widetilde{\Omega}_2 \triangleq \Omega_2 - \widehat{\Omega}_2$. After substituting (2.17) into (2.16), the closed–loop dynamics for the auxiliary tracking error signal $\eta_f(t)$ is obtained to have the following form

$$\dot{\eta}_f = -K_f\,\eta_f - J_j(q)\,r + \frac{\partial f_t(l)}{\partial l}R_a\eta_\theta + \widetilde{\Omega}_2 - v_{R1}. \tag{2.21}$$

At this stage, the backstepping design procedure requires the dynamics of $\eta_\theta(t)$, which can be obtained by taking the time derivative of (2.5), inserting (2.17) then pre–multiplying both sides of the resulting equation by J and applying (1.2), (1.3) and (1.4) as

$$J\dot{\eta}_\theta = \Omega_3 + \Omega_4 + \tau_a \tag{2.22}$$

where the right hand side is segregated into the auxiliary terms $\Omega_3\left(q, \dot{q}, l, \dot{\theta}, t\right) \in \mathbb{R}^m$ containing measurable/known variables, and $\Omega_4\left(q, \dot{q}, l, \dot{\theta}, \phi_r, J, B, t\right) \in \mathbb{R}^m$ containing uncertain system parameters, and are explicitly defined as follows

$$\begin{aligned}
\Omega_3 \triangleq\ & -R_a f_t(l) + J\frac{d\Lambda}{dt}\left(K_f\,\eta_f + J_j(q)\,r + \Omega_1 + \widehat{\Omega}_2 + v_{R1}\right) \\
& + J\Lambda\left\{K_f\left(\Omega_1 + \frac{\partial f_t(l)}{\partial l}R_a\dot{\theta}\right) + \frac{d}{dt}\left\{J_j(q)\right\}r + J_j(q)\left(\ddot{q}_d + \alpha\dot{e}\right)\right. \\
& \quad + \frac{\partial}{\partial q}\left(\Omega_1 + \widehat{\Omega}_2 + v_{R1}\right)\dot{q} + \frac{\partial}{\partial l}\left(\Omega_1 + \widehat{\Omega}_2 + v_{R1}\right)\left(J_j(q)\,\dot{q} + R_a\dot{\theta}\right) \\
& \quad \left. + \frac{\partial}{\partial t}\left(\Omega_1 + \widehat{\Omega}_2 + v_{R1}\right)\right\}
\end{aligned} \tag{2.23}$$

and

$$\begin{aligned}\Omega_4 \triangleq & -B\dot{\theta} - d_2 + J\Lambda\left\{K_f\,\Omega_2 - \left(J_j(q) - \frac{\partial}{\partial \dot{q}}\left(\Omega_1 + \widehat{\Omega}_2 + v_{R1}\right)\right)\right. \\ & \left.\times\left[M^{-1}(q)\left(J_j^T(q) f_t(l) + V_m(q,\dot{q})\dot{q} + F_d\dot{q} + G(q) + d_1\right)\right]\right\}.\end{aligned} \tag{2.24}$$

Based on the previous development and the ensuing stability analysis, the control torque input signal $\tau_a(t)$ have been designed as follows

$$\tau_a = -K_\theta \eta_\theta - \left(\frac{\partial f_t(l)}{\partial l} R_a\right)^T \eta_f - \Omega_3 - \widehat{\Omega}_4 - v_{R2} \tag{2.25}$$

where, similar to the design of (2.17), $K_\theta \in \mathbb{R}^{m\times m}$ is a positive definite, constant, diagonal gain matrix, Ω_3 was defined in (2.23), $\widehat{\Omega}_4\left(\hat{\phi}_r, \hat{J}, \hat{B}, t\right) \in \mathbb{R}^m$ is the estimate of $\Omega_4(\phi_r, J, B, t)$ with $\left(\hat{\cdot}\right)$ being used to illustrate the constant best guess estimates of $(\cdot)$, and $v_{R2}(t)$ is the robust term defined in the following form [39]

$$v_{R2} = \frac{\rho_4^2}{\varepsilon_2}\eta_\theta \tag{2.26}$$

where $\varepsilon_2 \in \mathbb{R}$ is a positive constant, and $\rho_4(e, r, l, \eta_\theta, t) \in \mathbb{R}$ is a positive bounding function designed to satisfy

$$\rho_4(e, r, l, \eta_\theta, t) \geq \left\|\widetilde{\Omega}_4\right\| \tag{2.27}$$

with $\widetilde{\Omega}_4 \triangleq \Omega_4 - \widehat{\Omega}_4 \in \mathbb{R}^m$. After substituting the control torque input given by (2.25) into (2.22),the closed–loop error dynamics for $\eta_\theta(t)$ have been obtained as shown below

$$J\dot{\eta}_\theta = -K_\theta \eta_\theta - \left(\frac{\partial f_t(l)}{\partial l} R_a\right)^T \eta_f + \widetilde{\Omega}_4 - v_{R2}. \tag{2.28}$$

A schematic representation of the controller formulation is presented in Figure 2.1. Having formed the closed–loop dynamics for the error signals $r(t)$, $\eta_f(t)$ and $\eta_\theta(t)$, it is time to analyse the stability of the overall system and the convergence of the link position tracking error $e(t)$.

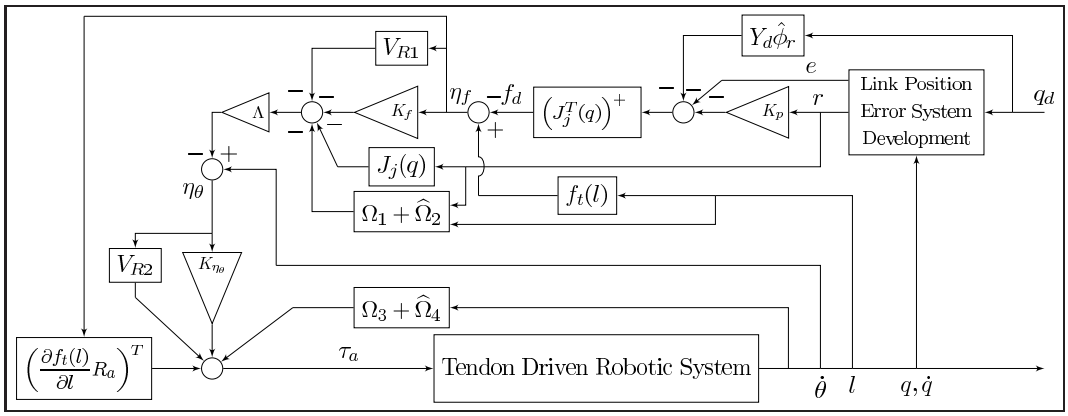

Figure 2.1: An illustration of the controller formulation.

2.2. Stability Analysis

The stability of the closed–loop system will be investigated by utilizing Lyapunov based arguments. Following theorem formalizes the stability analysis.

Theorem 2.1: The robust controller of (2.25) *and the auxiliary control inputs* (2.10) *and* (2.17) *with the robust terms* (2.19) *and* (2.26) *guarantees uniform ultimate boundedness of the link position tracking error* $e(t)$ *in the sense that*

$$\|e(t)\| \leq \sqrt{\frac{a}{b}\|x(0)\|^2 \exp(-\beta t) + \frac{2\varepsilon}{b\beta}(1-\exp(-\beta t))} \tag{2.29}$$

where $x(t) \triangleq \left[\begin{array}{cccc} e^T & r^T & \eta_f^T & \eta_\theta^T \end{array}\right]^T \in \mathbb{R}^{2(n+m)\times 1}$ *is the combined error signal, a, b,* β, $\varepsilon \in \mathbb{R}$ *are positive scalars defined explicitly as*

$$a \triangleq \max\{1, m_2, \bar{J}\} \tag{2.30}$$

$$b \triangleq \min\{1, m_1, \lambda_{\min}(J)\} \tag{2.31}$$

$$\beta \triangleq \frac{2\min\left\{\min\{\lambda_{\min}(K_r), \lambda_{\min}(\alpha)\} - \frac{1}{4k_n}, \lambda_{\min}\left(K_f\right), \lambda_{\min}\left(K_\theta\right)\right\}}{\max\{1, m_2, \bar{J}\}} \tag{2.32}$$

$$\varepsilon \triangleq \frac{1}{4k_n} + \varepsilon_1 + \varepsilon_2 \tag{2.33}$$

where m_1, m_2, $\bar{J}$, ε_1, ε_2, k_n, K_f, K_θ *and* K_r *were previously defined, and the notation* $\lambda_{\min}(\cdot)$ *is used to denote the minimum eigenvalue of a matrix. Proof 2.1: To prove the Theorem, one can start by defining a non–negative scalar function of the form*

$$V = \frac{1}{2} r^T M r + \frac{1}{2} e^T e + \frac{1}{2} \eta_f^T \eta_f + \frac{1}{2} \eta_\theta^T J \eta_\theta \tag{2.34}$$

which can be bounded from below and above as

$$\frac{1}{2} \min\{1, m_1, \lambda_{\min}(J)\} \|x\|^2 \leq V \leq \frac{1}{2} \max\{1, m_2, \bar{J}\} \|x\|^2 . \tag{2.35}$$

Taking the time derivative of (2.34) *along* (2.12), (2.2), (2.21) *and* (2.28), *making use of* (1.7), *and then canceling common terms yields to*

$$\begin{aligned} \dot{V} &= -r^T K_r r - e^T \alpha e - \eta_f^T K_f \eta_f - \eta_\theta^T K_\theta \eta_\theta \\ &\quad + r^T \left[\chi - k_n \rho_1^2 r\right] + r^T \left[\widetilde{F} - k_n \rho_2^2 r\right] \\ &\quad + \eta_f^T \left[\widetilde{\Omega}_2 - v_{R1}\right] + \eta_\theta^T \left[\widetilde{\Omega}_4 - \frac{\rho_4^2}{\varepsilon_2} \eta_\theta\right] . \end{aligned} \tag{2.36}$$

Note that using the definition given in (2.19) *the* $\eta_f^T \left[\widetilde{\Omega}_2 - v_{R1}\right]$ *term can be bounded as follows [39]*

$$\begin{aligned} \eta_f^T \left[\widetilde{\Omega}_2 - v_{R1}\right] &\leq \rho_3 \left\|\eta_f\right\| - \frac{\rho_3^2 \left\|\eta_f\right\|^2}{\varepsilon_1} \\ &\leq \rho_3 \left\|\eta_f\right\| \left(1 - \frac{\rho_3 \left\|\eta_f\right\|}{\varepsilon_1}\right) \\ &\leq \varepsilon_1 . \end{aligned} \tag{2.37}$$

After applying (2.8), (2.11), (2.27) *and* (2.37), *the right hand side of* (2.36) *can be upper bounded to have the following form*

$$\begin{aligned}\dot{V} \leq & -\lambda_{\min}(K_r)\|r\|^2 - \lambda_{\min}(\alpha)\|e\|^2 - \lambda_{\min}(K_f)\left\|\eta_f\right\|^2 \\ & -\lambda_{\min}(K_\theta)\|\eta_\theta\|^2 + \left[\rho_1\|z\|\|r\| - k_n\rho_1^2\|r\|^2\right] \\ & + \left[\rho_2\|r\| - k_n\rho_2^2\|r\|^2\right] + \left[\rho_4\|\eta_\theta\| - \frac{\rho_4^2\|\eta_\theta\|^2}{\varepsilon_2}\right] + \varepsilon_1.\end{aligned} \tag{2.38}$$

Applying the nonlinear damping argument (i.e., first by adding and subtracting $1/4k_n$ *and then completing the squares) to the first and second bracketed terms of* (2.38)*, the right hand side can further be bounded as*

$$\begin{aligned}\dot{V} \leq & -\left(\min\{\lambda_{\min}(K_r), \lambda_{\min}(\alpha)\} - \frac{1}{4k_n}\right)\|z\|^2 - \lambda_{\min}(K_f)\left\|\eta_f\right\|^2 \\ & -\lambda_{\min}(K_\theta)\|\eta_\theta\|^2 + \left[\rho_4\|\eta_\theta\| - \frac{\rho_4^2\|\eta_\theta\|^2}{\varepsilon_2}\right] + \varepsilon_1 + \frac{1}{4k_n}.\end{aligned} \tag{2.39}$$

where $z(t)$ *was previously defined in* (2.9)*. Finally, using a similar manipulation to that of* (2.37) *to the bracketed term of* (2.39)*, we obtain*

$$\dot{V} \leq -\min\left\{\min\{\lambda_{\min}(K_r), \lambda_{\min}(\alpha)\} - \frac{1}{4k_n}, \lambda_{\min}(K_f), \lambda_{\min}(K_\theta)\right\}\|x\|^2 + \varepsilon \tag{2.40}$$

where ε *was previously defined in* (2.33)*. Using the definition of* $x(t)$ *and the upper bound of* $V(t)$ *given in* (2.35)*, the upper bound of* $\dot{V}(t)$ *given* (2.40) *can be reformulated as*

$$\dot{V} \leq -\beta V + \varepsilon \tag{2.41}$$

where β *was defined in* (2.32)*. The solution of the above differential inequality yields*

$$V(t) \leq V(0)\exp(-\beta t) + \frac{\varepsilon}{\beta}(1 - \exp(-\beta t)) \tag{2.42}$$

and from (2.35)*, the following upper bound for* $x(t)$ *can be obtained*

$$\|x(t)\| \leq \sqrt{\frac{a}{b}\|x(0)\|^2\exp(-\beta t) + \frac{2\varepsilon}{b\beta}(1 - \exp(-\beta t))} \tag{2.43}$$

where a and b were previously defined in (2.30) *and* (2.31)*, respectively. Based on the definition of* $x(t)$ *and* (2.43)*, it can be shown that the tracking error term* $e(t)$ *is bounded as stated in* (2.29)*. Similar to the* $e(t)$*, it can be shown that* $r(t)$*,* $\eta_f(t)$ *and* $\eta_\theta(t)$ *by an exponential envelope, based on the definition of* $x(t)$*. Since e, r,* q_d *and* $\dot{q}_d$ *are bounded signals then* $\dot{e}$*, q,* $\dot{q}$ *are also bounded signals according to* (2.1) *and* (2.2)*. From definition of* f_d *given in* (2.10) *and utilising the boundedness of q, e and r, it can be shown that* f_d *is bounded and based on the definition of* η_f *given in* (3.8) $f_t(l)$ *is bounded and so* $l(t)$ *is bounded. In view of* (2.17)*, we can conclude that* $\bar{\theta}_d$ *is bounded based on the boundedness of the signals in it. Then using the definition of* η_θ *given in* (2.5)*, it can be shown that* $\dot{\theta}$ *is also bounded. Since q,* $\dot{q}$*, l and* $\dot{\theta}$ *are bounded, then* $\dot{l}$ *and* θ *are also bounded based on the dynamics given in* (1.4)*. Based on the definition of* τ_a *given in* (2.25) *and the boundedness of the signals therein,* τ_a *remains bounded, as well.* ■

2.3. Remarks

In this chapter, a full state feedback, nonlinear robust controller for TDRMs subject to parametric uncertainty in system dynamics have been presented. Despite the lack of exact knowledge of system parameters and presence of external disturbances, the proposed controller ensured practical trajectory tracking in the sense that; the norm of the link position tracking error signal is forced to enter an ultimate bound in finite time. Stability of the closed–loop system and boundedness of system states are proven via Lyapunov based arguments.the proposed controller requires the full state feedback of all system states (i.e. both position and velocity information of the robot joints and the actuators) and the exact knowledge of the tendon tensile forces generated by tendon expansions. From the illustration given Figure 2.1, it is obvious that the implementation of the proposed controller is far more complex compared to most conventional controllers. However thanks to the current state of micro–controllers the controller algorithm is still implementable in real time.

In the controller design it was assumed that the force/elongation characteristic of the tendon is perfectly known. It should be mentioned that the proposed robust controller can be modified to compensate for simplistic tendon transmission models

(i.e. linear). However as presented in [12], [13], [14] the actual tendon characteristics includes highly nonlinear terms as hysteresis. In an actual implementation due to the robust nature of proposed controller, some of these uncertainties might be compensated by readjusting the controller gains upto a point. Still additional uncertainties like the elastic tendon characteristics would result in higher tracking errors in an actual implementation.

The results given in this chapter are printed in volume 80 of Journal of Intelligent and Robotic Systems (pp.3–14) in October of 2015 [40].

3. PSFB ADAPTIVE CONTROLLER

FSFB model based control of tendon driven systems require a significant amount of sensory equipments to measure the necessary system states like positions and velocities of links and actuators since tendon driven systems are usually designed to be an over-actuated systems. In this chapter, it is focused on model based partial state feedback (PSFB) controller for tendon driven robot manipulators that does not require neither acceleration nor velocity measurements of both links and actuators. Moreover an extension on eliminating the actuator side position measurements have been investigated, as well. The proposed adaptive PSFB controller only requires link and actuator position measurements and tension measurements of each tendons while the whole dynamical system parameters are uncertain. Specifically, the proposed semi–global adaptive PSFB trajectory tracking controller deals with parametric uncertainties via three different parameter update rules. The need for link velocity measurements are eliminated by utilizing a nonlinear link velocity filter during the error system development, and the lack of actuator velocity measurements have been overcome with the help of a set of linear filters. Based on the backstepping type model based controller development procedure presented in the previous chapter, the proposed adaptive controller ensures boundedness of all the signals under the closed–loop operation, and semi–global asymptotic tracking of the link position error.

The rest of this chapter is organized as follows. Control objectives and detailed formulation of the adaptive PSFB controller are given in Sections 3.1. Main stability result and proof of the result can be seen in Section 3.2. An extension on eliminating the actuator side position measurements and related stability analysis have been presented in Section 3.3. Concluding remarks are given in Section 3.4.

3.1. Development of Adaptive PSFB Controller

The control objective is to design an adaptive link position tracking controller for the tendon driven robot manipulator model given by (1.2), (1.3) and (1.4) under the restrictive constraint that the dynamical system parameters of (1.2) and (1.3) are uncertain, and velocity and acceleration measurements of both robot links and actua-

tors are not available. Unknown disturbances given by d_1 in (1.2) and d_2 in (1.3) have been neglected due to the adaptive structure of the controller design. Specifically, the controller should ensure the robot links to asymptotically follow a desired trajectory despite the uncertain model parameters while only link and actuator position measurements and tendon tension force measurements are available. To this end a link velocity independent error system for robotic manipulator have been developed with the help of a link velocity filter design and uncertain manipulator and actuator parameters are updated via three different adaptation rules. Need for actuator velocity measurements can be eliminated with the help of a set of linear filters and back–stepping procedure have been implemented twice during the controller development process to design the actuator input signals. Since the aim of the controller is the desired output tracking of the links, the resultant performance of the controller-filter couples can be quantified by the link position tracking error $e(t) \in \mathbb{R}^n$ which can be defined as

$$e \triangleq q_d - q \tag{3.1}$$

where it is assumed that the desired link position signal $q_d(t)$ and its time derivatives are sufficiently smooth and bounded functions of time. We define a filtered tracking error like term $\eta(t) \in \mathbb{R}^n$ as follows

$$\eta \triangleq \dot{e} + \alpha_1 e + \alpha_2 e_f \tag{3.2}$$

where α_1, $\alpha_2 \in \mathbb{R}$ are positive constant filter gains, and $e_f(t) \in \mathbb{R}^n$ is an auxiliary filter variable having the following dynamic expression

$$\dot{e}_f = -\alpha_3 e_f + \alpha_2 e - k\eta \ , \ e_f(0) = 0_{m\times 1} \tag{3.3}$$

where $\alpha_3 \in \mathbb{R}$ is a positive constant filter gain and $k \in \mathbb{R}$ is a positive constant control gain.

3.1.1. Link Trajectory Tracking Controller Design

After taking the time derivative of (3.2), pre–multiplying both sides by $M(q)$, substituting (1.2), (3.2) and (3.3), adding and subtracting $Y_d\phi_r$ and $V_m(q,\dot{q})\eta$ to the right hand–side of the resulting equation and using the Property *1.3:* we can obtain the following expression

$$M(q)\dot{\eta} = -V_m(q,\dot{q})\eta + Y_d\phi_r - \alpha_2 kM(q)\eta + J_j^T(q)f_t(l) + \chi \tag{3.4}$$

where $\chi(t) \in \mathbb{R}^n$ is an auxiliary signal defined as

$$\begin{aligned}
\chi \triangleq\ & M(q)\ddot{q}_d + V_m(q,\dot{q}_d)\dot{q}_d + F_d\dot{q} + G(q) \\
& -Y_d\phi_r + \alpha_1 M(q)\left(\eta - \alpha_1 e - \alpha_2 e_f\right) \\
& +\alpha_2 M(q)\left(-\alpha_3 e_f + \alpha_2 e\right) \\
& -V_m(q,\eta)\left(\dot{q}_d + \alpha_1 e + \alpha_2 e_f\right) \\
& +V_m(q,\dot{q}_d)\left(\alpha_1 e + \alpha_2 e_f\right) \\
& +V_m(q,\dot{q}_d + \alpha_1 e + \alpha_2 e_f)\left(\alpha_1 e + \alpha_2 e_f\right).
\end{aligned} \tag{3.5}$$

Based on (1.5), (1.9), (1.11) and boundedness of the desired trajectory and its derivatives, it can be shown that

$$\|\chi\| \leq \rho(\|x\|)\|x\| \tag{3.6}$$

where $\rho(\cdot)$ is a positive scalar bounding function, and $x(t) \in \mathbb{R}^{3n}$ is defined as follows

$$x \triangleq \begin{bmatrix} e^T & e_f^T & \eta^T \end{bmatrix}^T. \tag{3.7}$$

Based on the manipulator model given in (1.2), it is necessary to show that tendon tension forces have to stabilize the robot dynamics. As a powerful tool to reach the lower level dynamics, a back–stepping procedure have been applied to design the desired tendon tension forces which can ensure the robot links track a desired trajectory.

To obtain this end, an auxiliary error term, denoted by $\eta_f(t) \in \mathbb{R}^m$ can be defined as follows

$$\eta_f \triangleq f_t(l) - f_d \tag{3.8}$$

where $f_d(t) \in \mathbb{R}^m$ is an auxiliary control input. After adding and subtracting $J_j^T(q) f_d(t)$ to the right–hand side of (3.4), we obtain the following

$$\begin{aligned} M(q)\dot{\eta} &= -V_m(q,\dot{q})\eta + Y_d\phi_r - \alpha_2 k M(q)\eta \\ &\quad + \chi + J_j^T(q)\eta_f + J_j^T(q) f_d. \end{aligned} \tag{3.9}$$

To stabilise the open–loop robot dynamics given in (3.9), and motivated by the subsequent stability analysis, we design the auxiliary control input $f_d(t)$ as

$$f_d = \left[J_j^T(q)\right]^+ \left\{-Y_d\hat{\phi}_r + kK_s e_f - K_s e\right\} \tag{3.10}$$

where $K_s \in \mathbb{R}$ is a positive scalar gain, $\left[J_j^T(q)\right]^+ \triangleq J_j(q)\left[J_j^T(q)J_j(q)\right]^{-1} \in \mathbb{R}^{m\times n}$ is the pseudo inverse of $J_j^T(q)$, and $\hat{\phi}_r(t) \in \mathbb{R}^p$ is the estimate of ϕ_r updated via the following

$$\dot{\hat{\phi}}_r = \Gamma Y_d^T \eta \tag{3.11}$$

where $\Gamma \in \mathbb{R}^{p\times p}$ is a positive definite, constant, diagonal adaptation gain matrix. From (3.11), it is clear that the right–hand side depends on $\eta(t)$ which is not available. Subsequently, we will provide an implementable (*i.e.*, link velocity independent) form. The control gain k is chosen as

$$k = \frac{1}{m_1}\left[1 + k_{n1}\rho^2(\|x\|)\right] \tag{3.12}$$

with k_{n1} being a positive constant nonlinear damping gain. Substituting (3.10) into (3.9) yields the closed–loop dynamics to be obtained as follows

$$\begin{aligned} M(q)\dot{\eta} &= -V_m(q,\dot{q})\eta + Y_d\tilde{\phi}_r - \alpha_2 k M(q)\eta \\ &\quad + \chi + J_j^T(q)\eta_f + kK_s e_f - K_s e \end{aligned} \tag{3.13}$$

where $\tilde{\phi}_r(t) \in \mathbb{R}^p$ is the parameter estimation error and defined as

$$\tilde{\phi}_r \triangleq \phi_r - \hat{\phi}_r. \tag{3.14}$$

3.1.2. Partial Stability Analysis for Manipulator Dynamics

In this subsection, the partial stability analysis for robot dynamics given by (1.2) have been presented. The results of this analysis will afterwards be used in the composite stability analysis of the overall closed–loop system.

A non–negative Lyapunov–like function, denoted by $V_r(\eta, e, e_f, \tilde{\phi}_r) \in \mathbb{R}$, can be defined as follows

$$V_r \triangleq \frac{1}{2}\eta^T M(q)\eta + \frac{1}{2}e^T K_s e + \frac{1}{2}e_f^T K_s e_f + \frac{1}{2}\tilde{\phi}_r^T \Gamma^{-1}\tilde{\phi}_r. \tag{3.15}$$

Taking the time derivative of (3.15), then substituting (3.2), (3.3), (3.11), (3.13), making use of (1.7) and then cancelling common terms, yields to

$$\dot{V}_r = \eta^T\left[-\alpha_2 k M(q)\eta + \chi\right] - \alpha_1 K_s \|e\|^2 - \alpha_3 K_s \left\|e_f\right\|^2 + \eta^T J_j^T(q)\eta_f. \tag{3.16}$$

Using the definition of the control gain k in (3.12), and the upper bounds of $M(q)$ in (1.5) and $\chi(t)$ in (3.6), one can reach the following upper bound for the right–hand side of (3.16)

$$\dot{V}_r \leq -\alpha_2 \|\eta\|^2 - \alpha_1 K_s \|e\|^2 - \alpha_3 K_s \left\|e_f\right\|^2 + \eta^T J_j^T(q)\eta_f + \frac{1}{4\alpha_2 k_{n1}}\|x\|^2 \tag{3.17}$$

where the following nonlinear damping argument [3] was also utilized

$$-\alpha_2 k_{n1}\rho^2(\|x\|)\|\eta\|^2 + \|\eta\|\rho(\|x\|)\|x\| \leq \frac{1}{4\alpha_2 k_{n1}}\|x\|^2. \tag{3.18}$$

Using the definition of $x(t)$ in (3.7), another upper bound can be reached as

$$\dot{V}_r \leq -\gamma\|x\|^2 + \eta^T J_j^T(q)\eta_f \tag{3.19}$$

where γ is some positive bounding constant satisfying $\min\{\alpha_2, \alpha_1 K_s, \alpha_3 K_s\} - \frac{1}{4\alpha_2 k_{n1}} > 0$. From (3.19) it can be seen that to ensure the stability and the convergence of the tracking error signal we need to ensure $\eta_f(t)$ converges to zero.

3.1.3. Actuator Side Velocity Filter Design

Since the stability of the robot manipulator requires the convergence of η_f as can be seen in (3.19), we continue the design process by investigating the dynamics of η_f. At this stage, the control problem becomes more complicated due to the unavailability of the actuator velocity information. To overcome the lack of the actuator velocity measurements, a set of linear filters have been developed as presented below. The actuator dynamics given in (1.3), can be reformed to obtain the following expression

$$\ddot{\theta} = J^{-1}\left[\tau_a - B\dot{\theta} - R_a f_t(l)\right]. \tag{3.20}$$

To write the actuator dynamics in a state space form, a new vector $r(t) \in \mathbb{R}^{2m}$ and auxiliary state variables $r_1(t), r_2(t) \in \mathbb{R}^m$ have been defined as follows

$$r = \begin{bmatrix} r_1 \\ r_2 \end{bmatrix} \triangleq \begin{bmatrix} \theta \\ \dot{r}_1 + J^{-1} B r_1 \end{bmatrix}. \tag{3.21}$$

Taking the time derivative of $r_2(t)$ and then substituting (3.20) and (3.21) yields to

$$\dot{r}_2 \triangleq J^{-1}\tau_a - J^{-1} R_a f_t(l). \tag{3.22}$$

The actuator dynamics can be written in the following state space form

$$\dot{r} = A_0 r + \begin{bmatrix} k_{f_1} I_m \\ k_{f_2} I_m \end{bmatrix} r_1 + A_1 \begin{bmatrix} r_1 \\ 0_{m\times 1} \end{bmatrix} + A_2 \begin{bmatrix} 0_{m\times 1} \\ f_t(l) \end{bmatrix} + \begin{bmatrix} 0_{m\times 1} \\ J^{-1}\tau_a \end{bmatrix} \tag{3.23}$$

where k_{f_1}, $k_{f_2} \in \mathbb{R}$ are constant positive filter gains, A_0, A_1, $A_2 \in \mathbb{R}^{m\times m}$ are Hurwitz matrices, and are defined as [41]

$$A_0 \triangleq \begin{bmatrix} -k_{f_1} I_m & I_m \\ -k_{f_2} I_m & 0_{m\times m} \end{bmatrix}, \tag{3.24}$$

$$A_1 \triangleq \begin{bmatrix} -J^{-1}B & 0_{m\times m} \\ 0_{m\times m} & -J^{-1}B \end{bmatrix}, \tag{3.25}$$

$$A_2 \triangleq \begin{bmatrix} -J^{-1}R_a & 0_{m\times m} \\ 0_{m\times m} & -J^{-1}R_a \end{bmatrix}. \tag{3.26}$$

Based on the above dynamics, the following linear, actuator velocity independent filters are designed [42], [43]

$$\dot{\varepsilon}_0 = A_0\varepsilon_0 + \begin{bmatrix} k_{f_1}I_m \\ k_{f_2}I_m \end{bmatrix} r_1; \qquad \varepsilon_0 \triangleq \begin{bmatrix} \varepsilon_{01}^T & \varepsilon_{02}^T \end{bmatrix}^T \tag{3.27}$$

$$\dot{\varepsilon}_1 = A_0\varepsilon_1 + \begin{bmatrix} r_1 \\ 0_{m\times 1} \end{bmatrix}; \qquad \varepsilon_1 = \begin{bmatrix} \varepsilon_{11}^T & \varepsilon_{12}^T \end{bmatrix}^T \tag{3.28}$$

$$\dot{\varepsilon}_2 = A_0\varepsilon_2 + \begin{bmatrix} 0 \\ f_t(l) \end{bmatrix}; \qquad \varepsilon_2 = \begin{bmatrix} \varepsilon_{21}^T & \varepsilon_{22}^T \end{bmatrix}^T \tag{3.29}$$

$$\dot{\upsilon}_0 = A_0\upsilon_0 + \begin{bmatrix} 0_{m\times 1} \\ \tau_a \end{bmatrix}; \qquad \upsilon_0 = \begin{bmatrix} \upsilon_{01}^T & \upsilon_{02}^T \end{bmatrix}^T \tag{3.30}$$

where $\varepsilon_{01}(t)$, $\varepsilon_{02}(t)$, $\varepsilon_{11}(t)$, $\varepsilon_{12}(t)$, $\varepsilon_{21}(t)$, $\varepsilon_{22}(t)$, $\upsilon_{01}(t)$, $\upsilon_{02}(t) \in \mathbb{R}^m$ and thus $\varepsilon_0(t)$, $\varepsilon_1(t)$, $\varepsilon_2(t)$, $\upsilon_0(t) \in \mathbb{R}^{2m}$. Based on the structure of the filters, state estimator for $r(t)$, denoted by $\hat{r}(t) \in \mathbb{R}^{2m}$, is designed in the following manner

$$\hat{r} = \varepsilon_0 + A_1\varepsilon_1 + A_2\varepsilon_2 + \begin{bmatrix} J^{-1} & 0_{mxm} \\ 0_{mxm} & J^{-1} \end{bmatrix} \upsilon_0. \tag{3.31}$$

The state estimation error, denoted by $\tilde{r}(t) \in \mathbb{R}^{2m}$, is defined as follows

$$\tilde{r} = \begin{bmatrix} \tilde{r}_1 \\ \tilde{r}_2 \end{bmatrix} \triangleq r - \hat{r}. \tag{3.32}$$

where substituting (3.31) yields

$$\begin{bmatrix} \tilde{r}_1 \\ \tilde{r}_2 \end{bmatrix} = \begin{bmatrix} r_1 - \varepsilon_{01} + J^{-1}\left(B\varepsilon_{11} + R_a\varepsilon_{21} - \upsilon_{01}\right) \\ r_2 - \varepsilon_{02} + J^{-1}\left(B\varepsilon_{12} + R_a\varepsilon_{22} - \upsilon_{02}\right) \end{bmatrix}. \tag{3.33}$$

Now, $\dot{\theta}(t)$ can be obtained by computing $r_2(t)$ from (3.33) and substituting in (3.21) as

$$\dot{\theta} = \tilde{r}_2 + \varepsilon_{02} - J^{-1}B(\varepsilon_{12} + \theta) - J^{-1}R_a\varepsilon_{22} + J^{-1}\upsilon_{02}. \tag{3.34}$$

To analyse the stability of the filter, one can take the time derivative of (3.32) and obtain the following estimation error dynamics

$$\dot{\tilde{r}} = \dot{r} - \dot{\varepsilon}_0 - A_1\dot{\varepsilon}_1 - A_2\dot{\varepsilon}_2 + \begin{bmatrix} J^{-1} & 0_{mxm} \\ 0_{mxm} & J^{-1} \end{bmatrix} \dot{\upsilon}_0 \tag{3.35}$$

where the time derivative of (3.31) was utilized. Substituting (3.23) and the set of linear filters in (3.27) into (3.35), it is easy to obtain

$$\dot{\tilde{r}} = A_0\tilde{r}. \tag{3.36}$$

3.1.4. Partial Stability Analysis for Velocity Filter

To investigate the stability analysis for the actuator velocity error generating filters, a non–negative scalar function, denoted by $V_f(\tilde{r}) \in \mathbb{R}$, can be defined as follows

$$V_f \triangleq \tilde{r}^T P_0 \tilde{r} \tag{3.37}$$

where $P_0 \in R^{2m\times 2m}$ is a positive definite, symmetric, constant matrix chosen to satisfy

$$A_0^T P_0 + P_0 A_0 = -I_{2m}. \tag{3.38}$$

After taking the time derivative of (3.37), as follows

$$\dot{V}_f = \dot{\tilde{r}}^T P_0 \tilde{r} + \tilde{r}^T P_0 \dot{\tilde{r}} \tag{3.39}$$

and substituting (3.36) and (3.38) yields

$$\dot{V}_f = -\tilde{r}^T\tilde{r} = -\|\tilde{r}_1\|^2 - \|\tilde{r}_2\|^2. \tag{3.40}$$

3.1.5. Actuator Torque Input Design

Owing to the exponential stable structure of the linear filter design, the dynamics of auxiliary error signal $\eta_f(t)$ can be introduced and the stability of auxiliary error dynamics can be investigated by taking the time derivative of (3.8) which yields to

$$\begin{aligned}\dot{\eta}_f &= \frac{\partial f_t(l)}{\partial l}\left[J_j(q)\dot{q}+R_a\dot{\theta}\right] \\ &\quad -\left[J_j^T(q)\right]^+\left\{-\dot{Y}_d\hat{\phi}_r-Y_d\dot{\hat{\phi}}_r+kK_s\dot{e}_f-K_s\dot{e}\right\} \\ &\quad -\frac{d}{dt}\left[J_j^T(q)\right]^+\left\{-Y_d\hat{\phi}_r+kK_se_f-K_se\right\}.\end{aligned} \tag{3.41}$$

In the last line of the above expression, from the time derivative of the pseudo inverse of the Jacobian matrix, the time derivative of joint position vector and thus the auxiliary error signal $\eta(t)$ shows up. In view of this, the last line can be rewritten as

$$\frac{d}{dt}\left\{\left[J_j^T(q)\right]^+\right\}\left\{-Y_d\hat{\phi}_r+kK_se_f-K_se\right\}=\Psi_1(e,e_f,t)+\Psi_2(e,e_f,t)\eta \tag{3.42}$$

where $\Psi_1(e,e_f,t)\in\mathbb{R}^m$ and $\Psi_2(e,e_f,t)\in\mathbb{R}^{m\times m}$ are known and available functions. After pre–multiplying both sides of (3.41) with J and then making use of (3.2), (3.3), (3.11), (3.34), (3.42) to obtain

$$J\dot{\eta}_f=W_1\phi_1-J\Omega_1\eta+J\frac{\partial f_t(l)}{\partial l}R_a\tilde{r}_2+\frac{\partial f_t(l)}{\partial l}R_a\left(\upsilon_{02}-R_a\varepsilon_{22}\right) \tag{3.43}$$

where $W_1(e,e_f,l,\varepsilon_{02},\varepsilon_{12},\hat{\phi},t)\in\mathbb{R}^{m\times p_1}$ is a known and available regressor matrix and $\phi_1\in\mathbb{R}^{p_1}$ is an unknown constant parameter vector, and both are obtained from

$$\begin{aligned}W_1\phi_1 &= J\frac{\partial f_t(l)}{\partial l}\left\{J_j(q)\left(\dot{q}_d+\alpha_1e+\alpha_2e_f\right)+R_a\left(\varepsilon_{02}-J^{-1}B\left(\varepsilon_{12}+\theta\right)\right)\right\} \\ &\quad -J\left[J_j^T(q)\right]^+\left\{-\dot{Y}_d\hat{\phi}+kK_s\left(-\alpha_3e_f+\alpha_2e\right)-K_s\left(-\alpha_1e-\alpha_2e_f\right)\right\}-J\Psi_1.\end{aligned} \tag{3.44}$$

In (3.43), the auxiliary matrix $\Omega_1(e,e_f,t)\in\mathbb{R}^{m\times m}$, which includes known and measurable terms, is defined as

$$\Omega_1 \triangleq \frac{\partial f_t(l)}{\partial l} J_j(q) - \left[J_j^T(q)\right]^+ \left(Y_d \Gamma Y_d^T + k^2 K_s + K_s\right) + \Psi_2. \tag{3.45}$$

Since the derivative of υ_{02} which can be seen in (3.27) includes the actuator torque input signal, the second backstepping procedure can be constructed on υ_{02} by defining a new auxiliary error signal, denoted by $\eta_L(t) \in \mathbb{R}^m$, as

$$\eta_L(t) \triangleq \upsilon_{02} - u_L \tag{3.46}$$

where $u_L(t) \in \mathbb{R}^m$ is an auxiliary input like term. Utilizing (3.46), and adding and subtracting $\frac{\partial f_t(l)}{\partial l} R_a u_L(t)$ to the right–hand side of (3.43) results in

$$J\dot{\eta}_f = W_1 \phi_1 + J\Omega_1 \eta + J\frac{\partial f_t(l)}{\partial l} R_a \tilde{r}_2 + \frac{\partial f_t(l)}{\partial l} R_a \left(u_L + \eta_L - R_a \varepsilon_{22}\right). \tag{3.47}$$

From the subsequent stability analysis, the auxiliary input $u_L(t)$ can be designed in the following manner

$$u_L = \Lambda \left(-K_f \eta_f - W_1 \hat{\phi}_1 + \frac{\partial f_t(l)}{\partial l} R_a^2 \varepsilon_{22} \right) \tag{3.48}$$

where the auxiliary variable $\Lambda(l) \in \mathbb{R}^{m \times m}$ is defined as

$$\Lambda \triangleq \left[\frac{\partial f_t(l)}{\partial l} R_a \right]^{-1} \tag{3.49}$$

and $K_f \in \mathbb{R}$ is a control gain designed as

$$K_f = k_f + k_{n2} \bar{J}^2 \left\| \Omega_1 \right\|_{i\infty}^2 + k_{n3} \bar{J}^2 \left\| \Lambda \right\|_{i\infty}^2 + k_{n4} \left\| J_j^T(q) \right\|_{i\infty}^2 \tag{3.50}$$

where $k_f \in \mathbb{R}$ is a constant control gain, k_{n2}, k_{n3}, $k_{n4} \in \mathbb{R}$ are constant scalar nonlinear damping gains, and $\bar{J}$ was introduced in (1.12). In (3.48), $\hat{\phi}_1(t) \in \mathbb{R}^{p_1}$ is the estimate of the unknown parameter vector ϕ_1, and is updated according to

$$\dot{\hat{\phi}}_1 = \Gamma_1 W_1^T \eta_f \tag{3.51}$$

with $\Gamma_1 \in \mathbb{R}^{p_1 \times p_1}$ being a positive definite, constant, diagonal, adaptation gain matrix. After substituting (3.48) into (3.47), closed–loop dynamics for $\eta_f(t)$ can be obtained as

$$J\dot{\eta}_f = -K_f \eta_f + W_1 \tilde{\phi}_1 + J\Omega_1 \eta + J\frac{\partial f_t(l)}{\partial l} R_a \tilde{r}_2 + \frac{\partial f_t(l)}{\partial l} R_a \eta_L \tag{3.52}$$

where $\tilde{\phi}_1(t) \in \mathbb{R}^{p_1}$ is the parameter estimation error vector and is defined as

$$\tilde{\phi}_1 \triangleq \phi_1 - \hat{\phi}_1. \tag{3.53}$$

In this stage controller design requires investigating the dynamics of $\eta_L(t)$. Taking the time derivative of (3.46), and then substitute (1.4), (3.2), (3.11), (3.27), (3.34), (3.43), and after some straightforward mathematical manipulations yields to

$$\dot{\eta}_L = \Omega_2 + W_2 \phi_2 + \Omega_3 \eta + \Omega_4 \tilde{r}_2 + \tau_a \tag{3.54}$$

where $W_2(\cdot) \in \mathbb{R}^{m \times p_2}$ is an available regressor matrix, $\phi_2 \in \mathbb{R}^{p_2}$ includes unknown system parameters, $\Omega_2(\cdot) \in \mathbb{R}^m$, $\Omega_3(\cdot) \in \mathbb{R}^{m \times n}$, $\Omega_4(\cdot) \in \mathbb{R}^{m \times m}$ are auxiliary terms that include known and available signals. According to the subsequent stability analysis, the actuator control input τ_a can be designed as follows

$$\tau_a = -K_L \eta_L - \Omega_2 - W_2 \hat{\phi}_2 - \left[\frac{\partial f_t(l)}{\partial l} R_a\right]^T \eta_f \tag{3.55}$$

with $K_L \in \mathbb{R}$ being a control gain designed as

$$K_L = k_L + k_{n5} \|\Omega_3\|_{i\infty}^2 + k_{n6} \|\Omega_4\|_{i\infty}^2 \tag{3.56}$$

where $k_L \in \mathbb{R}$ is a constant control gain, k_{n5}, $k_{n6} \in \mathbb{R}$ are constant scalar nonlinear damping gains, and $\hat{\phi}_2(t) \in \mathbb{R}^{p_2}$ is the estimate of the uncertain parameter vector ϕ_2 which is designed to be updated as follows

$$\dot{\hat{\phi}}_2 = \Gamma_2 W_2^T \eta_L \tag{3.57}$$

with $\Gamma_2 \in \mathbb{R}^{p_2 \times p_2}$ being a positive definite, constant, diagonal, adaptation gain matrix. After substituting (3.55) into (3.54), the closed–loop dynamics for $\eta_L(t)$ can be obtained as

$$\dot{\eta}_L = -K_L \eta_L + W_2 \tilde{\phi}_2 + \Omega_3 \eta + \Omega_4 \tilde{r}_2 - \left[\frac{\partial f_t(l)}{\partial l} R_a \right]^T \eta_f \tag{3.58}$$

where $\tilde{\phi}_2(t) \in \mathbb{R}^{p_2}$ is the parameter estimation error vector and defined as

$$\tilde{\phi}_2 \triangleq \phi_2 - \hat{\phi}_2. \tag{3.59}$$

3.1.6. Partial Stability Analysis for Auxiliary Error Dynamics

As the third step of the stability analysis, a non–negative scalar function, denoted by $V_a\left(\eta_f, \eta_L, \tilde{\phi}_1, \tilde{\phi}_2\right) \in \mathbb{R}$ can be defined as

$$V_a \triangleq \frac{1}{2}\eta_f^T J \eta_f + \frac{1}{2}\eta_L^T \eta_L + \frac{1}{2}\tilde{\phi}_1^T \Gamma_1^{-1} \tilde{\phi}_1 + \frac{1}{2}\tilde{\phi}_2^T \Gamma_2^{-1} \tilde{\phi}_2. \tag{3.60}$$

Taking the time derivative of (3.60), substituting (3.51), (3.52), (3.57), (3.58), using the control gains K_f in (3.50) and K_L in (3.56), an upper bound for $\dot{V}_a(t)$ can be obtained as

$$\begin{aligned} \dot{V}_a \leq & -k_f \left\|\eta_f\right\|^2 - k_L \left\|\eta_L\right\|^2 + \frac{\|\eta\|^2}{4k_{n2}} + \frac{\|\tilde{r}_2\|^2}{4k_{n3}} \\ & -k_{n4} \left\|J_j^T(q)\right\|_{i\infty}^2 \left\|\eta_f\right\|^2 + \frac{\|\eta\|^2}{4k_{n5}} + \frac{\|\tilde{r}_2\|^2}{4k_{n6}}. \end{aligned} \tag{3.61}$$

3.2. Main Result and Overal Stability analysis

In this section, the stability of the closed–loop system will be investigated by utilizing Lyapunov–based arguments.

Theorem 3.1: For the tendon driven robot manipulator system given by dynamic equations (1.2)*,* (1.3) *and* (1.4)*, link position tracking adaptive controller given by* (3.10)*,*

(3.48), (3.55), *and adaptation laws given by* (3.11), (3.51), (3.57), *in conjunction with actuator velocity error generating filter given by* (3.27) *and* (3.31), *semi–global asymptotic link position tracking is guaranteed in the sense that*

$$\|e(t)\| \to 0 \text{ as } t \to \infty \tag{3.62}$$

provided the nonlinear damping gains are selected to satisfy the following conditions

$$\min\left\{\gamma, 1, k_f, k_L\right\} > \sum_{i=2}^{6} \frac{1}{4k_{ni}} \tag{3.63}$$

$$k_{n1} > \frac{\lambda_2}{\lambda_1}\|s(0)\|^2 + 1 \tag{3.64}$$

where $\gamma \in \mathbb{R}$ *is some positive bounding constant satisfying* $\min\{\alpha_2, \alpha_1 K_s, \alpha_3 K_s\} - \frac{1}{4\alpha_2 k_{n1}} > \gamma > 0$, *and* $s(t) \in \mathbb{R}^{(3n+p)\times 1}$, λ_1, $\lambda_2 \in \mathbb{R}$ *are defined as follows*

$$s \triangleq \begin{bmatrix} e^T & e_f^T & \eta^T & \tilde{\phi}_r^T \end{bmatrix}^T \tag{3.65}$$

$$\lambda_1 \triangleq \frac{1}{2}\min\left\{m_1, \lambda_{\min}(K_s), \lambda_{\min}\left(\Gamma^{-1}\right)\right\} \tag{3.66}$$

$$\lambda_2 \triangleq \frac{1}{2}\max\left\{m_2, \lambda_{\max}(K_s), \lambda_{\max}\left(\Gamma^{-1}\right)\right\} \tag{3.67}$$

where $\lambda_{\min}(\cdot)$ *denotes the minimum eigenvalue of a matrix.*

Proof 3.1: In order to investigate the closed–loop system stability, a non–negative scalar function, denoted by $V(t) \in \mathbb{R}$, *can be constructed by summing* (3.15), (3.37), (3.60), *as*

$$V \triangleq V_r + V_f + V_a. \tag{3.68}$$

After taking the time derivative of (3.68), *substituting* (3.19), (3.40) *and* (3.61), *and then simplifying the resulting expression, the following expression will be obtained*

$$\begin{aligned}\dot{V} \leq & -\gamma\|x\|^2 - \|\tilde{r}_1\|^2 - \|\tilde{r}_2\|^2 - k_f\left\|\eta_f\right\|^2 - k_L\|\eta_L\|^2 \\ & + \frac{\|\eta\|^2}{4k_{n2}} + \frac{\|\tilde{r}_2\|^2}{4k_{n3}} + \frac{\|\eta\|^2}{4k_{n5}} + \frac{\|\tilde{r}_2\|^2}{4k_{n6}} \\ & + \eta^T J_j^T(q)\eta_f - k_{n4}\left\|J_j^T(q)\right\|_{i\infty}^2\left\|\eta_f\right\|^2.\end{aligned} \tag{3.69}$$

Applying a similar nonlinear damping argument to the one in (3.18) *to the last line of* (3.69)*, the upper bound for* $\dot{V}(t)$ *can be written as*

$$\begin{aligned}\dot{V} \leq & -\gamma\|x\|^2 - \|\tilde{r}_1\|^2 - \|\tilde{r}_2\|^2 - k_f\left\|\eta_f\right\|^2 - k_L\|\eta_L\|^2 \\ & + \frac{\|\eta\|^2}{4k_{n2}} + \frac{\|\tilde{r}_2\|^2}{4k_{n3}} + \frac{\|\eta\|^2}{4k_{n4}} + \frac{\|\tilde{r}_2\|^2}{4k_{n5}} + \frac{\|\tilde{r}_2\|^2}{4k_{n6}}.\end{aligned} \tag{3.70}$$

The expression given in (3.70) *can further be upper bounded as follows*

$$\dot{V} \leq -\left(\min\left\{\gamma, 1, k_f, k_L\right\} - \sum_{i=2}^{6}\frac{1}{4k_{ni}}\right)\|z\|^2 \tag{3.71}$$

where $z(t) \in R^{(3n+4m)\times 1}$ *is defined as follows*

$$z \triangleq \begin{bmatrix} x^T & \tilde{r}_1^T & \tilde{r}_2^T & \eta_f^T & \eta_L^T \end{bmatrix}^T. \tag{3.72}$$

Provided the gain condition in (3.63) *is satisfied, the upper bound for* $\dot{V}(t)$ *in* (3.71) *can be reformulated as*

$$\dot{V} \leq -\delta\|z\|^2 \tag{3.73}$$

for some positive bounding constant $\delta \in \mathbb{R}$*. Standard signal chasing arguments can now be utilized to demonstrate boundedness of all the signals under the closed–loop operation. Barbalat's Lemma [42] can then be utilized to prove that* $z(t)$ *is asymptotically stable, and thus it is easy to see that the tracking objective is met in the sense that* (3.62) *is satisfied.* ■

3.3. Eliminating Actuator Side Measurements

Need for position measurements of the actuators requires a high resolution position sensor for each actuator. Since tendon driven robotic systems are generally over-actuated systems, actuator side position measurements increases the sensor costs dramatically. If model parameters of the actuator dynamics given in (1.3) exactly known, the proposed adaptive controller can be modified with the help of an actuator side state observer in order to eliminate the position measurements of the actuators. The resultant controller–observer couple can still deal with uncertainties in the link dynamics while only requires the link position measurements and tendon tension measurements.

3.3.1. Design of Model Dependent State Observer

The actuator dynamics given in (3.20) can be reformed to have a useful state space form by defining state variables $x_1(t) = \theta$, $x_2(t) = \dot{\theta} \in \mathbb{R}^m$ as follows

$$\begin{bmatrix} \dot{x}_1 \\ \dot{x}_2 \end{bmatrix} = \begin{bmatrix} x_2 \\ J^{-1}\tau_a - J^{-1}Bx_2 - J^{-1}R_a f_t(l) \end{bmatrix}. \tag{3.74}$$

In order to quantify the observation performance, the velocity observation error vector $\tilde{x}_2 \in \mathbb{R}^m$ have been defined as follows

$$\tilde{x}_2 \triangleq x_2 - \hat{x}_2 \tag{3.75}$$

where $\hat{x}_2$ is the observed velocity of the actuators. Similar to the controller formulation presented in the previous sections, the convergence of the auxiliary error signal η_f to the zero need to be proved, as well. To investigate the dynamics of η_f, one can take the time derivative of (3.8), make use of the tension dynamics given in (1.4) and add and subtract $\frac{\partial f_t(l)}{\partial l} R_a \hat{x}_2$ to obtain

$$\dot{\eta}_f = \Omega_0 + \Omega_1 \eta + \frac{\partial f_t(l)}{\partial l} R_a \tilde{x}_2 + \frac{\partial f_t(l)}{\partial l} R_a \hat{x}_2 \tag{3.76}$$

where $\Omega_0 \in \mathbb{R}^m$ and $\Omega_1 \in \mathbb{R}^{m \times n}$ include known and measurable terms and can be calculated as follows

$$\frac{\partial f_t(l)}{\partial l} J_j(q)\dot{q} - \frac{d}{dt} f_d = \Omega_0 + \Omega_1 \eta. \tag{3.77}$$

Since the observed velocity of the actuators can not be designed directly, the desired version the observed velocity can be designed and inserted to the controller development by the help of backstepping procedure. To apply the backstepping on $\hat{x}_2$, a new auxiliary input tracking error vector $\eta_b(t) \in \mathbb{R}^m$ can be designed as follows

$$\eta_b(t) \triangleq \hat{x}_2 - x_{2d}. \tag{3.78}$$

where $x_{2d}(t) \in \mathbb{R}^m$ is the desired velocity observation vector which will be designed as an auxiliary input term. To this end, adding and subtracting $\frac{\partial f_t(l)}{\partial l} R_a x_{2d}$ to (3.76) yields to

$$\dot{\eta}_f = \Omega_0 + \Omega_1 \eta + \frac{\partial f_t(l)}{\partial l} R_a \tilde{x}_2 + \frac{\partial f_t(l)}{\partial l} R_a \eta_b + \frac{\partial f_t(l)}{\partial l} R_a x_{2d}. \tag{3.79}$$

According to the subsequent stability analysis, the auxiliary input x_{2d} can be designed in the following manner

$$x_{2d} = \Lambda\left(-K_f \eta_f - \Omega_0\right) \tag{3.80}$$

where the auxiliary variable $\Lambda(l) \in \mathbb{R}^{m\times m}$ was defined in (3.49) and $K_f \in \mathbb{R}^{m\times m}$ is the controller gain matrix which is defined as

$$K_f \triangleq k_f + k_{n2} \left\|\Omega_1\right\|_{i\infty}^2 + k_{n3} \lambda_{\max}\left(J_j^T(q)\right)^2 \tag{3.81}$$

where $k_f \in \mathbb{R}^{m\times m}$is a constant, diagonal control gain matrix, $k_{n2}, k_{n3} \in \mathbb{R}^1$ are constant scalar nonlinear damping gains. After substituting (3.80) in to the (3.79) closed loop dynamics for η_f can be obtained as

$$\dot{\eta}_f = -K_f \eta_f + \Omega_1 \eta + \frac{\partial f_t(l)}{\partial l} R_a \tilde{x}_2 + \frac{\partial f_t(l)}{\partial l} R_a \eta_b. \tag{3.82}$$

Before going further in the design process, the state observer design for $\hat{x}_2$ need to be presented. According to actuator dynamics given in (3.74) and to the subsequent stability analysis actuator side state observer can be designed as follows

$$\dot{\hat{x}}_2 = J^{-1}\left(\tau_a - B\hat{x}_2 - R_a f_t(l)\right) + \frac{\partial f_t(l)}{\partial l} R_a \eta_f + \Omega_7 \eta_b. \tag{3.83}$$

To prove the convergence of the velocity observer to the zero, the state observer error term can be defined defined and obtained as follows

$$\dot{\tilde{x}}_2 \triangleq \dot{x}_2 - \dot{\hat{x}}_2 = -J^{-1} B\tilde{x}_2 - \frac{\partial f_t(l)}{\partial l} R_a \eta_f - \Omega_7 \eta_b. \tag{3.84}$$

In this step, the control design requires the convergence of the auxiliary error signal η_b to the zero. To investigate the dynamics of η_b one can take the time derivative of (3.78), take the other necessary derivatives in the resulting equation and than substitute (3.83) (3.76), (1.4), (3.2) and do some more mathematical manipulations to obtain

$$\dot{\eta}_b = \Omega_5 + \Omega_6 \eta + \Omega_7 x_2 + J^{-1}\tau_a \tag{3.85}$$

where $\Omega_5 \in \mathbb{R}^m$, $\Omega_7 \in \mathbb{R}^{m\times m}$ and $\Omega_6 \in \mathbb{R}^{m\times n}$ include the known terms. According to the subsequent stability analysis, the actuator control input τ_a can be designed as follows

$$\tau_a = J\left\{-K_b\eta_b - \Omega_5 - \Omega_7\hat{x}_2 - \frac{\partial f_t(l)}{\partial l} R_a \eta_f\right\} \tag{3.86}$$

with

$$K_b = k_b + k_{n4}\left\|\Omega_6\right\|_{i\infty}^2 \tag{3.87}$$

where $k_b \in \mathbb{R}^{m\times m}$is a constant, diagonal control gain matrix, $k_{n4} \in \mathbb{R}^1$ is constant scalar nonlinear damping gain. After substituting (3.86) in to the (3.85) closed loop dynamics for η_b can be obtained as

$$\dot{\eta}_b = -K_b\eta_b + \Omega_6\eta + \Omega_7\tilde{x}_2 - \frac{\partial f_t(l)}{\partial l} R_a \eta_f. \tag{3.88}$$

3.3.2. Stability Result of the Extension

Stability of the new observer side of the closed loop signals will be investigated with the help of a non–negative scalar function which can be defined as

$$V_o = \frac{1}{2}\eta_f^T \eta_f + \frac{1}{2}\eta_b^T \eta_b + \frac{1}{2}\tilde{x}_2^T \tilde{x}_2. \tag{3.89}$$

Taking the time derivative of (3.89), substituting (3.82), (3.88), (3.84), using definitions of gains K_f and K_b given in (3.81) and (3.87) and applying the other similar steps as applied to $\dot{V}_r$, the upper bound for $\dot{V}_o$ can be arranged as follows

$$\begin{aligned} \dot{V}_o \quad \leq \quad & -k_f \left\|\eta_f\right\|^2 - k_b \left\|\eta_b\right\|^2 - J^{-1}B \left\|\tilde{x}_2\right\|^2 + \frac{\left\|\eta\right\|^2}{4k_{n2}} \\ & + \frac{\left\|\tilde{x}_2\right\|^2}{4k_{n3}} - k_{n4}\lambda_{\max}\left(J_j^T(q)\right)^2 \left\|\eta_f\right\|^2 asdf \frac{\left\|\eta\right\|^2}{4k_{n4}}. \end{aligned} \tag{3.90}$$

To investigate the overall closed loop system stability, a non–negative scalar function can be constructed by summation of (3.15) and (3.89) as follows

$$V_E = V_r + V_o. \tag{3.91}$$

After taking the time derivative of (3.91) and substituting (3.19) and (3.90) and than simplifying the resulting expression the following inequality can be obtained

$$\begin{aligned} \dot{V}_E \quad \leq \quad & -\gamma \left\|x\right\|^2 - k_f \left\|\eta_f\right\|^2 - k_b \left\|\eta_b\right\|^2 - J^{-1}B \left\|\tilde{x}_2\right\|^2 \\ & + \frac{\left\|\eta\right\|^2}{4k_{n2}} + \frac{\left\|\eta\right\|^2}{4k_{n4}} + \eta^T J_j^T(q)\eta_f - k_{n4}\lambda_{\max}\left(J_j^T(q)\right)^2 \left\|\eta_f\right\|^2. \end{aligned} \tag{3.92}$$

Applying the nonlinear damping tool given in (3.18) to the last line of (3.92), the upper bound for $\dot{V}_E$ can further be written in the following manner

$$\dot{V}_E \leq -\gamma \left\|x\right\|^2 - J^{-1}B \left\|\tilde{x}_2\right\|^2 - k_f \left\|\eta_f\right\|^2 - k_b \left\|\eta_b\right\|^2 + \frac{\left\|\eta\right\|^2}{4k_{n2}} + \frac{\left\|\eta\right\|^2}{4k_{n3}}. \tag{3.93}$$

The expression given in (3.93) can be further upper bounded as follows

$$\dot{V}_E \leq -\left(\min\left\{\gamma, 1, k_f, k_b\right\} - \sum_{i=2}^{6} \frac{1}{4k_{ni}}\right) \left\|z_E\right\|^2 \tag{3.94}$$

where $z(t) \in R^{3n+4m}$ is defined as follows

$$z_E \triangleq \left[\begin{array}{cccc} x^T & \tilde{x}_2^T & \eta_f^T & \eta_b^T \end{array} \right]^T. \tag{3.95}$$

If the gain condition given below

$$\min\left\{\gamma, 1, k_f, k_b\right\} > \sum_{i=2}^{6} \frac{1}{4k_{ni}} \tag{3.96}$$

is satisfied then the upper bound for $\dot{V}_E$ given in (3.94) can be reformulated as a negative semi definite function as

$$\dot{V}_E \leq -\delta \left\|z\right\|^2 \tag{3.97}$$

where δ is a some positive bounding constant. Based on the definition of z_E in (3.95) and by using standard signal chasing arguments it can be shown that

$$\left\|e(t)\right\| \to 0 \text{ as } t \to \infty. \tag{3.98}$$

More over all signals in z_E converges to zero and all signals in the closed loop system are bounded.

3.4. Remarks

In this chapter, two different partial state feedback adaptive controller formulations for tendon driven robotic manipulators subject to parametric uncertainty in the system dynamics have been presented. In the first controller formulation; the proposed controller ensured the link position tracking error signal is forced to go to zero despite the lack of exact knowledge of the system parameters and lack of velocity measurements of both links and actuators. In the second formulation, actuator side position measurements are also eliminated via a model based state observer in case of having exact knowledge of the actuator parameters. Stability of the closed–loop systems and boundedness of system states are proven via Lyapunov based arguments for both of the controllers.

Note that, although the control input in (3.10) depends on $e_f(t)$ (which obviously requires link velocity measurements), we can construct an implementable (*i.e.*, link velocity independent) form of the auxiliary control input $f_d(t)$. To construct the link velocity independent version of the filter given by (3.3), we insert (3.2) into (3.3) to reach the following expression

$$\dot{e}_f = -k\dot{e} + (\alpha_2 - k\alpha_1)\, e - (\alpha_3 + k\alpha_2)\, e_f. \tag{3.99}$$

We now define, an auxiliary signal, denoted by $w(t) \in \mathbb{R}^n$, as

$$w \triangleq e_f + ke \tag{3.100}$$

whose time derivative can be obtained as

$$\dot{w} = (\alpha_2 - k\alpha_1)\, e - (\alpha_3 + k\alpha_2)\,(w - ke) \tag{3.101}$$

where (3.99) and (3.100) were utilized. From (3.101), it is clear that $w(t)$ can be obtained from link position measurements only, and thus from (3.100), one can obtain an implementable form of $e_f(t)$. After this, the implementable form of (3.11) is given as

$$\begin{aligned} \hat{\phi}_r \;=\; & \Gamma \int_0^t Y_d^T(\sigma)\left(\alpha_1 e(\sigma) + \alpha_2 e_f(\sigma)\right) d\sigma \\ & + \Gamma Y_d^T(t)\, e(t) - \Gamma Y_d^T(0)\, e(0) \\ & + \Gamma \int_0^t \dot{Y}_d^T(\sigma)\, e(\sigma)\, d\sigma. \end{aligned} \tag{3.102}$$

The results given in this chapter are presented in 2014 IEEE Conference on Control Applications (CCA), Antibes, France[44] and 2015 54th IEEE Conference on Decision and Control (CDC), Osaka, Japan[45].

4. NUMERICAL SIMULATIONS

To verify the performance of the three different proposed controllers (i.e. FSFB, PSFB, extended PSFB), some numerical simulations have been performed on a two link robot manipulator driven by six tendons as shown in Figure 4.1. MATLAB Simulink environment have been used to perform the simulations. In this chapter, simulation studies will be presented to compare the results of the simulations properly.

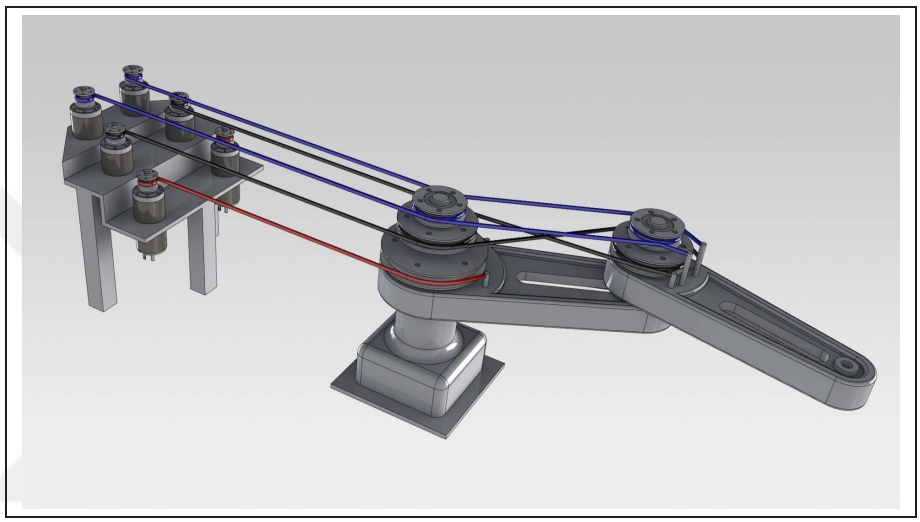

Figure 4.1: Overall view of two link planar robot driven by six tendons.

The dynamical parameters of the robot used in our simulation studies has the following model matrices

$$M = \begin{bmatrix} p_1 + 2p_3\cos(q_2) & p_2 + p_3\cos(q_2) \\ p_2 + p_3\cos(q_2) & p_2 \end{bmatrix} \tag{4.1}$$

$$V_m = \begin{bmatrix} -p_3\sin(q_2)\dot{q}_2 & -p_3\sin(q_2)(\dot{q}_1 + \dot{q}_2) \\ p_3\sin(q_2)\dot{q}_1 & 0 \end{bmatrix} \tag{4.2}$$

$$F_d = \begin{bmatrix} f_{d1} & 0 \\ 0 & f_{d2} \end{bmatrix} \tag{4.3}$$

and the Jacobian matrix is defined as follows [13],

$$J_j = s_1 \begin{bmatrix} 1 & -1 & 1 & -1 & 1 & -1 \\ 0 & 0 & -1 & 1 & 1 & -1 \end{bmatrix}^T. \tag{4.4}$$

The linearly parametrized version of robot dynamics given in (1.2) has been used in controller formulation and stability analysis. This linearisation can be performed in the following manner.

$$Y\phi_r = \begin{bmatrix} \ddot{q}_1 & \ddot{q}_2 & Y_{13} & \dot{q}_1 & 0 \\ 0 & \ddot{q}_1+\ddot{q}_2 & Y_{23} & 0 & \dot{q}_2 \end{bmatrix} \begin{bmatrix} p_1 \\ p_2 \\ p_3 \\ f_{d1} \\ f_{d2} \end{bmatrix} \tag{4.5}$$

where

$$Y_{13} = (2\ddot{q}_1+\ddot{q}_2)\cos(q_2) - \dot{q}_2\sin(q_2)(2\dot{q}_1+\dot{q}_2) \tag{4.6}$$

$$Y_{23} = \ddot{q}_1 cos(q_2) + \dot{q}_1\dot{q}_1\sin(q_2) \tag{4.7}$$

Tendon tensile forces can be calculated as a function of tendon expansions in the following manner [13],

$$f_{t,i}(l_i) = \begin{cases} s_2 l_i + s_3 l_i^3 & l_i \geqslant 0 \\ 0 & l_i < 0 \end{cases} \tag{4.8}$$

for $i = 1,..,6$ where l_i are the tendon expansions and $f_{t,i}(l_i)$ are the members of the vector of the tendon tensile forces which is defined as follows

$$f_t(l) = \begin{bmatrix} f_{t,1}(l_1) & f_{t,2}(l_2) & f_{t,3}(l_3) & f_{t,4}(l_4) & f_{t,5}(l_5) & f_{t,6}(l_6) \end{bmatrix}^T. \tag{4.9}$$

The robot parameter values can be seen in Table 4.1 for the simulations. It should be noted that most of the system and tendon parameters used in our simulation studies are taken from [13]. The actuator part of the tendon mechanism has identical six DC motors which have the inertia of 10 gcm^2 and viscous friction of $0.25 \times 10^{-3}\, Nm\sec/rad$, each actuator is assumed to have a gearbox mechanism having 1/32 gear ratio and the pulleys mounted on the actuators have a radius of 10 cm. The desired trajectory of the robot is selected as

$$q_{d1} = q_{d2} = 0.5sin(0.5t)(1 - exp(-0.3t^3))\ rad \tag{4.10}$$

with the initial positions of each link being set to 0.5 rad.

Table 4.1: Simulation Setup TDRM model parameter values.

Parameter	Value	Unit
p_1	0.006	kgm^2
p_2	0.003	kgm^2
p_3	0.002	kgm^2
f_{d1}	0.005	$Nm\sec$
f_{d2}	0.001	$Nm\sec$
s_1	0.015	m
s_2	7907.5	N/m
s_3	1.7898×10^8	N/m^3

4.1. Simulation Studies for FSFB Robust Controller

The proposed FSFB robust controller presented in Chapter 2 should ensure the robot links follow a desired trajectory as closely as possible, despite the uncertain robot/actuator system parameters. During the simulation studies the best guessed estimates of the system parameters are selected to be 80 percent of the actual system parameters. To ease the tuning process an auxiliary gain

$$K_p = K_r + k_n(\rho_1^2 + \rho_2^2) \tag{4.11}$$

was taken and assumed to be a constant gain matrix. In view of (2.40), the controller gains were selected to ensure that

$$\min\left(\lambda_{\min}\left(K_r\right), \lambda_{\min}\left(\alpha\right)\right) - \frac{1}{4k_n} > 0 \tag{4.12}$$

is satisfied. Controller gain matrices are selected as shown in Table 4.2.

The simulation results are shown in Figures 4.2–4.4. Figure 4.2 shows the link position tracking errors in degrees and in inner figure the enlarged steady state error signals can be seen. Figure 4.3 presents the control torques applied to each actuators. Tendon tensile forces can be seen in 4.4. As can be viewed from Figure 4.2 after a very short period of time (less than 5 secs.) the tracking error terms for both joint converge to small values. During this time the controller inputs with the tendon tensile forces (see Figure 4.3) are in acceptable regions.

Table 4.2: Controller gains for FSBF controller simulations.

Controller Gains	**Adaptation Gains**
$\alpha = diag\{8, 10\}$	$\rho_3 = 1$
$K_p = diag\{2.8, 2.6\}$	$\rho_4 = 4$
$K_f = 5I_6$	$\varepsilon_1 = 0.01$
$K_\theta = 0.1I_6$	$\varepsilon_2 = 0.1$

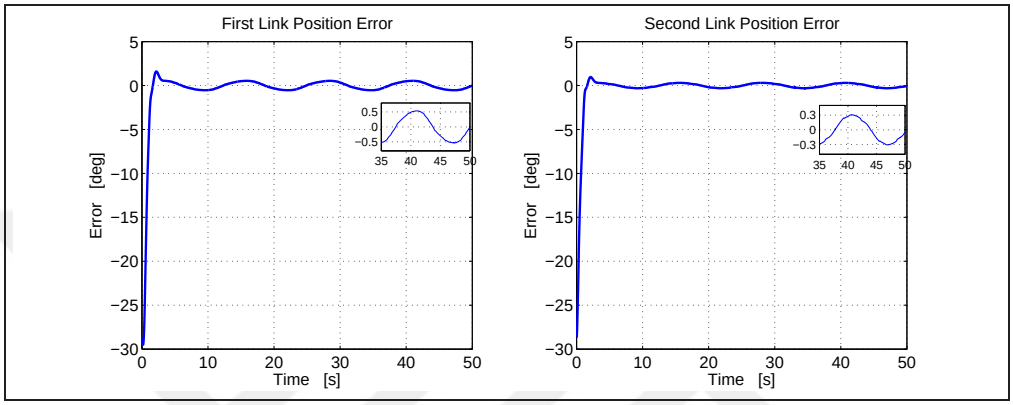

Figure 4.2: FSFB Controller: Position tracking errors for each link.

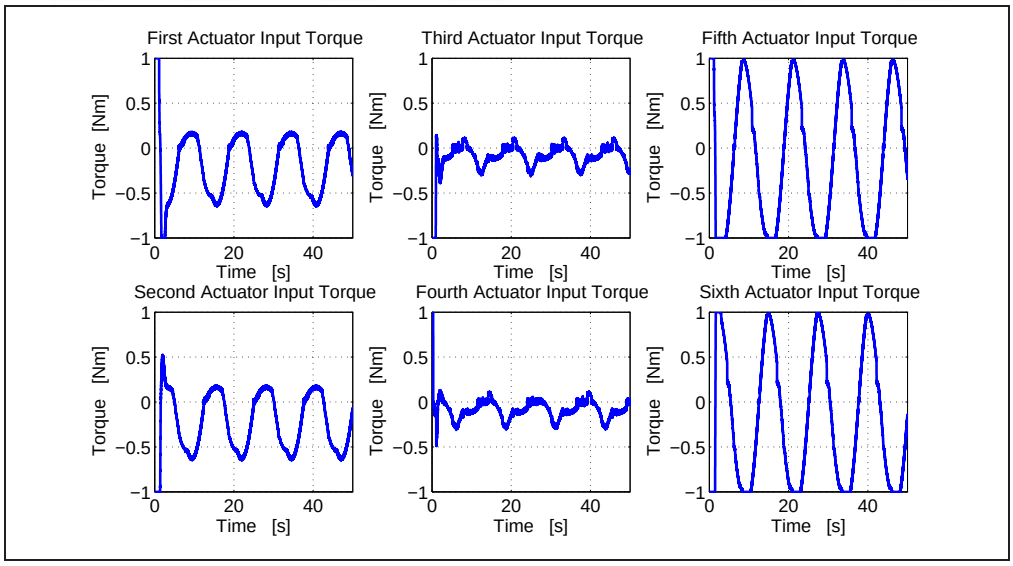

Figure 4.3: FSFB Controller: Control input torques.

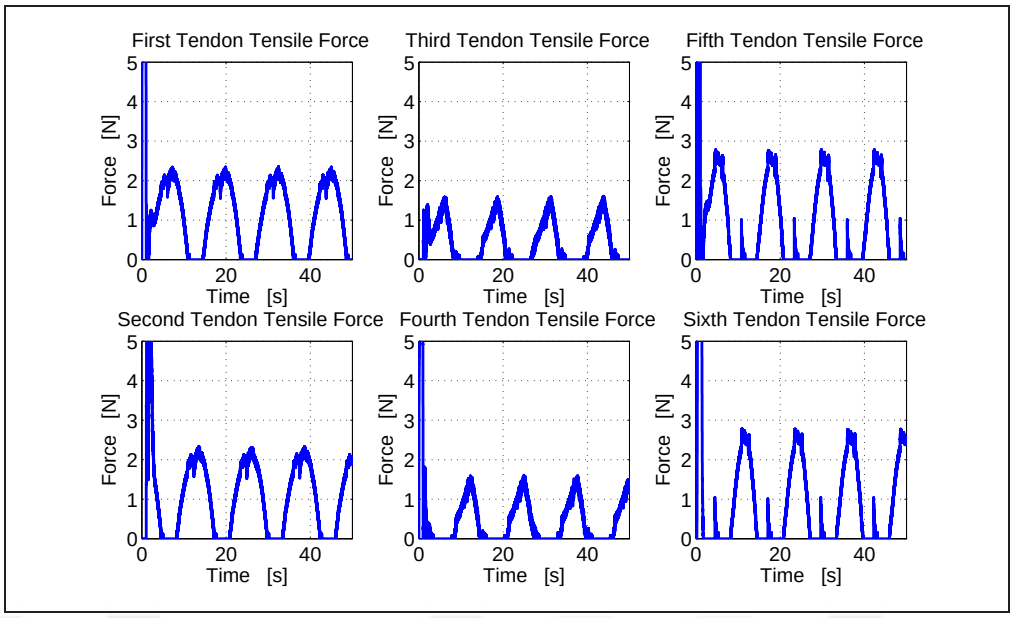

Figure 4.4: FSFB Controller: Tendon tensile forces.

4.2. Simulation Studies for Adaptive PSFB Controller

The adaptive PSFB controller presented in Section 2.1 should ensure the robot links to asymptotically follow a desired trajectory despite the uncertain model parameters while only link and actuator position measurements and tendon tension force measurements are available. All the initial estimations of the unknown parameters were taken as 0. According to the stability analysis estimations of the parameter values are expected to converge some constant values. Controller gains were selected as given in Table 4.3.

Table 4.3: Controller gains for PSFB controller simulations.

$\alpha_1 = diag\{6,6\}$	$\alpha_2 = diag\{15,15\}$	$\alpha_3 = diag\{10,10\}$
$k = diag\{0.1,0.6\}$	$K_s = diag\{30,20\}$	$K_f = 100I_6$
$K_L = 50I_6$	$k_{f1} = 30$	$k_{f2} = 30$
$\Gamma = diag\{15,5,2,8,8\}$	$\Gamma_1 = diag\{10^{-6}I_6, 10^{-8}I_6\}$	$\Gamma_2 = 10^{-3}I_{12}$

The simulation results are shown in Figures 4.5–4.6. Figure 4.5 shows the link position tracking errors. Figure 4.7 presents the control torques applied to each actuator, while Figure 4.8 presents the tendon tensile forces. Figure 4.6 shows the entries of the parameter estimation vector $\hat{\phi}_r(t)$. From Figure 4.5, it is clear that the tracking

control objective was successfully met.

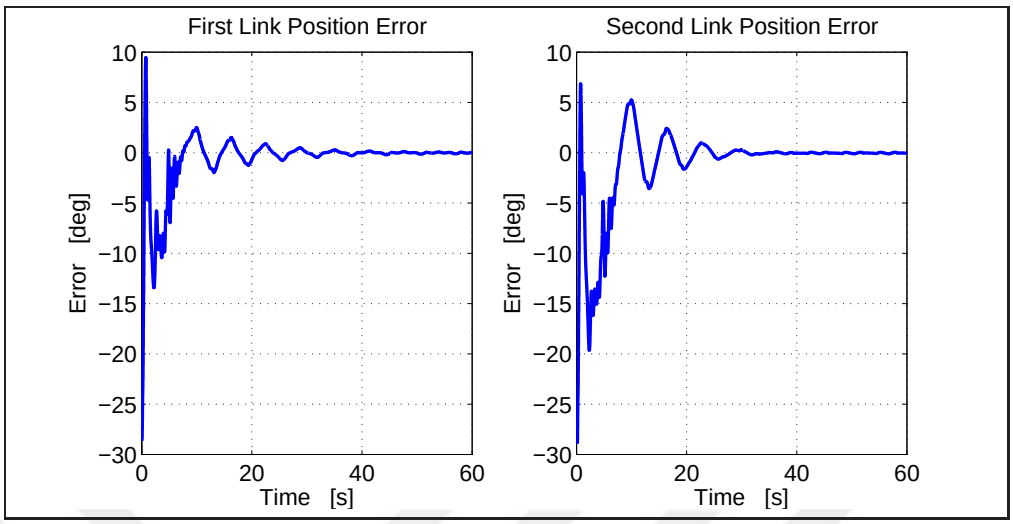

Figure 4.5: PSFB Controller: Link position tracking error $e(t)$.

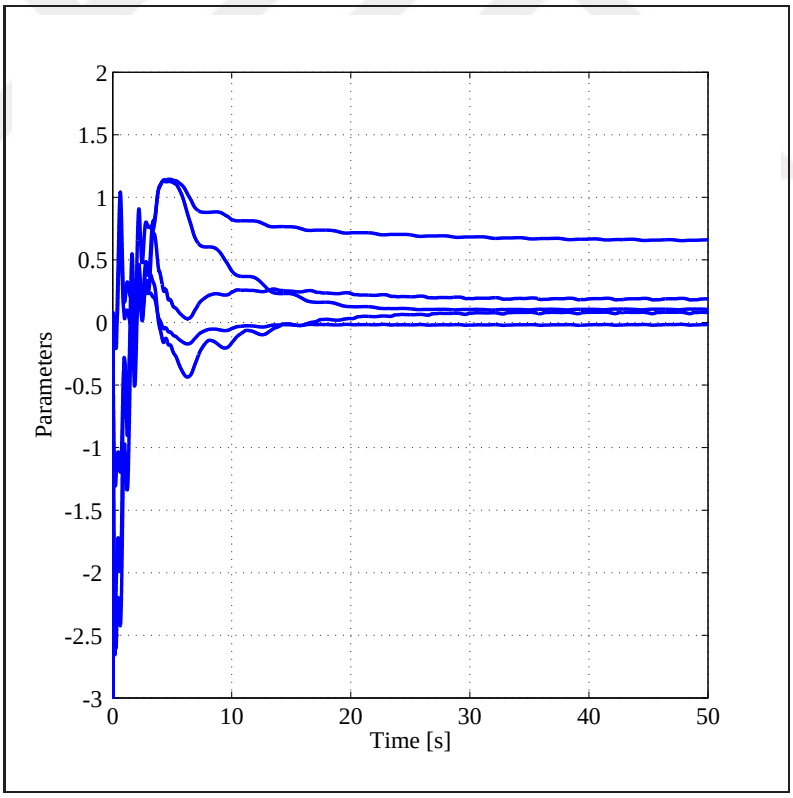

Figure 4.6: PSFB Controller: Entries of the parameter estimation vector $\hat{\phi}_r(t)$.

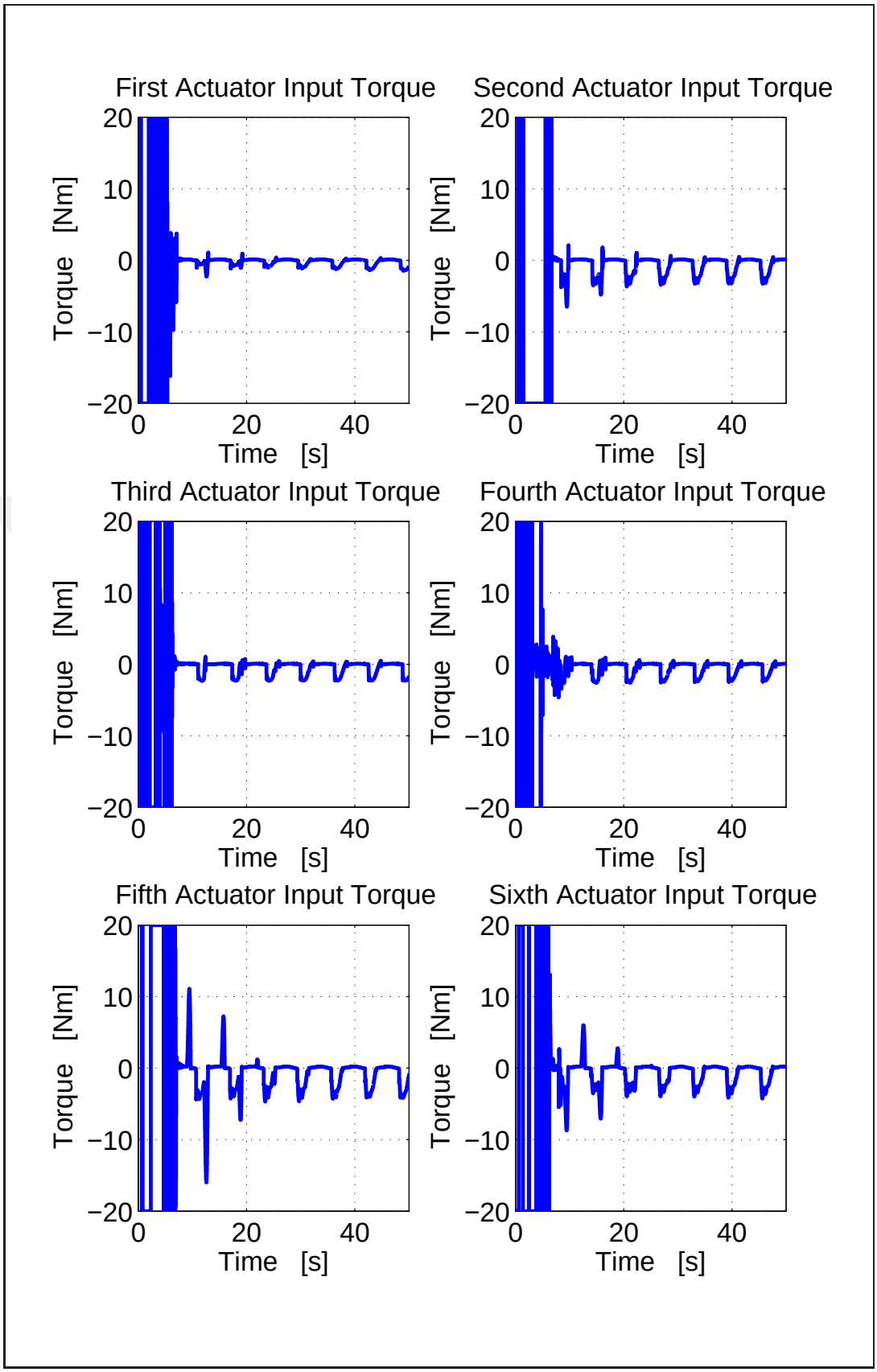

Figure 4.7: PSFB Controller: Actuator inputs $\tau_a(t)$.

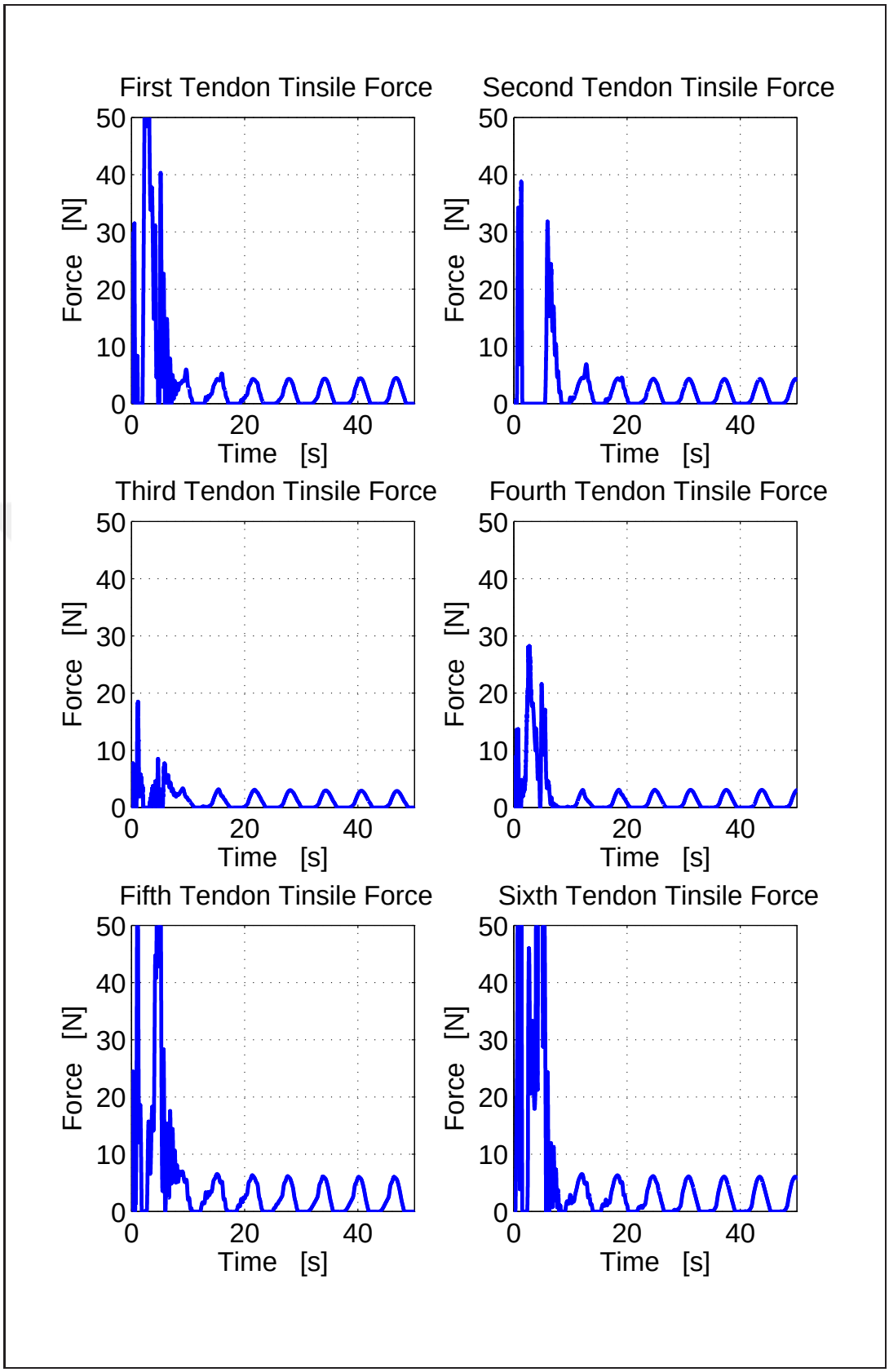

Figure 4.8: PSFB Controller: Tendon tensile forces $f_t(t)$.

4.3. Simulation Studies for Extended PSFB Controller

Similar to the previous controller, extended PSFB controller includes a parameter update law for robotic manipulator parameters and assures the asymptotic stability of the trajectory tracking error signal. Besides, the proposed controller can handle the control objective without actuator side position measurements while requires the exact knowledge of the actuator parameters. All of the unknown parameter initial estimation values are taken as 0 and controller gain matrices are selected as shown below.

Table 4.4: Controller gains for extended PSFB controller simulations.

$\alpha_1 = diag\{6,6\}$	$\alpha_2 = diag\{15,15\}$	$\alpha_3 = diag\{10,10\}$
$k = diag\{0.5,0.6\}$	$K_s = diag\{13,15\}$	$K_f = 100I_6$
$K_b = 100I_6$	$\Gamma = diag\{15,5,2,8,8\}$	

The simulation results are shown in Figures 4.9–4.12. Figure 4.9 shows the link position tracking errors. Figure 4.10 presents the control torques applied to each actuator, while Figure 4.11 presents the tendon tensile forces. Figure 4.12 shows the entries of the parameter estimation vector $\hat{\phi}_r(t)$. From Figure 4.9, it is clear that the tracking control objective was successfully met while accurate tuning of the controller gains could increase the controller performance.

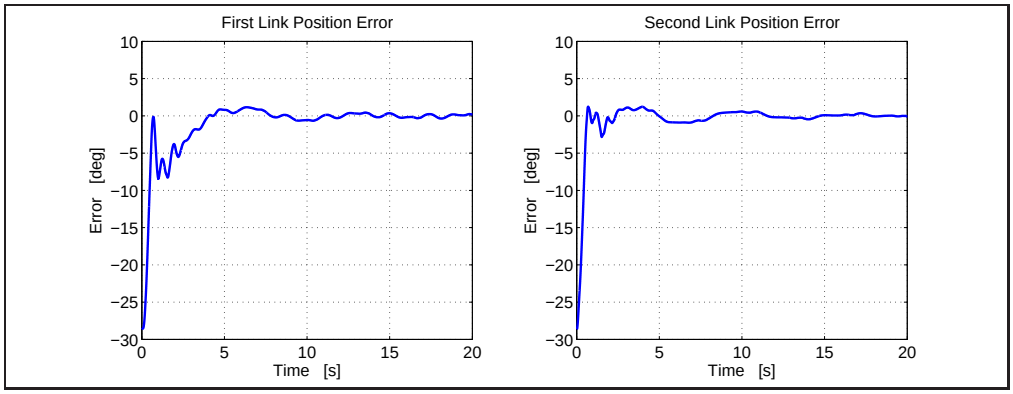

Figure 4.9: Extended PSFB Controller: Link Errors.

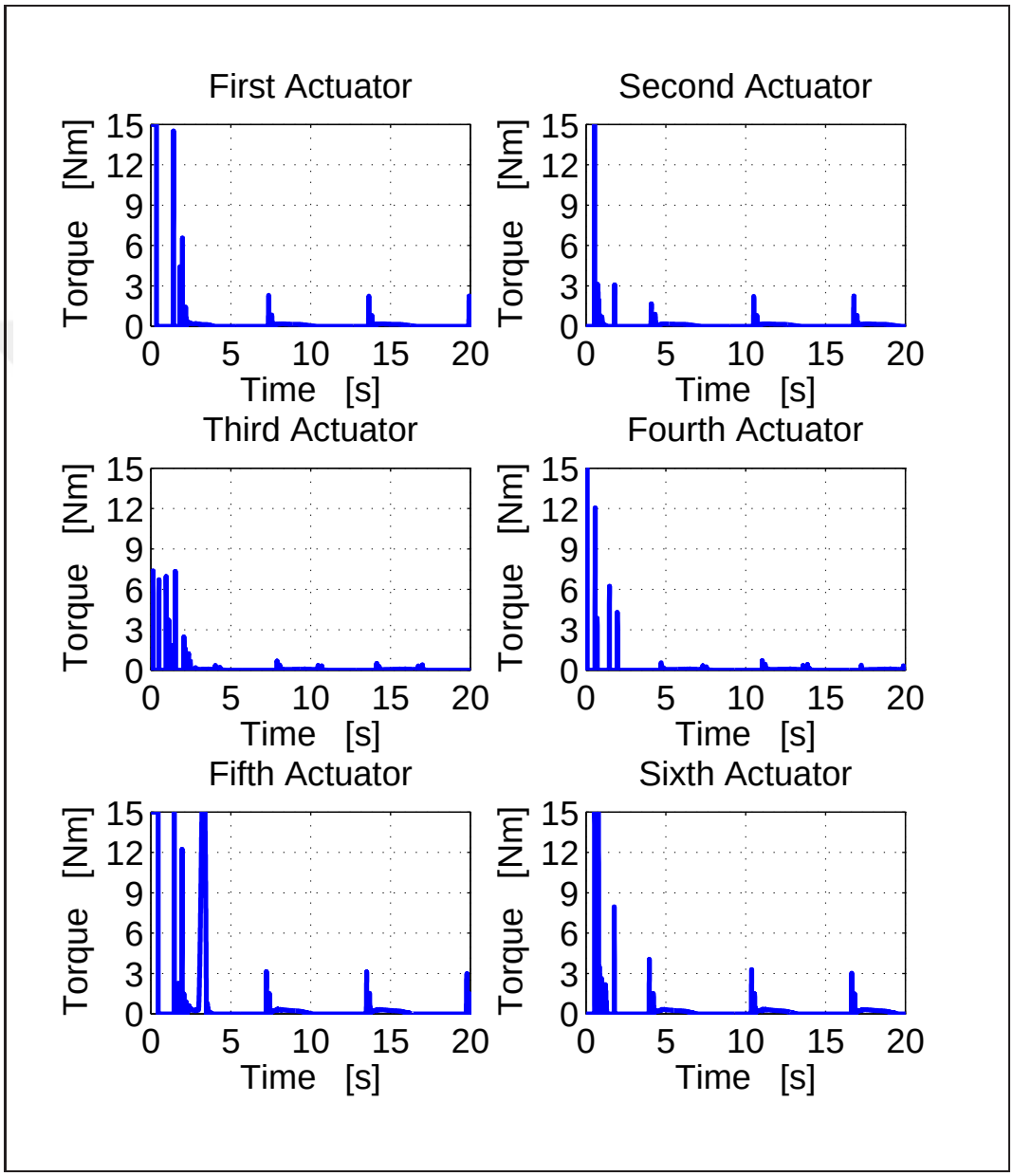

Figure 4.10: Extended PSFB Controller: Actuator inputs.

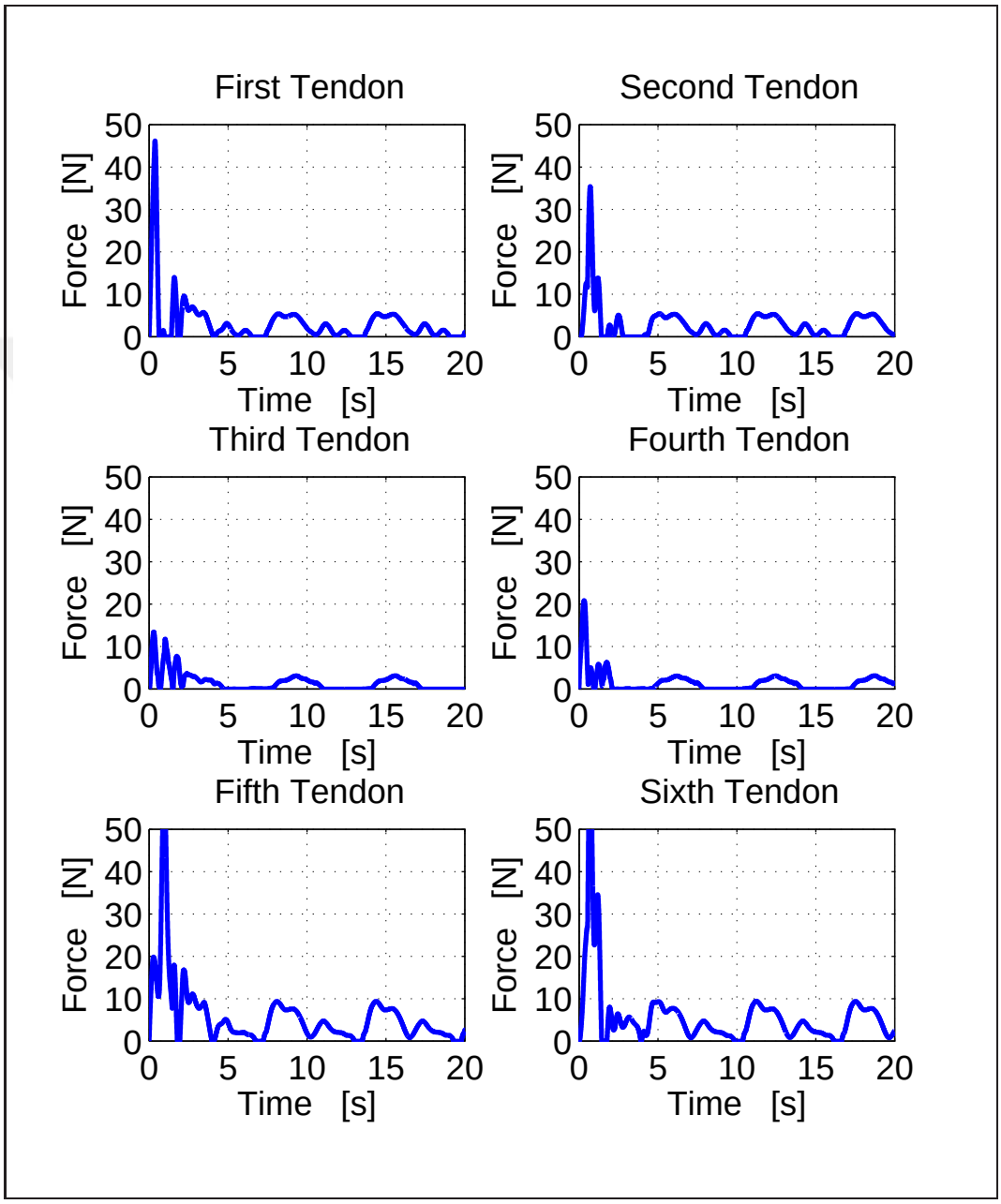

Figure 4.11: Extended PSFB Controller: Tendon tensile Forces.

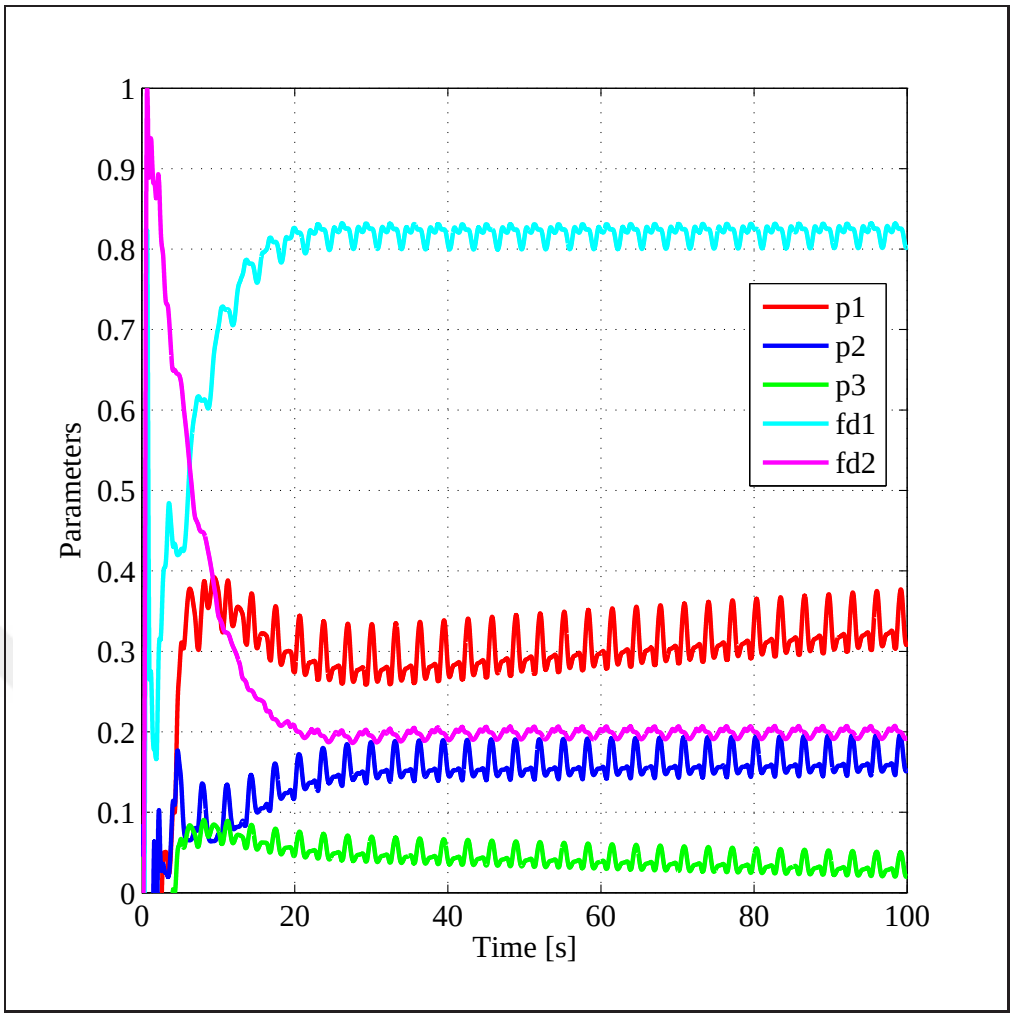

Figure 4.12: Extended PSFB Controller: Parameter updates for robot manipulator.

4.4. Remarks

In this chapter, simulation studies performed on an elastic tendon driven robotic system are presented. There different controllers (i.e. Robust FSFB, Adaptive PSFB, extended PSFB) have been simulated with the same system and desired link trajectories. The details of the controller algorithms used in the simulations can be seen in the previous chapters. As can be seen in the simulation results, controllers can deal with parametric uncertainties successfully and output error signal remains in an acceptable range even if the system state measurements are not available.

5. EXPERIMENTAL STUDIES

To verify the performance of the proposed Adaptive PSFB controller, some experimental studies on a two link robot manipulator driven by four tendons have been performed. Experimental validations are only performed to illustrate the performance and viability of the first PSFB method since it is impossible to determine the exact values of the actuator model parameters which are essential for the extended version of the PSFB controller. Besides, a very close estimation of the actuator parameters could force the tracing error signal in an acceptable range owing to the adaptation in the robotic manipulator dynamics.

5.1. Experimental Setup

Experimental setup includes a robotic manipulator with two links, four elastic tendons, four identical S-type load cells and their signal conditioning electronics, four identical brushed DC motors and 4 motor drivers (see Fig. 5.1). Electric motors

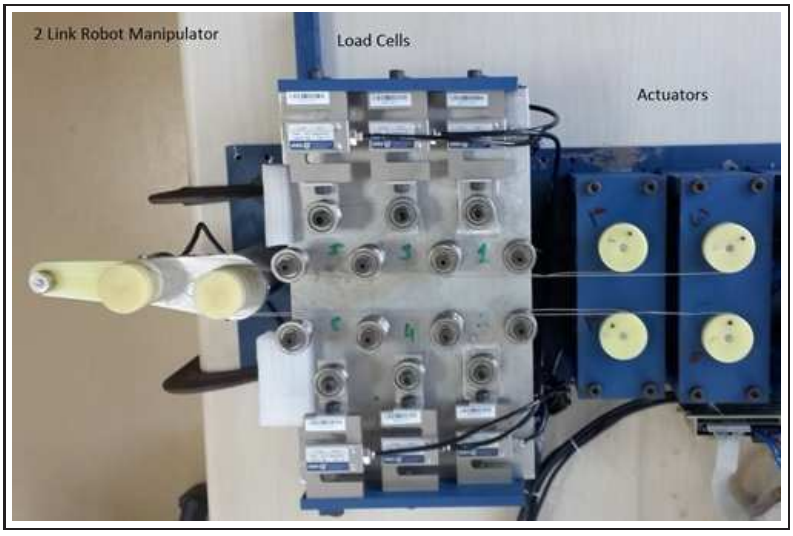

Figure 5.1: Two link planar robot manipulator driven by four tendons.

actuate robot links via elastic tendons and tensions on elastic tendons can be measured by means of load cells. The pulleys on the links and actuators have diameter of 40 mm. Link positions and actuator positions can be measured by means of incremental optic encoders with 20000 count per revolution. DC electric motors have 0.0302 Nm/A

torque constant under 24 V nominal supply voltage. Motor amplifiers work in torque mode and provides about 11 A maximum output current with the current gain of 2. One motor can produce about 20 N tension force on the tendons. Tendons are steel cables which have 0.8 mm diameter. The relationship between tendon expansion and tensile force represents a nonlinear behaviour due to a purely elastic behaviour of tendons [9]. Tendon expansions have been measured experimentally and the curve fitting process have been applied to the measurements to obtain the best approximated polynomial as explained in [13]. As a result, tensile forces can be calculated as a function of tendon expansions in the following manner

$$f_t(l_i) = \begin{Bmatrix} s_2 l_i + s_3 l_i^3 & l_i \geqslant 0 \\ 0 & l_i < 0 \end{Bmatrix}, i = 1, .., m \tag{5.1}$$

where l_i are the tendon expansions, $s_2 = 1550\ N/m$ and $s_3 = 1.48 \times 10^8\ N/m^3$ are constant elongation parameters and $f_t(l_i)$ are the members of the vector of the tendon tensile forces which is defined as follows

$$f_t(l) = \begin{bmatrix} f_t(l_1) & f_t(l_2) & \dots & f_t(l_m) \end{bmatrix}^T. \tag{5.2}$$

The tensile force definition given in (5.1) satisfies the assumptions *1.2:* to *1.4:*. Owing to the modular structure of the experimental setup, two different tendon-link connections have been demonstrated which are one link–two actuator and two link four actuator configurations as shown in Fig. 5.2.

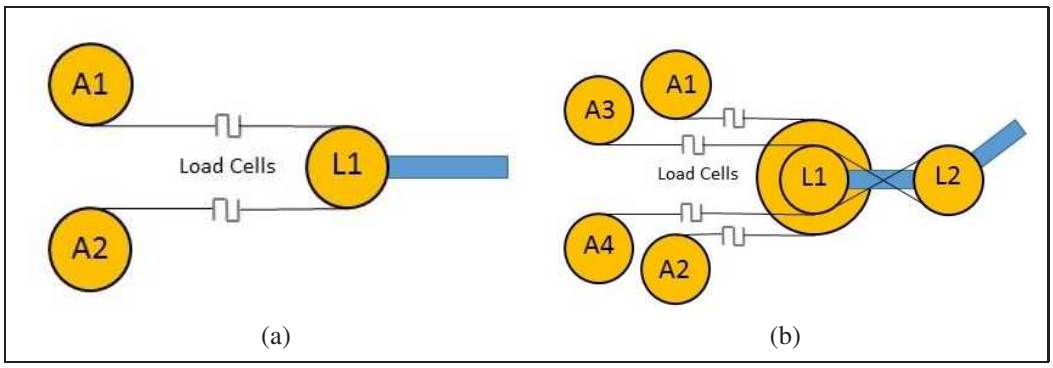

Figure 5.2: a) One link tendon configuration, b) Two links tendon configuration.

Jacobian matrices for the first and second configurations are defined as follows

$$J_j^T(q) = s_1 \begin{bmatrix} 1 & -1 \end{bmatrix}, \tag{5.3}$$

$$J_j^T(q) = s_1 \begin{bmatrix} 1 & -1 & 1 & -1 \\ 0 & 0 & -1 & 1 \end{bmatrix}, \tag{5.4}$$

respectively. Here $s_1 = 0.02\ m$. The desired trajectories of the robot was selected as

$$q_{d1} = 0.5\sin(t)(1-\exp(-t^3))\ rad, \tag{5.5}$$

$$q_{d2} = 0.5\sin(1.5t)(1-\exp(-t^3))\ rad \tag{5.6}$$

in order to see the effects of the nonlinearities in the robot dynamics, clearly. Initial positions of the robot links were set to 0 *rad*. All the initial estimations of the unknown parameters were taken as 0.

5.2. PID Controller Experimental Results

At the beginning of the experimental studies a standart PID Controller have been implemented as explained in [17] to see capabilities of the experimental setup. Actuator control input signals have been calculated as follows

$$\tau_a = J_j(q)(K_p e + K_d \frac{de}{dt} + K_i \int edt) + f_b \tag{5.7}$$

where f_b is the constant bias force, K_p, K_d, and K_i are PID controller gains and selected as shown in Table 5.1.

Table 5.1: Controller gains for PID controller experiments.

First link	**Second link**
$K_{p1} = 70$	$K_{p2} = 70$
$K_{d1} = 0.5$	$K_{d2} = 0.1$
$K_{i1} = 5$	$K_{i2} = 5$

Figure 5.3-5.4 represents the one link - two actuator configuration experimental results while Figure 5.5-5.6 represents two link - four actuator configuration experimental results. In Figure 5.3 link error and controller output signal of a one link robot manipulator can be seen. 5.4 shows the related tension force generated by the actuators. Figure 5.5 represents the link errors for two link robot configurations. Thanks to the over actuated structure of this configuration, link errors are a little bit better than the one link configuration while the control inputs are in a similar behaviour(See Figure 5.7). Related tension forces are presented in Figure 5.6.

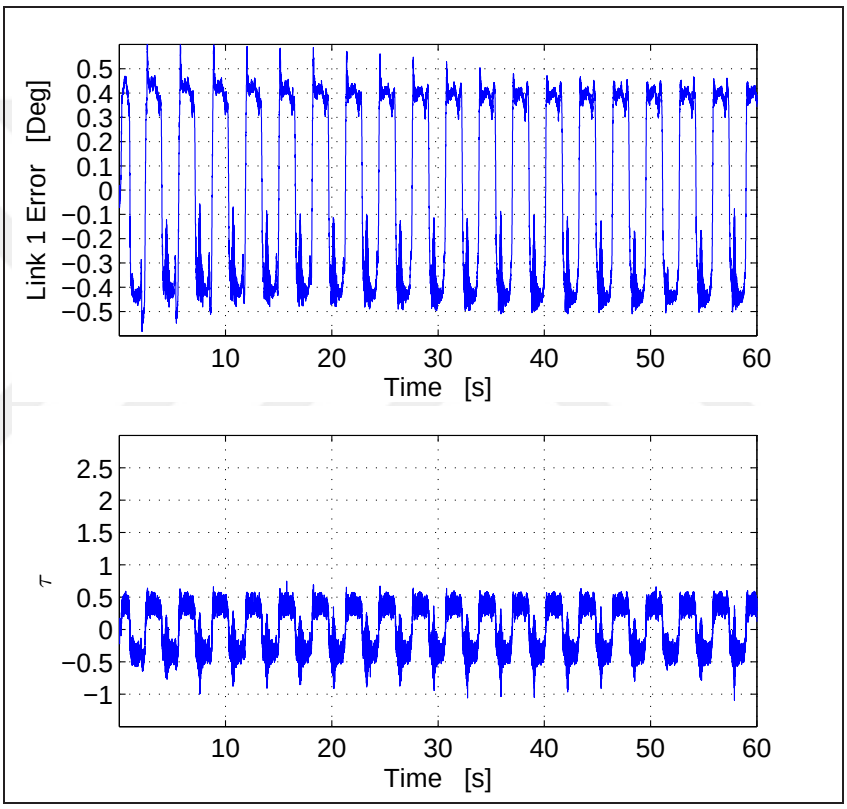

Figure 5.3: Link error and controller output for one link PID Controller.

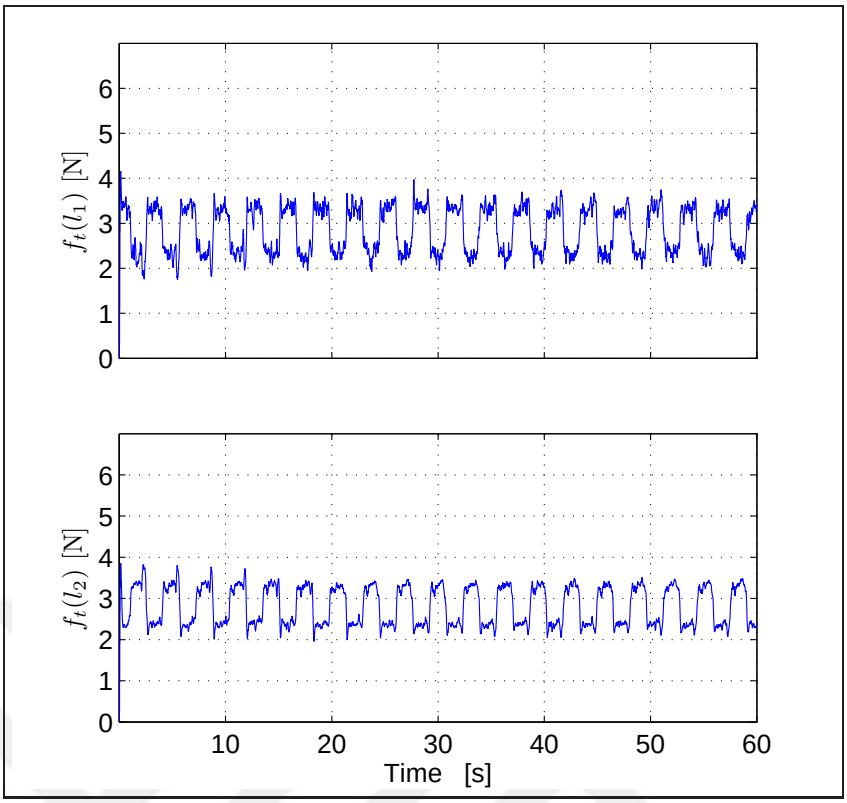

Figure 5.4: Tendon Tensions for one link PID Controller.

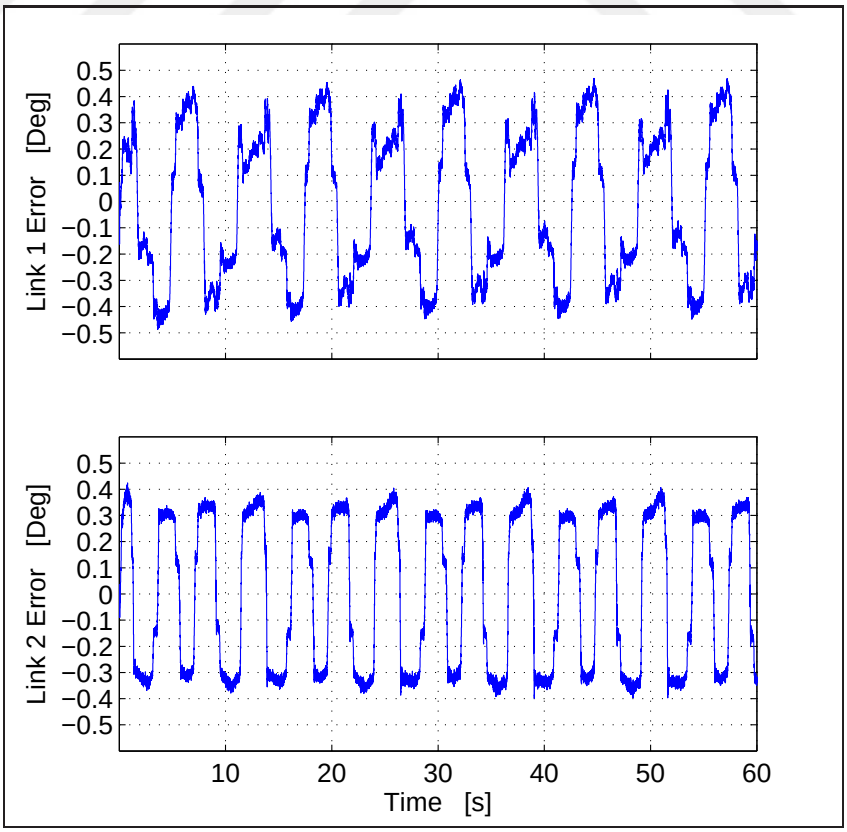

Figure 5.5: Link position tracking error $e(t)$ for two link PID Controller.

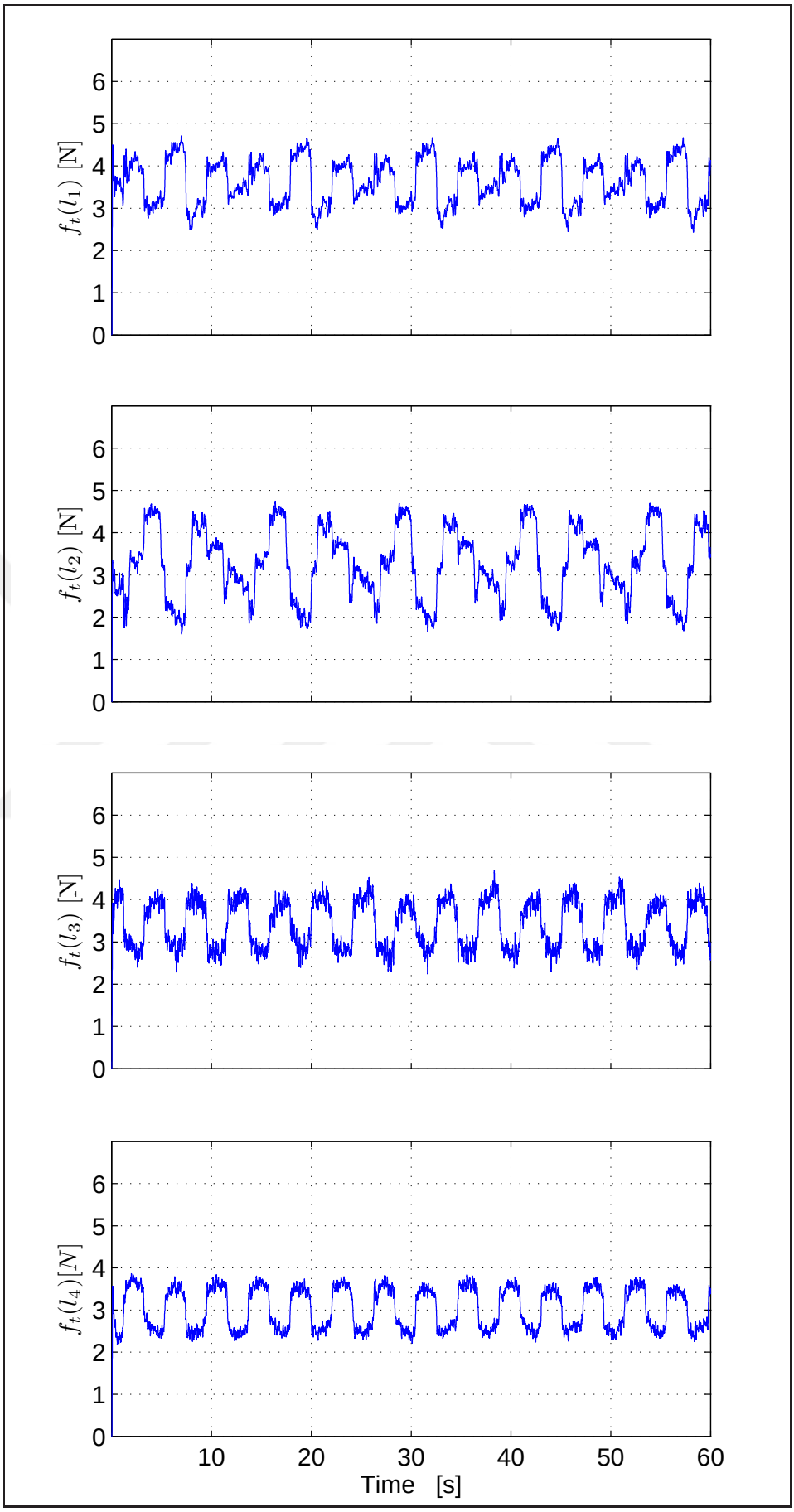

Figure 5.6: Tendon Tensions for two link PID Controller.

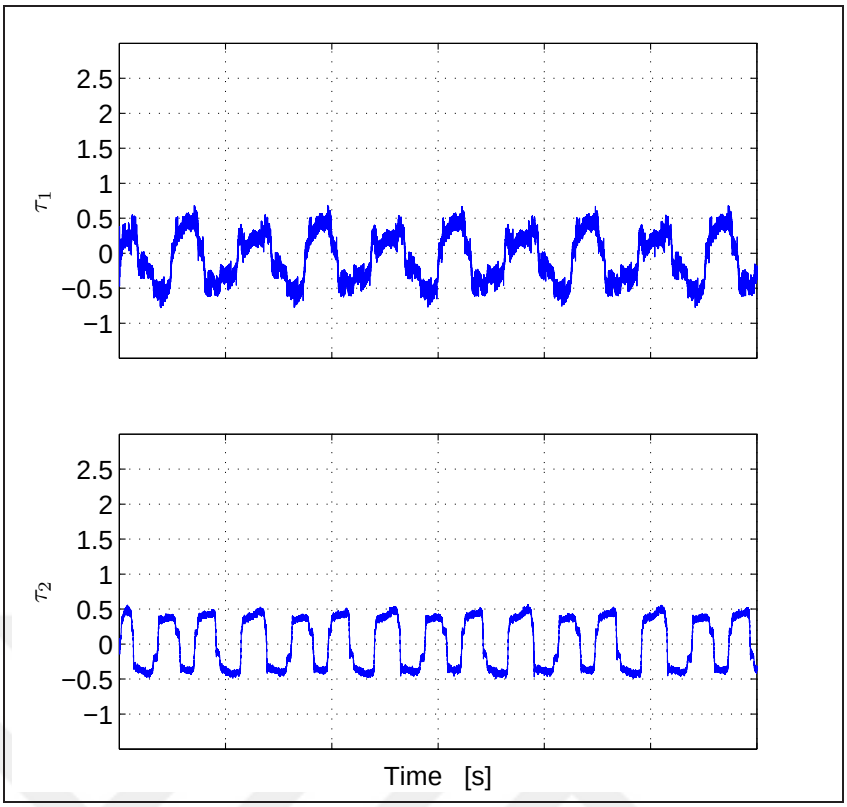

Figure 5.7: Controller output for two link PID Controller.

5.3. Feed-forward Controller Experimental Results

At the beginning of the controller development and implementation process, we applied the desired tendon tension signal given in (3.10) as a controller signal since it is a type of feed-forward computed torque controller signal. In this type of controller, actuator dynamics have been neglected but it gave us a valuable experience on implementing a model based controller formulation before implementing a very complicated controller algorithm. Controller gains for two link–four actuators configuration have been selected as shown in Table 5.2.

Table 5.2: Controller gains for Feed-Forward controller experiments.

$\alpha_1 = 2.4I_2$	$\alpha_2 = 0.1I_2$	$\alpha_3 = 0.001I_2$
$k = 4I_2$	$K_s = 0.93I_2$	
$\Gamma = diag\{0.01, 0.05, 0.007, 0.0001, 0.001\}$		

Figure 5.8 shows the link errors and Figure 5.9 shows the controller outputs including bias force f_b. Tendon tensile forces are presented in Figure 5.10.

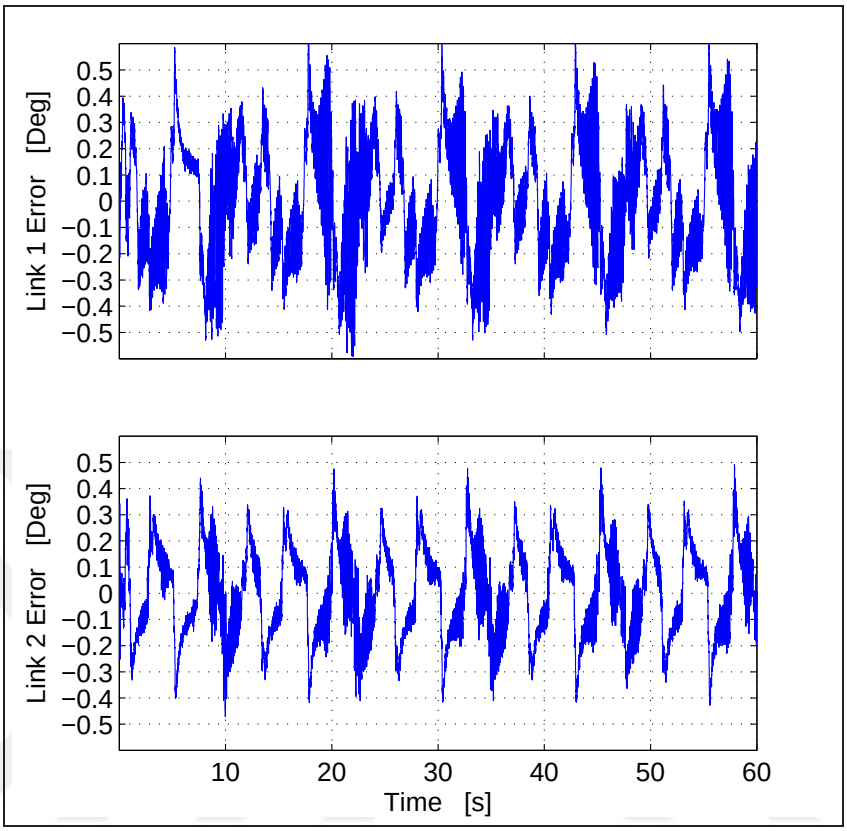

Figure 5.8: Link position tracking error $e(t)$ for two link Feed-forward Controller.

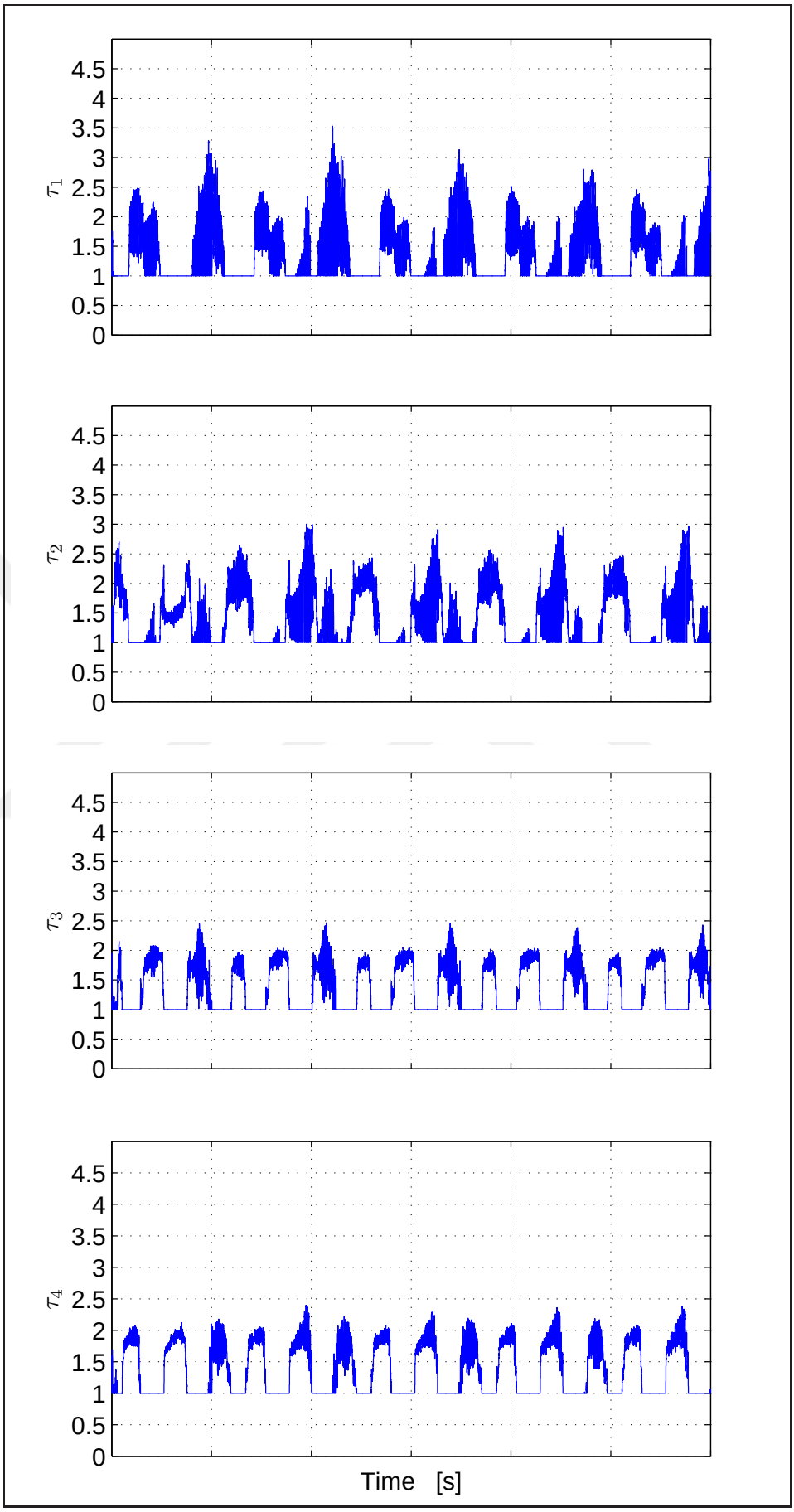

Figure 5.9: Controller output for two link Feed-forward Controller.

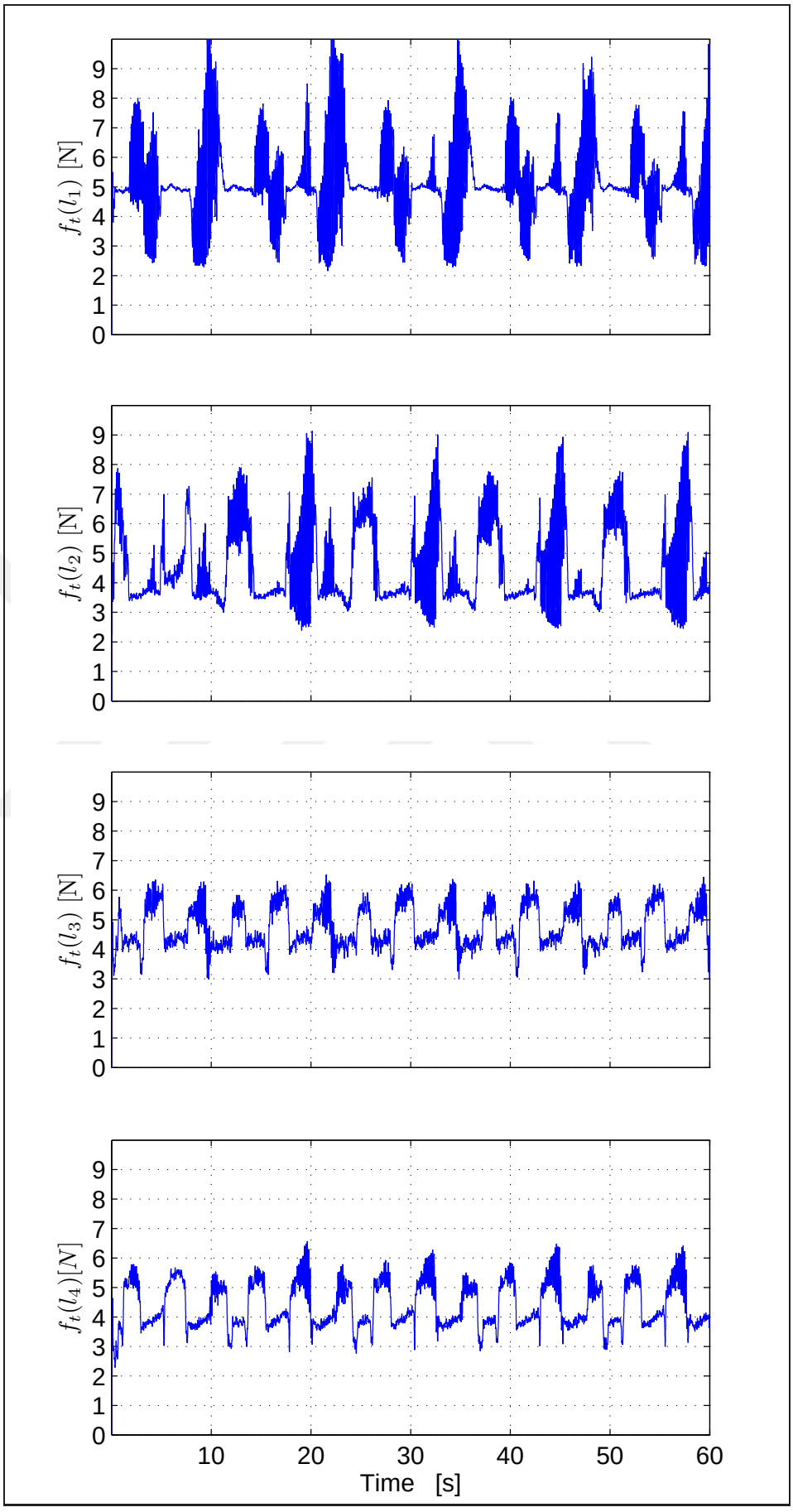

Figure 5.10: Tendon Tensions for two link Feed-forward Controller.

5.4. PSFB Controller Experimental Results

Controller gains for one link–two actuators configuration were selected as shown in Table 5.3.

Table 5.3: Controller gains for PSFB controller experiments.

$\alpha_1 = 13$	$\alpha_2 = 0.5$	$\alpha_3 = 0.2$
$k = 1.94$	$K_s = 3.05$	$K_f = 0.3I_2$
$K_L = 0.7I_2$	$k_{f1} = 0.078$	$k_{f2} = 0.078$
$\Gamma = diag\{0.3, 1.5\}$	$\Gamma_1 = 10^{-6}I_4$	$\Gamma_2 = 10^{-5}I_4$

In Fig. 5.11 link position tracking error of the one link robotic manipulator can be seen. The amplitude of the error signal is relatively small compared to the PID controller, Feed forward controller and similar studies in the literature (i.e. [13]) even-tough some of the model parameters are not known and most of the system states are not measured. Controller output signal is presented in Fig. 5.12 without the bias force component of the input torque. Total tendon tension forces included bias forces can be seen in Fig. 5.13.

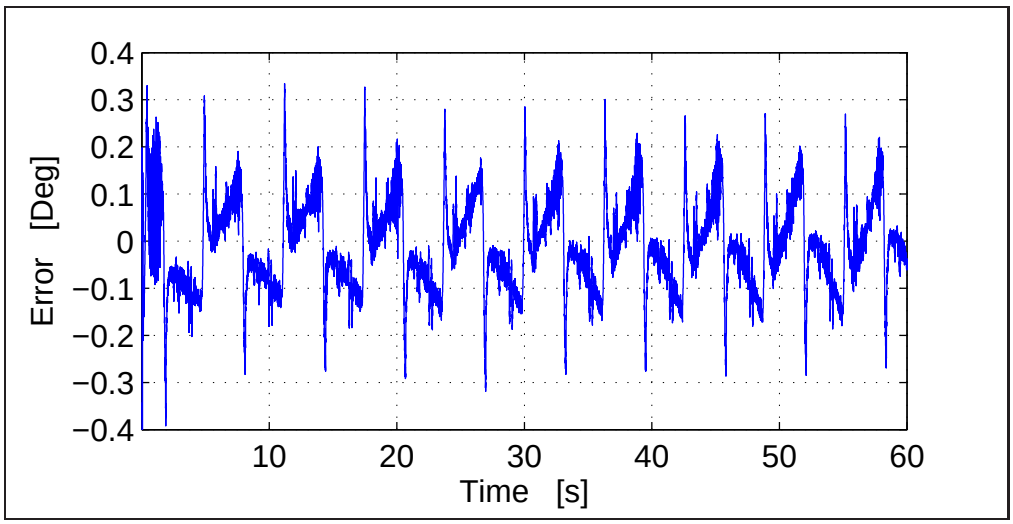

Figure 5.11: Link position tracking error $e(t)$ for one link configuration.

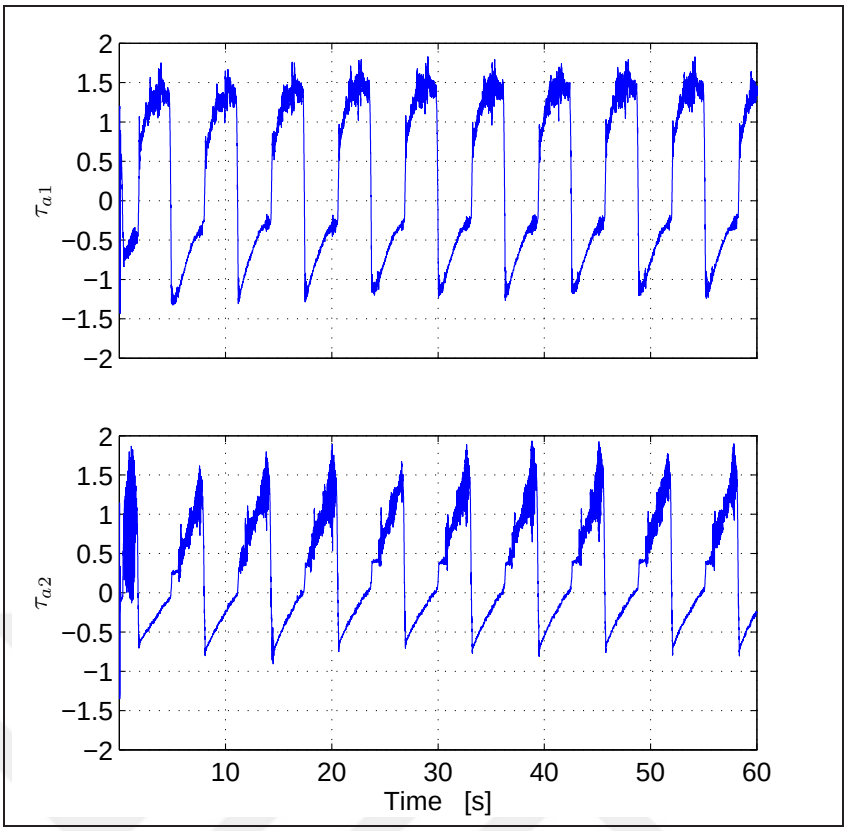

Figure 5.12: Controller output for one link two actuator configuration.

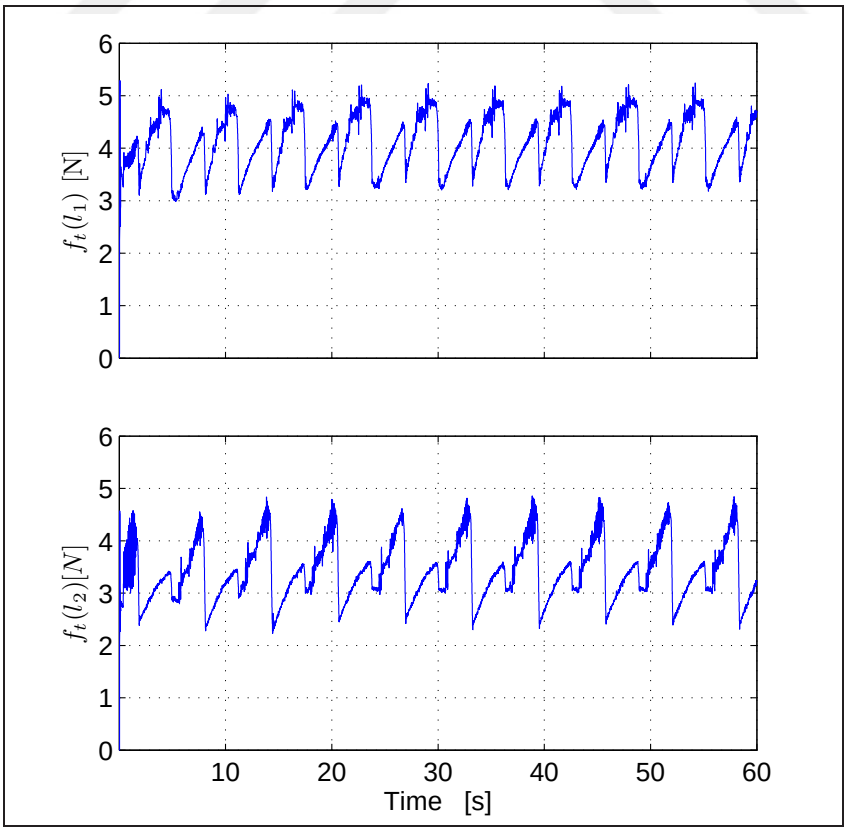

Figure 5.13: Tendon Tensions for one link two tendon configuration.

Controller gains for two link–four actuators configuration were selected as shown in Table 5.4

Table 5.4: Controller gains for PSFB controller experiments on two link robot.

$\alpha_1 = diag\{12,12\}$	$k = diag\{3.9,3.9\}$	$K_L = 0.35I_4$
$\alpha_2 = diag\{0.9,0.9\}$	$K_s = diag\{1.15,1.15\}$	$K_f = 0.01I_4$
$\alpha_3 = diag\{0.01,0.01\}$	$k_{f1} = 0.003$	$k_{f2} = 0.003$
$\Gamma = diag\{0.1,0.3,0.01,0.01,0.01\}$	$\Gamma_1 = 10^{-6}I_8$	$\Gamma_2 = 10^{-6}I_8$

Link position tracking errors of the two link robotic manipulator are given in Fig. 5.14 and controller output can be seen in Fig. 5.15. Figure 5.16 presents tendon tensile forces. The results of the experiments prove the effectiveness and facility of implementation of the proposed controller.

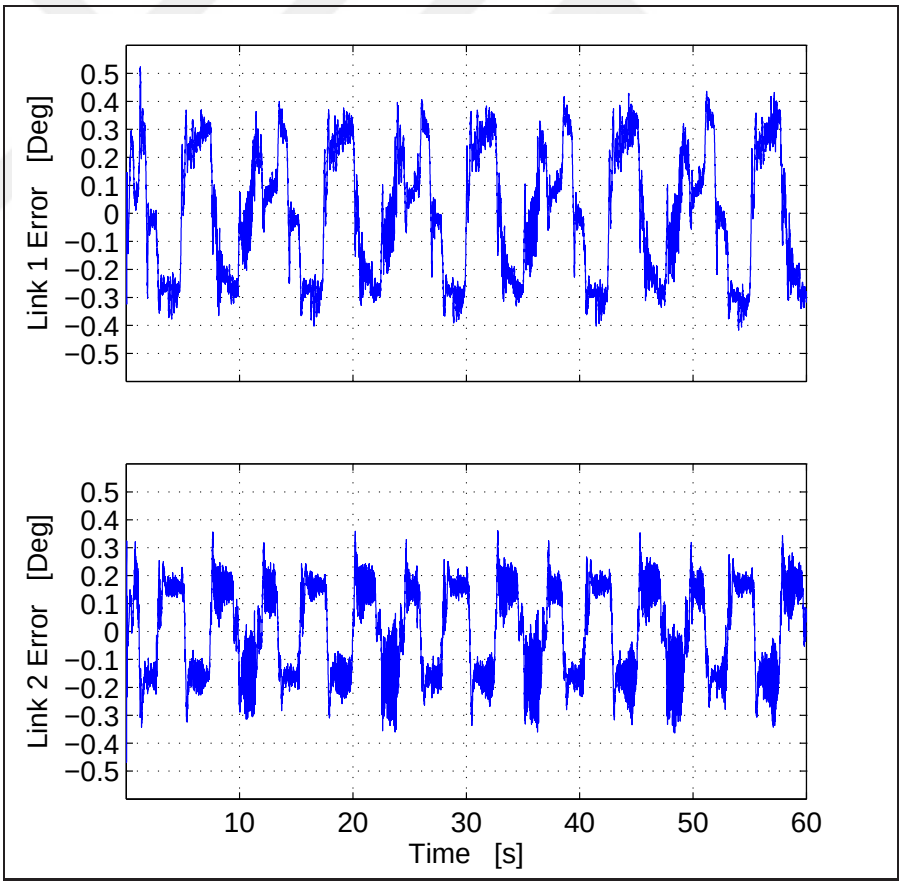

Figure 5.14: Link position tracking error $e(t)$ for two link configuration.

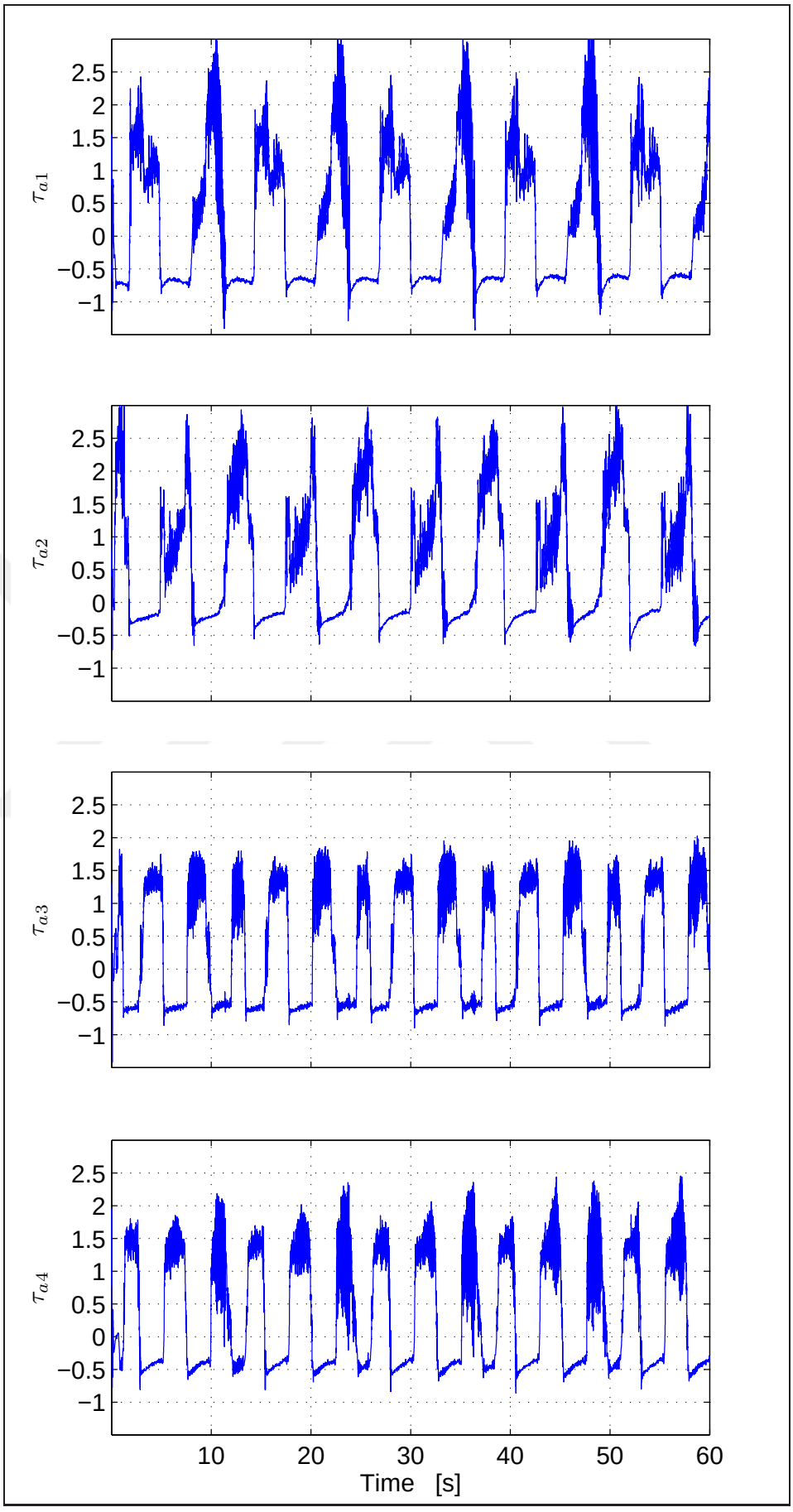

Figure 5.15: Controller output for two link four actuator configuration.

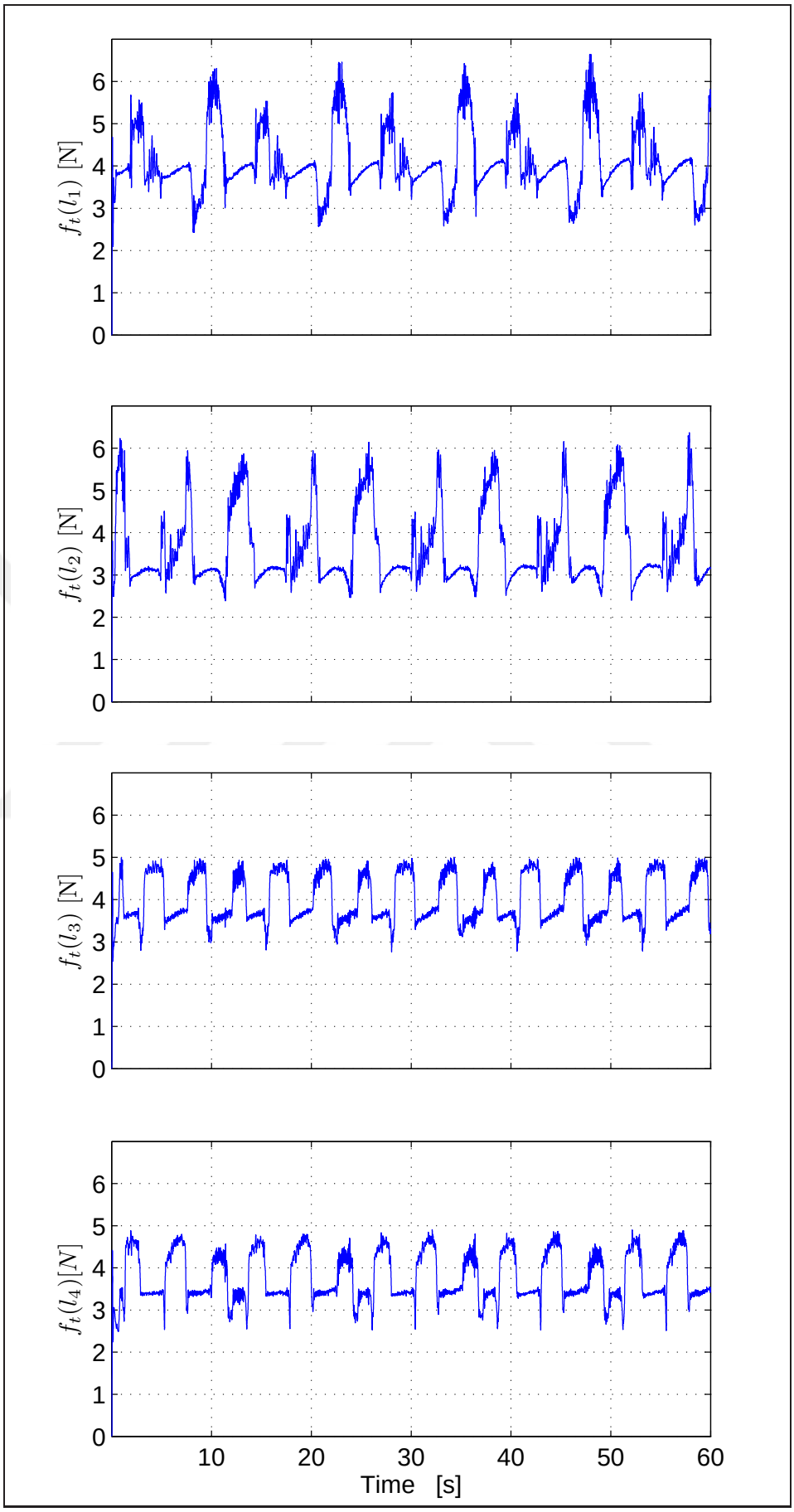

Figure 5.16: Tendon Tensions for two link four tendon configuration.

5.5. Remarks

In this chapter, experimental validations have been presented to illustrate the performance and viability of the adaptive PSFB controller. since it is impossible to determine the exact values of the actuator model parameters. Besides, a very close estimation of the actuator parameters could force the tracing error signal in an acceptable range owing to the adaptation in the robotic manipulator dynamics.According to the experimental results, PSFB Adaptive controller provides the best controller performans compared to the PID and Feedforward controllers.

6. EXTENSION ON A LEVITATION SYSTEM

Magnetic levitation is a key technology that allow high precision and frictionless movement and eliminate lubrication needs. Owing to these advantages, magnetic levitation technology is successfully implemented in many areas like high speed trains, special environment conveyance systems, frictionless bearings and high precision positioning systems. Recently, control performance of a magnetic levitation system becomes much more important as energy efficiency stands a major performance criteria of these kind of systems. Hybrid electromagnets consisting of permanent magnets and electromagnets in the same magnetic structure receive an increasing attention because they give an opportunity to implement the zero power control methods.

Levitation systems that consist of both permanent magnets and electromagnets have been investigated since the 1960s. In [46], a magnetic levitation system with hybrid electromagnets has been analysed, advantages and benefits of the usage of permanent magnets with electromagnets have been investigated and effects of the size and type of permanent magnets on these benefits have been presented. [47] is one of the important and pioneering work on this subject. In this work authors have investigated hybrid levitated carriage systems which consist of permanent magnets and electromagnets together and focused on decreasing the power consumption issue by the help of permanent magnets. It is carried out in this work that power consumption is the lowest when permanent magnets are chosen to overcome the mass of the levitated body and electromagnets are only powered to control the levitation which is also the main idea of the zero power control method. [48],[49] are focused on the optimal design based on the electromagnetic analysis of the hybrid electromagnets. In [50], it is shown that hybrid levitation systems have advantages for both large scale systems such as 50 kg and small scale systems such as 5 kg.

Magnetically levitated systems are represented with nonlinear mathematical expressions due to the nature of the magnetic fields but linear and nonlinear control algorithms are equally take place in the literature. [51], [52],[53],[54] and [55] can be given as an example of nonlinear robust controllers. [56] and [57] applied nonlinear control techniques with backstepping approach on active magnetic bearings without permanent magnets nevertheless in [56], authors have been proposed a full state feed-

back controller which requires the exact knowledge of the model parameters and in [57], Sivrioglu did not take into consideration the voltage dynamics of the electromagnets. [58] represents a nonlinear control method applied to the maglev trains. A flatness based nonlinear control of magnetic bearings have been investigated in [59] with both voltage control and current control approaches. A robust trajectory tracking controller for magnetic levitation systems have been presented in [60] with a very simplified model of the current dynamics. In [61], a detailed model of a 4 pole hybrid electromagnet is presented and 3-degree-of-freedom (DOF) motion control is investigated via linear control methods with zero power control method. [62] and [63] can be stated as examples of zero power control methods in recent years.

In this chapter, a back stepping type, model based controller have been investigated to ensure that a 1-DOF levitation system with hybrid electromagnets can track a desired smooth trajectory under the constraint that the model parameters are uncertain and the air gap velocity measurement is not available. The time dependency of the electrical subsystem parameters have been ignored and taken into account as parametric uncertainties during the controller development and stability analysis processes.

The rest of the chapter is organized in the following manner. The dynamical model of a 1-DOF levitation system is presented in Section 6.1. Controller formulation is given in Section 6.2. The corresponding stability analysis can be seen in Section 6.3. Numerical simulations are presented in Section 6.4. Concluding remarks are given in Section 6.5.

6.1. Modelling of the Levitation System

A hybrid U type electromagnet composed of electromagnets and permanent magnets can be seen in Fig. 6.1. Electrodynamic model of this levitation system can be written as

$$m\ddot{z} = mg - F_e(z,i) + F_d. \tag{6.1}$$

Here, m is the total mass of the levitated body, z is the total air gap of the magnetic circuit which is the sum of thickness of the permanent magnet (l_{pm}) and distance between

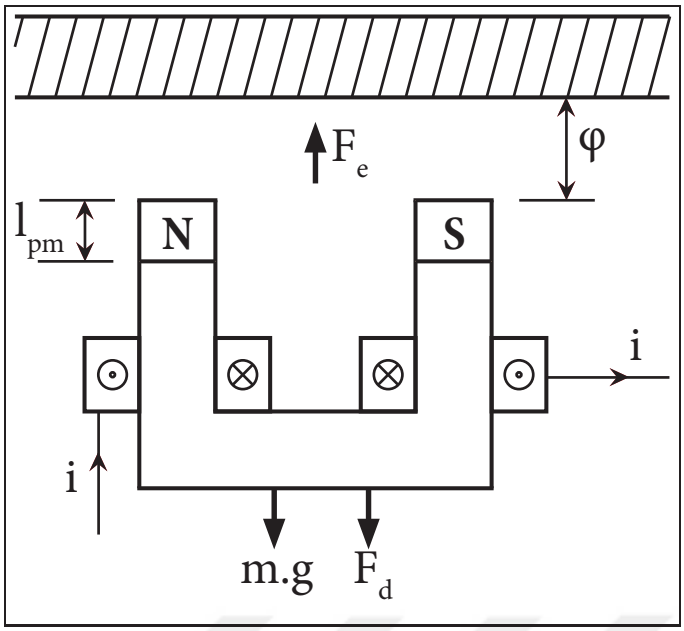

Figure 6.1: A suspension system consisting of a U type hybrid electromagnet.

the poles and upper part (φ) and can be represented as

$$z = \varphi + l_{pm}, \tag{6.2}$$

$\ddot{z}$ is the acceleration of the system, i represents the total equivalent current of the magnetic circuit which is the sum of current passing through the electromagnet coils (i_c) and the equivalent current of the permanent magnets (I_{pm}) and can be represented as

$$i = i_c + I_{pm}, \tag{6.3}$$

$F_e(z,i)$ is the total electromagnetic force produced by the coils and permanent magnets and F_d is a bounded disturbance term. According to the flux linkage model, electromagnetic force can be calculated as follows [64]

$$F_e(z,i) = -\frac{\partial}{\partial z}\int_0^i \lambda(z,i)di \tag{6.4}$$

where $\lambda(z,i)$ represents the flux linkage. If the magnetic circuit is assumed to be linear, $\lambda(z,i)$ can be calculated by the following formula

$$\lambda(z,i) = 2N^2\mu_0 S\frac{i}{z} \tag{6.5}$$

where N is the number of coil turns for each coil, S is the cross-sectional area of the electromagnet poles, μ_0 is the constant permeability of the air. Substituting (6.5) into (6.4), total electromagnetic force can be calculated as follows

$$F_e(z,i) = N^2\mu_0 S\frac{i^2}{z^2}. \tag{6.6}$$

After substituting (6.6) into the mathematical model given in (6.1), a useful form of the electromechanical dynamics of the system can be written as follows

$$M\ddot{z} = Mg - \phi(z)u(i) + \frac{1}{N^2\mu_0 S}F_d \tag{6.7}$$

where

$$M \triangleq \frac{m}{N^2\mu_0 S}, \quad \phi(z) \triangleq \frac{1}{z^2}, \quad u(i) \triangleq i^2. \tag{6.8}$$

It is assumed that M satisfies the following condition.

$$m_1 \leq M \leq m_2 \tag{6.9}$$

where $m_1, m_2 \in \Re$ are scalar bounding constants. Electrical dynamics of the electromagnets can be written as follows [65]

$$L(z)\frac{di}{dt} + Ri_c + B(z,i)\frac{dz}{dt} = v \tag{6.10}$$

here $L(z)$ is the inductance of the coils and can be calculated with the help of the magnetic flux linkage model as follows

$$L(z) = \frac{\partial\lambda(z,i)}{\partial i} = \frac{N^2\mu_0 S}{z} \tag{6.11}$$

and $B(z,i)$ is the back EMF (Electro-Motive Force) factor and can be calculated as follows

$$B(z,i) = \frac{\partial\lambda(z,i)}{\partial z} = -N^2\mu_0 S\frac{i}{z^2}. \tag{6.12}$$

R is the electrical resistance of the coils and v is the voltage input of the system. Although electrical model parameters L, B are time dependent and their values change during the operation, they have a constant part and a time dependent part and constant part is respectively big compared to the time dependent part [65]. During the controller development we assume that electrical model parameters L, B, R are constants and time varying parts of these parameters will be added as parametric uncertainties to the system model. A robust controller will be designed to handle these uncertainties. More over electrical subsystem parameters are asummed to be satisfied the following conditions.

$$l_1 \leq L \leq l_2 \tag{6.13}$$

$$b_1 \leq B \leq b_2 \tag{6.14}$$

where $l_1, l_2, b_1, b_2 \in \Re$ are scalar bounding constants.

6.2. Problem Formulation and Controller Development

The aim of this section is to design an air gap distance tracking controller for a magnetic levitation system consisting of hybrid U-type electromagnet given by model equations (6.7) and (6.10) under the constraint that air gap velocity cannot be measurable and model parameters are not known exactly. Specifically; the proposed controller should force the desired air gap trajectory tracking error to converge to a zone close to zero despite the uncertain model parameters and lack of velocity measurement. I design a model based robust controller to over come parametric uncertainties and the need of velocity measurement is eliminated by using a velocity independent filter term. The tracking error signal $e(t) \in \Re$ is defined as follows

$$e \triangleq z_d - z \tag{6.15}$$

where z_d is the desired air gap trajectory signal and its first, second and third time derivatives are assumed to be sufficiently smooth and bounded functions of time. To

eliminate the need for velocity measurement, a filtered tracking error like term $\eta(t) \in \Re$ is defined as follows

$$\eta \triangleq \dot{e} + \alpha_1 e + \alpha_2 e_f \tag{6.16}$$

where α_1, α_1 are positive constant filter gains and $e_f(t) \in \Re$ is an auxiliary filter variable having the following dynamic relationship

$$\dot{e}_f \triangleq -\alpha_3 e_f + \alpha_2 e - k\eta; \quad e_f(0) = 0 \tag{6.17}$$

where α_3 is a positive constant filter gain and k is a positive constant control gain.

The controller design can be started by taking the time derivative of (6.16), then multiply it with M and substitute mechanical system dynamics given by (6.7) as well as (6.16) and (6.17) to obtain open loop system dynamics as follows

$$M\dot{\eta} = M(\ddot{z}_d - g) + \chi - Mk\alpha_2\eta + \phi(z)u(i) \tag{6.18}$$

where

$$\chi \triangleq M\alpha_1\left(\eta - \alpha_1 e - \alpha_2 e_f\right) + M\alpha_2\left(-\alpha_3 e_f + \alpha_2 e\right) + \frac{1}{N^2\mu_0 S}F_d. \tag{6.19}$$

It can be shown that χ can be upper bounded as follows

$$\chi \leq \rho_1 \|x\| + \rho_2 \tag{6.20}$$

where ρ_1, ρ_2 are bounding constants and defined as

$$\rho_1 \triangleq m_2 \max(\alpha_1, \alpha_2), \tag{6.21}$$

$$\frac{1}{N^2\mu_0 S}F_d \leq \rho_2 \tag{6.22}$$

$$x = \begin{bmatrix} e & e_f & \eta \end{bmatrix}^T \tag{6.23}$$

where m_2 was defined in (6.9). To apply back-stepping procedure on $u(i)$ an auxiliary control input $u_d(t) \in \Re$ and an auxiliary error signal $\eta_u(t) \in \Re$ have been defined as follows

$$\eta_u \triangleq u - u_d. \tag{6.24}$$

Finally adding and subtracting $\phi(z)u_d$ to obtain the open loop error dynamics as follows

$$M\dot{\eta} = M(\ddot{z}_d - g) + \chi - Mk\alpha_2\eta + \phi(z)\eta_u + \phi(z)u_d. \tag{6.25}$$

Based on the subsequent stability analysis auxiliary control input u_d can be designed as follows

$$u_d \triangleq \phi(z)^{-1}\left\{-\hat{M}(\ddot{z}_d - g) + kK_s e_f - K_s e\right\} \tag{6.26}$$

where $\hat{M}$ is a constant, best guessed estimation value of M, K_s is a positive constant controller gain.

Remark 6.1: It is assumed that u_d is lower bounded by zero since u defined in (6.8) *cannot track u_d when it is negative.*

Substituting (6.26) into (6.25) results the closed loop dynamics as follows

$$M\dot{\eta} = \tilde{M}(\ddot{z}_d - g) + \chi - Mk\alpha_2\eta + kK_s e_f - K_s e + \phi(z)\eta_u \tag{6.27}$$

where

$$\tilde{M} = M - \hat{M} \tag{6.28}$$

which satisfies the following bounding condition

$$\left|\tilde{M}(\ddot{z}_d - g)\right| \leq \rho_3 \tag{6.29}$$

where ρ_3 is a positive bounding constant. The controller gain k is chosen as

$$k = \frac{1}{m_2}\left[1 + k_{n1}\left(\rho_1^2 + \rho_2^2 + \rho_3^2\right)\right] \tag{6.30}$$

where k_{n1} is a positive constant nonlinear damping gain. To ensure the stability of (6.27), stability of η_u need to be proven, as well. To investigate the dynamics of η_u, I take the time derivative of (6.24), pre-multiply the resulting equation by L, substitute the electrical model given by (6.10) as well as (6.16) and time derivative of (6.26) and obtain the open loop current error dynamics as follows

$$L\dot{\eta}_u = 2iv(t) + W_1\phi_1 + \Omega_0 - \phi(z)\eta \tag{6.31}$$

where

$$\begin{aligned} W_1\phi_1 \triangleq\ & -2i\left[Ri_c + B\left(\dot{z}_d + \alpha_1 e + \alpha_2 e_f\right)\right] \\ & + L\phi(z)^{-1}\left[\hat{M}\dddot{z}_d + kK_s\left(-\alpha_3 e_f + \alpha_2 e\right) + K_s\left(-\alpha_1 e - \alpha_2 e_f\right)\right] \\ & - L\frac{\partial}{\partial z}\left\{\phi(z)^{-1}\right\}\left(\dot{z}_d + \alpha_1 e + \alpha_2 e_f\right)\left(-\hat{M}\left(\ddot{z}_d - g\right) + kK_s e_f - K_s e\right) \end{aligned} \tag{6.32}$$

and

$$\begin{aligned} \Omega_0 \triangleq\ & \Big[2iB + L\phi(z)^{-1}K_s(k^2+1) + \phi(z) \\ & + L\frac{\partial}{\partial z}\left\{\phi(z)^{-1}\right\}\left(-\hat{M}\left(\ddot{z}_d - g\right) + kK_s e_f - K_s e\right)\Big]\eta. \end{aligned} \tag{6.33}$$

Here, it is assumed that Ω_0 satisfies the following boundary condition

$$\Omega_0 \leq \rho_4\left(\|x\|\right)\|x\| \tag{6.34}$$

where $\rho_4(\cdot)$ is a boundary function. Based on the subsequent stability analysis control voltage $v(t)$ can be designed as follows

$$v(t) = \frac{1}{2i}\left(-K_u\eta_u - W_1\hat{\phi}_1\right) \tag{6.35}$$

where $W_1\hat{\phi}_1$ represents the best guessed estimation value of $W_1\phi_1$, K_u is a positive constant controller gain.

Remark 6.2: To avoid the singularity in the control law, i_c is assumed to be saturated to satisfy $|i_c| < I_{pm}$.

Closed loop dynamics can be obtained by substituting (6.35) into (6.31) as follows

$$L\dot{\eta}_u = -K_u\eta_u + W_1\tilde{\phi}_1 + \Omega_0 - \phi(z)\eta \tag{6.36}$$

where

$$W_1\tilde{\phi}_1 \triangleq W_1\phi_1 - W_1\hat{\phi}_1 \tag{6.37}$$

which can be upper bounded as follows

$$W_1\tilde{\phi}_1 \leq \rho_5 \tag{6.38}$$

where ρ_5 is a positive bounding constant. The controller gain K_u can be chosen as

$$K_u = k_u + k_{n2}(\rho_4^2 + \rho_5^2). \tag{6.39}$$

where k_{n2} is a positive constant nonlinear damping gain and k_u is a positive, constant controller gain.

6.3. Stability Analysis

In this section, the stability theorem have been presented and the proof of the theorem have been investigated by utilizing Lyapunov-based arguments.

Theorem 6.1: For a one DOF levitation system given by electromechanical equations (6.1) *and* (6.10)*, the air gap tracking controller given by* (6.26) *and* (6.35) *guarantees the uniformly ultimately boundedness of the air gap tracking error $e(t)$ in the sense that*

$$\|e(t)\| \leq \sqrt{\frac{a}{b}\|x_R(0)\|^2 \exp(-\beta t) + \frac{2\varepsilon}{b\beta}(1-\exp(-\beta t))} \tag{6.40}$$

where $x_R(t) \triangleq \begin{bmatrix} \eta & e & e_f & \eta_u \end{bmatrix}^T$ *is the combined error signal,* a, b, β, ε *are positive scalars defined explicitly as*

$$a \triangleq \max\{m_2, K_s, l_2\} \tag{6.41}$$

$$b \triangleq \min\{m_1, K_s, l_1\} \tag{6.42}$$

$$\beta \triangleq \frac{\min(\alpha_2, \alpha_1 K_s, \alpha_3 K_s, k_u) - \max(\frac{1}{4k_{n1}\alpha_2}, \frac{1}{4k_{n2}})}{0.5\max\{m_2, K_s, l_2\}} \tag{6.43}$$

$$\varepsilon \triangleq \frac{1}{4k_{n1}\alpha_2} + \frac{1}{4k_{n2}}. \tag{6.44}$$

Proof 6.1: To investigate the stability of the proposed controller a non-negative Lyapunov-like function have been defined as follows

$$V = \frac{1}{2}M\eta^2 + \frac{1}{2}K_s e^2 + \frac{1}{2}K_s e_f^2 + \frac{1}{2}L\eta_u^2 \tag{6.45}$$

which can be lower bounded and upper bounded as

$$\frac{1}{2}\min\{m_1, K_s, l_1\}\|x_R\|^2 \leq V \leq \frac{1}{2}\max\{m_2, K_s, l_2\}\|x_R\|^2 \tag{6.46}$$

where

$$x_R = \begin{bmatrix} \eta & e & e_f & \eta_u \end{bmatrix}^T. \tag{6.47}$$

Taking time derivative of (6.45) *and substituting closed loop dynamics given by* (6.27), (6.36) *and definitions of* (6.16), (6.17) *and then cancelling the common terms yields to*

$$\begin{aligned} \dot{V} &= \eta\left(\tilde{M}(\ddot{z}_d - g) + \chi - Mk\alpha_2\eta\right) - \alpha_1 K_s e^2 \\ &\quad -\alpha_3 K_s e_f^2 + \eta_u\left(-K_u\eta_u + W_1\tilde{\phi}_1 + \Omega_0\right). \end{aligned} \tag{6.48}$$

The derivative of V given in (6.48) *can be upper bounded by using the definitions of k given in* (6.30) *and K_u given in* (6.39) *and using the bounds given in* (6.20), (6.29), (6.34) *and* (6.38) *as follows*

$$\begin{aligned} \dot{V} \leq & -\alpha_2\eta^2 - \alpha_1 K_s e^2 - \alpha_3 K_s e_f^2 - k_u \eta_u^2 \\ & + \frac{1}{4k_{n1}\alpha_2}\|x\|^2 + \frac{1}{4k_{n1}\alpha_2} + \frac{1}{4k_{n2}}\|x\|^2 + \frac{1}{4k_{n2}} \end{aligned} \tag{6.49}$$

where the following nonlinear damping tool also utilised

$$k_{ni}\rho_i^2\|\cdot\|^2 - \rho_i\|\cdot\| + \frac{1}{4k_{ni}} = \left(\sqrt{k_{ni}}\rho_i\|\cdot\| - \frac{1}{2\sqrt{k_{ni}}}\right)^2 \geq 0. \tag{6.50}$$

The expression given in 6.49 can be further upper bounded by the help of using the definition of $x_R(t)$ given in (6.47) *and the upper bound of $V(t)$ given in (6.46) as follows*

$$\dot{V} \leq -\beta V + \varepsilon \tag{6.51}$$

where β was previously defined in (6.43) and ε was previously defined in (6.44). The solution of the above differential inequality yields

$$V(t) \leq V(0)\exp(-\beta t) + \frac{\varepsilon}{\beta}(1 - \exp(-\beta t)) \tag{6.52}$$

and from direct application of (6.46) the following upper bound for $x_R(t)$ can be obtained

$$\|x_R(t)\| \leq \sqrt{\frac{a}{b}\|x_R(0)\|^2\exp(-\beta t) + \frac{2\varepsilon}{b\beta}(1 - \exp(-\beta t))} \tag{6.53}$$

where a, b were previously defined in (6.41) and (6.42). Based on the definition of $x_R(t)$ and (6.53), it can be shown that the tracking error term $e(t)$ is bounded as stated in (6.40). Moreover applying standard signal chasing argument it can be shown that all signals in the closed-loop error system are bounded. ■

6.4. Simulation Studies

To see the behaviour of the proposed controller some simulation studies have been performed on a 1 DOF levitation system as shown in Figure 6.1. System parameters are listed in Table 6.1. Although the most common desired air gap is a set point

Table 6.1: 1 DOF Levitation system parameters.

Parameter Name	Symbol	Value [Unit]
Mass	m	5 [kg]
PM equivalent current	I_{pm}	$12.5[A]$
PM thickness	l_{pm}	$3[mm]$
Number of Coil Turns	N	$200[turns]$
Cross sectional Area of PM poles	S	$9[cm^2]$
Resistant of Coil	R	$1.6[\Omega]$
Permeability of free space	μ_0	$4\pi * 10^{-7}[NA^{-2}]$

in the levitation systems, the proposed controller can deal with time dependent and differentiable trajectories, as well. To see this property more clear; two different desired air gap trajectories for the levitated object are selected as $z_{d1} = 0.0122(1-e^{-t})m$ and $z_{d2} = (0.0122+0.001\sin 0.3t)(1-e^{-t})m$. To keep the control voltage and current close to zero, levitation point is selected to be the air gap value which the electromagnetic force produced by permanent magnets equals the total mass, similar to that of the zero power control. Controller gains are selected as $k = 3.1$, $K_s = 8$, $K_u = 1.5$, $\alpha_1 = 2$, $\alpha_2 = 0.43$, $\alpha_3 = 0.05$ for both of the desired trajectories.

Simulation results are shown in Figure 6.2-6.6. In Figure 6.2 convergence of the error signal can be seen clearly as well as the behaviour of the auxiliary control input. Control voltage and the current passing through the coils can be seen in Fig. 6.3. Figure 6.4 and Figure 6.5 shows trajectory tracking performance of the proposed controller with a sinusoidal desired trajectory. As stated in the previous sections, L and B are time dependent parameters but in the controller design and simulations we use constant estimations of the related parameters. Figure 6.6 represents the time dependent parameter values of L and B during both kinds of trajectory and constant estimated values of the parameters. Our controller can deal with the difference between the estimation value and real value of the parameters.

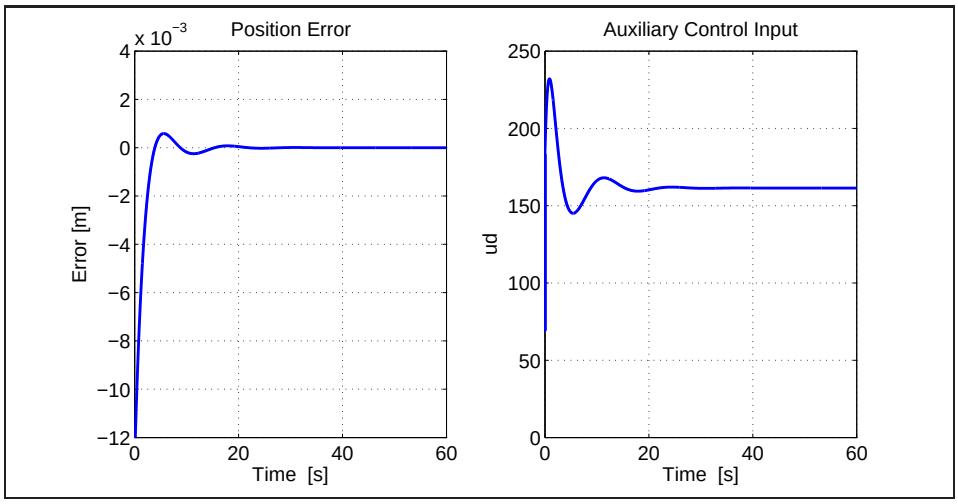

Figure 6.2: Position error and auxiliary control input($z_d = z_{d1}$).

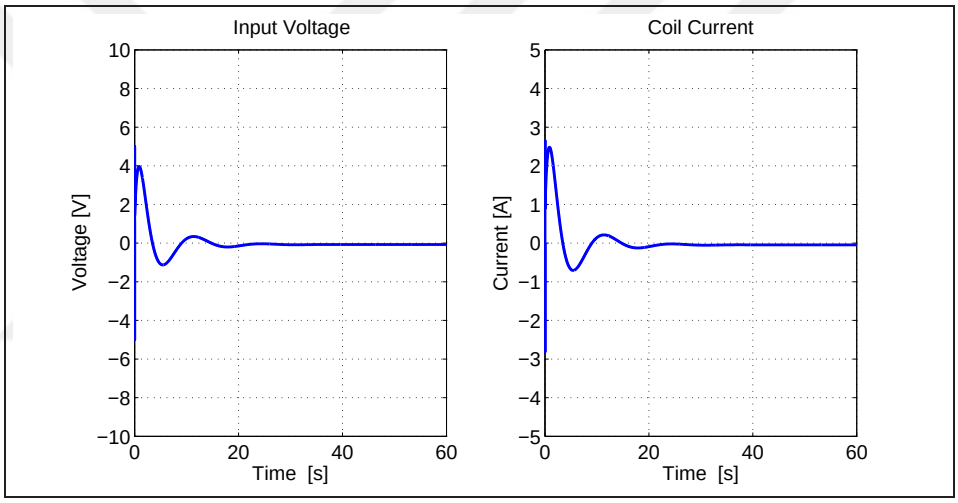

Figure 6.3: Control Voltage and Coil Current($z_d = z_{d1}$).

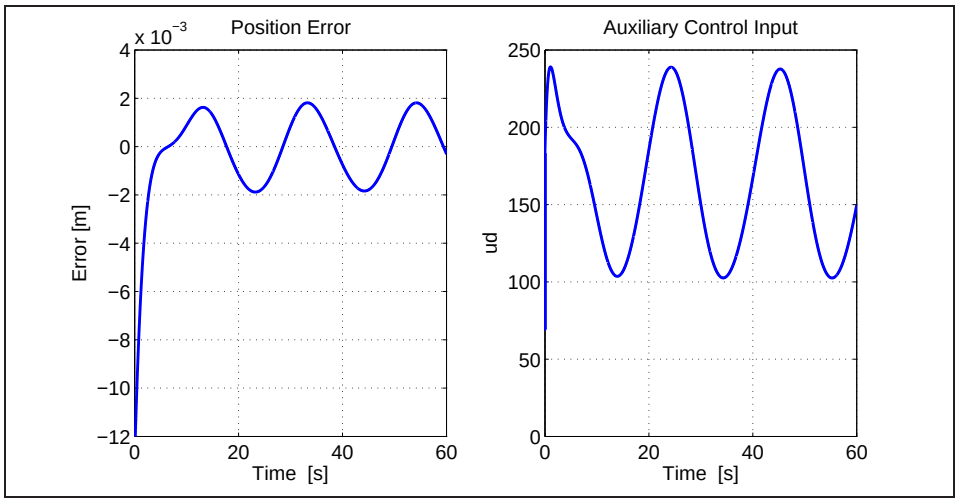

Figure 6.4: Position error and auxiliary control input($z_d = z_{d2}$).

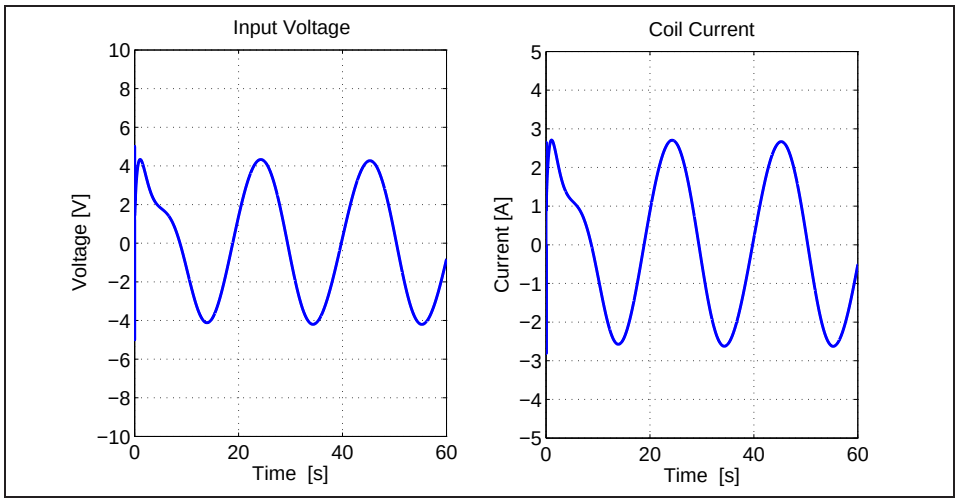

Figure 6.5: Control Voltage and Coil Current($z_d = z_{d2}$).

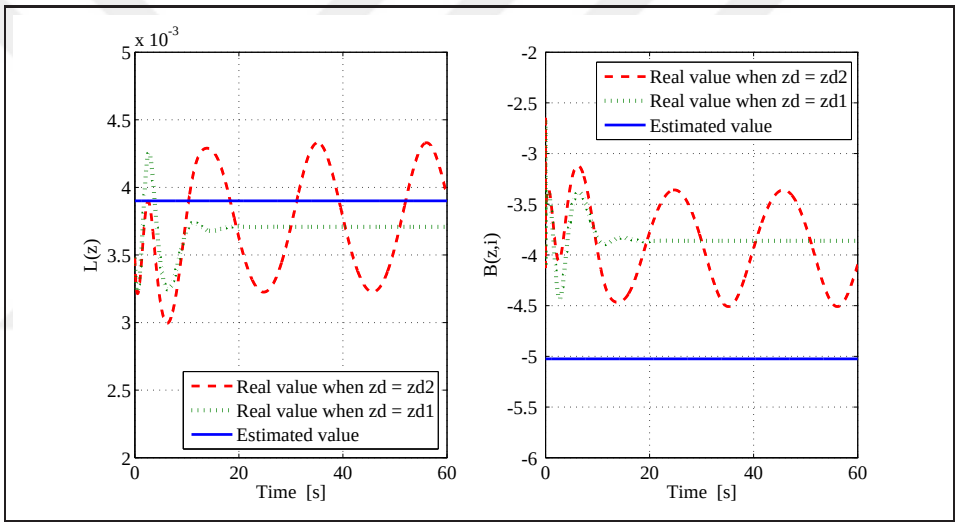

Figure 6.6: Time varying model parameters.

6.5. Remarks

In this chapter, a partial state feedback nonlinear model based robust controller for a one degree-of-freedom levitation have been presented. It is assumed that the target system includes parametric uncertainty in system dynamics. The proposed controller ensures that the absolute value of the air gap trajectory tracking error signal is forced to enter an ultimate bound in finite time despite the lack of exact knowledge of system parameters, unavailability of the velocity measurements and presence of external disturbances. Stability of the closed-loop system and boundedness of system

states are proven via Lyapunov based arguments. Simulation studies are performed to illustrate the effectiveness and viability of the proposed method.

The results given in this chapter are presented in 2015 54th IEEE Conference on Decision and Control (CDC), Osaka, Japan[66].

7. CONCLUSIONS

In this thesis, some partial state feedback controller formulations have been developed for two different kind of electromechanical systems with different dynamical properties while both of them include parametric uncertainties in the system models. The most important outcome of this thesis is novel model based controller design approaches for tendon driven robotic systems and levitation systems with hybrid electromagnets. Especially, the proposed controller design technique for over actuated tendon driven robotic systems allows to design various kinds of implementable partial state feedback controllers which reduces the sensor needs and system costs, as well.

A brief overview and a detailed model of a tendon driven robotic system have been presented in Chapter 1. The model presented here includes nonlinear robot dynamics, actuator dynamics as well as nonlinear elastic tendon dynamics. In Chapter 2, a novel controller design and the stability analysis have been presented for a tendon driven robotic system with parametric uncertainties in the overall system model and provides a robust solution to deal with uncertainties. The proposed controller proves the uniformly ultimately boundedness of the output tracking error signal with the help of Lyapunov like analysis tools. Partial state feedback solutions of the proposed controller design approach have been investigated in Chapter 3. Since the tendon actuated robotic systems are over actuated systems, elimination of any system state measurement would simplify the robotic hardware and decrease the total system costs. Nevertheless it requires heavy mathematical work out and a trustable theoretical background for stability analysis. In Chapter 3, two different partial state feedback controller formulations have been presented. The first one is a fully adaptive controller formulation and can deal with parametric uncertainties of manipulator subsystem parameters and actuator subsystem parameters while it requires link positions, tendon tensions and actuator position measurements. The second controller formulation shows how to eliminate the actuator side position measurements in case of having exact knowledge of the actuator parameters. It still provides and adaptation rule for the manipulator parameters. Since it is very hard to define the actuator parameters, the experimental evaluation could not be implemented, only simulation results are available to see the controller performance. Besides, a proper estimation of the actuator parameters can provide an

acceptable output performance owing to the adaptation in the manipulator side. To prove the effectiveness of controllers, both of the simulation results and experimental results are presented in Chapter 4 and Chapter 5, respectively.

In Chapter 6, a partial state feedback controller formulation for a one degree-of-freedom levitation system with hybrid electromagnets have been investigated. The levitation system model considers mechanical and electrical subsystem models and the voltage applied to the coils have been designed as a controller signal. Since it is very hard to measure the air gap velocity, it is eliminated via a filtered error like term. System parameters of the levitation system can change during the operation in certain bounds and robust structure of the proposed controller can deal with parametric uncertainties. Uniformly ultimately boundedness of the output error term have been proven via Lyapunov-like analysis tools not only for set point control but also trajectory tracking control of the levitated object. Some simulation results can be seen at the end of the chapter.

Future work includes many opportunities for researchers because output feedback control problem of tendon driven robots is still an open problem. Similarly an output feedback controller can be formulated for levitation systems by observing the coil currents. Reforming the proposed controllers for tendon driven robots to dexterous robotic hands and continuum tendon robotic systems and their experimental implementations would be a challenging issue, as well. Experimental implementation of a levitation system with four pole hybrid electromagnet would be an interesting issue with reformulating the controller algorithm as a model based zero power controller.

REFERENCES

[1] Kokotovic P., Arcak M., (2001), "Constructive nonlinear control: a historical perspective", Automatica, 37(5), 637-662.

[2] Berghuis H., Nijmeijer H., (1993),"A passivity approach to controller-observer design for robots", IEEE Transactions on Robotics and Automation, 9(6), 740-754.

[3] Kokotovic P., (1992), "The joy of feedback: nonlinear and adaptive", IEEE Control Systems, 12(3), 7-17.

[4] Dixon W.E., Zergeroglu E., Dawson D.M., Hannan M.W., (2000),"Global adaptive partial state feedback tracking control of rigid-link flexible-joint robots", Robotica, 18(3), 25-336.

[5] Kaloust J., Qu Z., (1994), "Continuous robust control design for nonlinear uncertain systems without a priori knowledge of control direction", American Control Conference,3494-3498, Orlando, FL, USA, 29 June-1 July.

[6] Khalil H. K.,(2008), "High-gain observers in nonlinear feedback control", International Conference on Control, Automation and Systems, xlvii-lvii, Seoul, South Korea, 14-17 October.

[7] Zhang X., Behal A., Dawson D. M., Xian B., (2005) "Output Feedback Control for a Class of Uncertain MIMO Nonlinear Systems With Non-Symmetric Input Gain Matrix", Proceedings of the 44th IEEE Conference on Decision and Control, 7762-7767.

[8] Okur B., Zergeroglu E., Seker M., Tatlicioglu E.,(2014), "Nonlinear robust control of 3 phase inverter with output LC filter", 19th IFAC World Congress, 529–533, Cape Town, South Africa, 24-29 August.

[9] Palli G., Borghesan G., Melchiorri C., (2012), "Modeling, identification, and control of tendon-based actuation systems", IEEE Transactions on Robotics, 28(2), 277–290.

[10] Kaneko M., Paetsch W., Tolle H., (1992), "Input-Dependent Stability of Joint Torque Control of Tendon-Driven Robot Hands", IEEE Tr. on Industrial Electronics, 39(2), 96–104.

[11] Mason M. T., Salisbury J. K., (1985), "Robot Hands and the Mechanics of Manipulation", MIT Press.

[12] Ma S., Hirose S., Yashinada H., (1993), “Design and experiments for a coupled tendon-driven manipulator”, IEEE Control Systems Magazine, 13(1), 30–36.

[13] Kobayashi H., Ozawa R., (2003), “ Adaptive Neural Network Control of Tendon Driven Mechanisms with elastic tendons”, Automatica, 39, 1509–1519.

[14] Chang S., Lee J., Yen H., (2005), “Kinematic and Compliance Analysis for Tendon Driven Robotic Mechanisms with Flexible Tendons”, Mechanism and Machine Theory, 40, 728–739.

[15] Tsai L. W., (1994), “Design of tendon-driven manipulators,”, Technical Report No: 95-96, Institute of System Research, University of Meriland, USA.

[16] Palli G., (2007), “Model and control of tendon actuated robots”, Doctorate Thesis, University of Bologna.

[17] Lee J. J., (1991), “Tendon-Driven Manipulators: Analysis, Synthesis and Control”, Doctorate Thesis, University of Maryland.

[18] Agrawal V., Peine W. J., Yao B., (2010), “Modelling of transmission characteristics across a cable-conduit system”, IEEE Transactions on Robotics, 26(5), 914–924.

[19] Wang Z., Sun Z., Phee S. J., (2013), “Modeling tendon-sheath mechanism with flexible configurations for robot control”, Robotica, 31, 1131–1142.

[20] Lee Y.-H., Lee J.-J., (2003), “Modeling of the dynamics of tendon-driven robotic mechanisms with flexible tendons,” Mechanism and Machine Theory, 38(12), 1431 – 1447.

[21] Ozawa R., Kobayashi H., Hashirii K., (2014), “Analysis, classification, and design of tendon-driven mechanisms,” IEEE Transactions on Robotics, 30(2), 396–410.

[22] Jacobsen S. C., Wood J. E., Knutti D. F., Biggers K. B., (1984), “The UTAH/M.I.T. dextrous hand: Work in progress ”, Int. J. of Robotics Research, 3(4), 21–50.

[23] Lens T., Stryk O. V., (2013), “Design and dynamics model of a lightweight series elastic tendon-driven robot arm”, IEEE International Conference on Robotics and Automation (ICRA), 4512–4518, Karlsruhe, Germany, 6–10 May.

[24] Jacobsen S. C., Ko H., Iversen E. K., Davis C. C., (1990), “Control strategies for tendon-driven manipulators,” IEEE Control Systems Magazine, 10(2), 23–28.

[25] Lee J.-J., Tsai L.-W.,(1991) “Torque resolver design for tendon-drive manipulators”, Technical Report No: 91-52, Institute of System Research, University of Meriland, USA.

[26] Rombokas E., Theodorou E., Malhotra M., Todorov E., Matsuoka Y., (2012), “Tendon–driven control of biomechanical and robotic systems: A path integral reinforcement learning approach”, IEEE International Conference on Robotics and Automation, 208–214, St. Paul, Minnesota, USA, 14–18 May.

[27] Deshpande A. D., Ko J., Fox D., Matsuoka Y.,(2013), “Control strategies for the index finger of a tendon-driven hand”, The International Journal of Robotics Research, 3281), 115–128.

[28] Abdallah M. E., Platt R., Wampler C. W., (2013), “Decoupled torque control of tendon–driven fingers with tension management,” The International Journal of Robotics Research, 32(2),247–258.

[29] Nakayama T., Fujimoto H., (2007), “Trajectory Tracking Control of Tendon Driven Robots Using Delayed Force Feedback, ”IEEE Int. Conf. on Mechatronics, 1–6 Kumamoto, Japan, 8–10 May.

[30] Haiya K., Komada S., Hirai J., (2009) “Control of Tendon–driven Robotic Mechanism by Nonlinear Springs and Hysteresis Characteristics, ”TEEE Int. Conf. on Mechatronics, pp. 1–6, Malaga, Spain, 14–17 April.

[31] Haiya K., Komada S., Hirai J., (2010), “Tension Control of Tendon Mechanisms by Compensation of Nonlinear Spring Characteristic Equation Error, ”IEEE Workshop on Advanced Motion Control, 42–47, Nagaoka, Japan, 21–24 March.

[32] Wimbock T., Ott C., Hirzinger G., (2010) “Immersion and invariance control for an antagonistic joint with nonlinear mechanical stiffness, ”IEEE Conf. on Decision and Control, 1128–1135, Atlanta, GA, USA, 15-17 December .

[33] Chalon M., Novel B. d’A., (2014) “Backstepping experimentally applied to an antagonistically driven finger with flexible tendons,” 19th IFAC World Congress, 217–223, Cape Town, South Africa, 24–29 August.

[34] Lewis F. L., Abdallah C. T., Dawson D. M., (1993), “Control of Robot Manipulators ”, Macmillan Publishing Co..

[35] Tomei P., (1991), “Adaptive PD Controller for Robot Manipulators,”IEEE Transactions on Robotics and Automation, 7(4), 565–570.

[36] Nicosia S., Tomei P., (1990), “Robot Control by Using Only Position Measurements, ”IEEE Transactions on Automatic Control, 35(9), 1058–1061.

[37] Ozbay U., Sahin H. T., Zergeroglu E., (2008), “Robust tracking control of kinematically redundant robot manipulators subject to multiple-self motion criteria, ”Robotica, 26, 711–728.

[38] Rao C. R., Mitra S. K., (1971), “Generalized Inverse of Matrices and Its Applications, ”Wiley.

[39] Dawson D. M., Bridges M. M., Qu Z., (1995), “Nonlinear Control of Robotic Manipulators for Environmental Waste and Restoration”, Prentice Hall.

[40] Okur B., Aksoy O., Zergeroglu E., Tatlicioglu E., (2015) “Nonlinear robust control of tendon-driven robot manipulators,” Journal of Intelligent and Robotic Systems, 80, 3–14.

[41] Sastry S., Bodson M., (1989), “Adaptive control: Stability, Convergence and Robustness”, Prentice Hall Co..

[42] Krstic M., Kanellakopoulos I., Kokotovic P., (1995), “Nonlinear and Adaptive Control Design”, John Wiley & Sons.

[43] Lim S. Y., Dawson D., Anderson K., (1996), “Re-examining the nicosia-tomei robot observer-controller from a backstepping perspective,” IEEE Transactions on Control Systems Technology, 4(3), 304–310.

[44] Okur B., Zergeroglu E., Tatlicioglu E., Aksoy O., (2014), “Nonlinear adaptive partial state feedback trajectory tracking control of tendon driven robot manipulators,” IEEE Conference on Control Applications, 228–233, Antibes, Nice, France, 8–10 October.

[45] Okur B., Zergeroglu E., Tatlicioglu E., (2015), “Nonlinear control of tendon driven robot manipulators: Elimination of actuator side position measurements,” 54th IEEE Conference on Decision and Control, 1491–1496, Osaka, Japan, 15–18 December.

[46] Atheron D., (1980), “Maglev using permanent magnet”, IEEE Transactions on Magnetics, 16(1), 146–148.

[47] Morishita M., (1989), “A new maglev system for magnetically levitated carrier system”, IEEE Transactions on Vehicular Technology, 38(4), 230–236.

[48] Onuki T., Toda Y., (1993), “Optimal design of hybrid magnet in maglev system with both permanent and electromagnets”, IEEE Transactions on Magnetics, 29(2), 1783–1786.

[49] Tzeng Y.-K., Wang T., (1994), “Optimal design of the electromagnetic levitation with permanent and electro magnets”, IEEE Transactions on Magnetics, 30(6), 4731–4733.

[50] Tzeng Y.-K., Wang T., (1995), “Dynamic analysis of the maglev system using controlled-pm electromagnets and robust zero-power-control strategy”, IEEE Transactions on Magnetics, 31(6), 4211–4213.

[51] Sinha P., Pechev A., (2004), “Nonlinear h–∞ controllers for electromagnetic suspension systems”, IEEE Transactions on Automatic Control, 49(4), 563–568.

[52] Im J. B., Cho S., Oh S., Ahn H., Kim S., Lee J., (2011), “Robust control using linear quadratic method in hybrid-electromagnetic suspension system”, 21st Interntional conference on Magnetically levitated systems and linear Derives, Daejon, Korea, 10–13 October.

[53] Sadrnia M. A., Jafari A. H., (2007), “Robust control design for maglev train with parametric uncertainties using Îij-synthesis”, World Congress on Engineering, London, U.K., 2–4 July.

[54] da Rocha P. H., Ferreira H. C., Porsch M. C., Sales R. M., (2009), “Fixed–point DSP implementation of nonlinear h–∞ controller for large gap electromagnetic suspension system”, Control Engineering Practice, 17(10), 1148–1156.

[55] Yang Z.-J., Tsubakihara H., Kanae S., Wada K., Su C.-Y., (2007), “Robust nonlinear control of a voltage-controlled magnetic levitation system with disturbance observer”, IEEE International Conference on Control Applications, 747–752, Singapore, 1–3 October.

[56] De Queiroz M., Dawson D., (1996), “Nonlinear control of active magnetic bearings: a backstepping approach”, IEEE Transactions on Control Systems Technology, 4(5), 545–552.

[57] Sivrioglu S., (2007), “Adaptive backstepping for switching control active magnetic bearing system with vibrating base”, IET Control Theory Aplications, 1, 1054–1059.

[58] Xu J., Zhou Y., (2011), “A nonlinear control method for the electromagnetic suspension system of the maglev train”, Journal of Modern Transportation, 19, 176–180.

[59] Levine J., Lottin J., Ponsart J.-C., (1996), “A nonlinear approach to the control of magnetic bearings”, IEEE Transactions on Control Systems Technology, 4(5), 524–544.

[60] Tran X.-T., Kang H.-J., (2014), “Arbitrary finite-time tracking control for magnetic levitation systems”, International Journal of Advanced Robotic Systems, 11, 1–8.

[61] LIU J., Yakushi K., Koseki T., (2002), “Robust control of a 4-pole electromagnet in semi-zero-power levitation scheme with a disturbance observer”, IEEJ Transactions on Industry Application, 122(1), 7–15.

[62] Cho H., Han H., Lee J., Kim B., Sung S., (2009), “Design considerations of em-pm hybrid levitation and propulsion device for magnetically levitated vehicle”, IEEE Transactions on Magnetics, 45(10), 4632–4635.

[63] Erkan K., Okur B., Koseki T., Yigit F., (2011), “Experimental evaluation of zero-power levitation control by transfer function approach for a 4-pole hybrid electromagnet”, IEEE International Conference on Mechatronics, 23–28, Istanbul, Turkey, 13–15 April.

[64] Chiba A., Fukao T., Ichikawa O., Osahima M., Takemoto M., Dorrell D., (2005), “Magnetic Bearings and Bearingless Drives ”, Elsevier.

[65] Woodsan H. H., Melcher J., (1968), “Electromechanical Dynamics - Part I:Discrete Systems”, Wiley.

[66] Okur B., Zergeroglu E., Erkan K., (2015), “Nonlinear robust control of a levitation system with hybrid electromagnets, ”54th IEEE Conference on Decision and Control, 6215–6220, Osaka, Japan, 15–18 December.

[67] Laumond J-P., Jacobs P.E., Taix M., Murray R.M., (1994), “A Motion Planner for Nonholonomic Mobile Robots”, IEEE Transactions on Robotics and Automation, 10(5), 120-135.

[68] Kobayashi H., Hyodo K., Ogane D., (1998), “On tendon-driven robotic mechanisms with redundant tendons ,”International Journal of Robotics Research, 17(5), 561–571.

[69] Krstic M., Kanellakopoulos I., Kokotovic P., (1995), “Nonlinear and Adaptive Control Design ”, John Wiley & Sons.

BIOGRAPHY

Beytullah OKUR was born in Samsun, Turkey, in 1984. He received the B.E. degree in Electronics Engineering Department from the Uludag University , Bursa, Turkey, in 2007 and the Master degree in Electronics Engineering from the Graduate School of Applied Sciences of Gebze Institute of Technology, Gebze, Kocaeli, Turkey, in 2011. In 2010, he joined the Department of Mechatronics Engineering, Yildiz Technical University, as a Research Assistant. He received the Ph. D. degree in Electronics Engineering from Graduate School of Applied Sciences of Gebze Technical University, Gebze, Kocaeli, Turkey, in 2016. His current research interests include nonlinear control techniques, tendon driven robots, levitation systems, power electronics, electrical machines and drives. He is married and has two children.

APPENDICES

Appendix A: List of Papers

Okur B., Aksoy O., Zergeroglu E., Tatlicioglu E, (2015), "Nonlinear robust control of tendon-driven robot manipulators," Journal of Intelligent and Robotic Systems, 80, 3–14.

Okur B., Zergeroglu E., Tatlicioglu E., Aksoy O., (2014), "Nonlinear adaptive partial state feedback trajectory tracking control of tendon driven robot manipulators," IEEE Conference on Control Applications, 228–233, Antibes, Nice, France, 8–10 October.

Okur B., Zergeroglu E., Tatlicioglu E., (2015), "Nonlinear control of tendon driven robot manipulators: Elimination of actuator side position measurements," 54th IEEE Conference on Decision and Control, 1491–1496, Osaka, Japan, 15–18 December.

Okur B., Zergeroglu E., Erkan K., (2015), "Nonlinear robust control of a levitation system with hybrid electromagnets," 54th IEEE Conference on Decision and Control, 6215–6220, Osaka, Japan, 15–18 December.